DB (H) C=440.12
629
1990

寄贈
吉田宏氏
昭和 年 月 日

Gravitational Lens Effect

by
Hiroshi Yoshida

Submitted on partial fulfillment of the requirements
for the degree of Doctor of Science
in Doctoral Program in University of Tsukuba
June, 1990

92303117

ABSTRACT

Some aspects of gravitational lens effect are discussed. The multiple quasar 1115+080 is analyzed as a multiple-image system due to this effect. In so doing we apply to the deflector of this system a dark lens model with dipole and quadrupole moments and thereby find that this model well produces observed data. We estimate the travel time differences between images, and the result is comparable with observed data. A new method is proposed to evaluate the deflector mass, and is applied to this system. By combining our mass estimations with Borgeest's method and with our own method, we can put some constraints on the Hubble constant.

We show further that apparent superluminal motions may be observed in gravitationally lensed systems such as 1115+080. It is found that images move with velocities greater than the light velocity when the source of lights crosses over one of the caustic lines.

Next the rotation of the polarization plane are discussed which is induced by a rotating deflector. We evaluate the rotation angle of the polarization plane by a rotating deflector with spheroidal symmetry, with the result that in the general cases of dark lens there are no differences between rotation angles of the polarization planes of the images.

Finally we discuss possible influence of the gravitational lens effect on determination of the density parameter Ω_0. It is found that the gravitational lens effect should not be neglected in the redshift-volume test which is one of the geometrical tests for Ω_0, and that when the effect is taken into account, Ω_0 is decreased, in agreement with the result of Hammer and Nottale.

CONTENTS

1. Introduction

The gravitational lens effect is one in which lights emitted from background sources are affected by the gravitational fields generated by foreground objects such as stars, galaxies, or clusters of galaxies. It has been known that this effect gives rise to the following phenomena.

i) Multiplication of images

The trajectory of lights emitted from a source is deflected by the gravitational fields which are generated by foreground objects. It then becomes possible that lights from the source propagate along some different paths to be received by the observers, and that the observers recognize these lights as images distinct from each other. Such a phenomenon is called the "multiplication of images". When multiple images are identified as lights emitted from one and the same source, the whole system of multiple images and the gravitational lensing objects (deflectors) is called the "multiple-image system".

ii) Gravitational distortion effect

Cross sections of light bundles may be distorted by the gravitational lens effect. This effect is called the "gravitational distortion effect". For some special alignments of the source and the deflector with respect to the observer, this effect will makes us observe those images with arc-like (ring-like) structure, which are called the giant arcs (Einstein rings).

iii) Gravitational amplification effect

Due to the gravitational lens effect not only is the shape of the cross section of a light bundle distorted, but its cross sectional area is changed. Then the apparent luminosity of each image is amplified or de-amplified. This effect is called the "gravitational amplification effect". In the case of amplification, the effect enables us to observe faint distant sources which may otherwise be unobservable. It is for this reason that the gravitational lens effect is sometimes called the "natural telescope".

iv) Time delay

The travel time of light from a source to the observer in the case of the gravitational lens effect differs from that in the case when no such effect is operating. This difference in arrival time is called the "time delay". In fact, the time delay results from the change of the length of light path (geometrical term) and also from the change of the spatial velocity of light due to the gravitational potential (potential term).

v) Gravitational Faraday effect

When the light passes through the gravitational field induced by a rotating deflector, the polarization plane of the light may rotate. This effect is called the "gravitational Faraday effect".

The gravitational lens effect provides a very powerful tool in the observational astrophysics. It plays important roles when and where objects such as multiple images, giant arcs or Einstein rings are observed. Strictly speaking, most astrophysical data cannot be free from the gravitational lens effects which are caused by the local inhomogeneities in the Universe. Therefore we must take into account the gravitational lens effect when investigating the structure of the Universe on the basis of such data. This can be done by statistically treating the gravitational lens effect. In fact, for the case when the multiple-image systems are recognized or when the universe is locally inhomogeneous, the role played by the gravitational lens effect in the observational astrophysics can be summarized as follows.

I. Multiple images, giant arcs or Einstein rings

Up to the present many candidates for multiple images, giant arcs or Einstein rings have been found. In such systems we can observe the following quantities: the relative positions of images, shapes of images, apparent luminosities of images, travel time differences between images and differences between rotation angles of polarization planes of images. From the data of such a system we can obtain the following information on the deflector.

i) The deflector mass

We can estimate the total masses or the mass distributions of the deflectors in such systems. Masses obtainable in this way differ from those estimated from the rotation curves of galaxies. Consideration of the gravitational lens effect thus provides us with more detailed information on such masses of galaxies than the case when we have only the rotation curves of galaxies.

ii) Travel time differences between multiple images

When the source has some intrinsic time evolution in its luminosity, we can determine the travel time differences between multiple images by observing, over long duration, differences between apparent luminosities of those images. The travel time differences between images put some constraints either on the Hubble constant or on the cosmological models employed well as on the structure of the deflector.

iii) Apparent superluminal motions

In some cases the images appear to move away from one another with velocities greater than the light velocity, although their sources move normally. Such motions are called the "apparent superluminal motions of images", and may be observed in the case like multiple-image systems.

iv) Gravitational Faraday effects

If the light source is a radio source, we can observe the differences between rotation angles of polarization planes corresponding to the respective images, the difference being due to the gravitational lens effect. We can distinguish such rotations from those of the polarization planes which are induced by the interstellar or intergalactic matters (the usual Faraday effect).

II. Statistical gravitational lens effects

In order to investigate the global structure of the Universe we often analyze the observed data on geometrical tests such as m-z relation, N-m relation or the redshift-volume test. The redshift-volume test is known to be less affected by the

galaxy-evolution effects than the case of other tests. Recently Loh and Spillar obtained the data on the redshift-volume test, and their results suggest that the density parameter $\Omega_0 \sim 1$. In their analysis they assumed that the Universe is homogeneous and isotropic not only globally but also locally, thus adopting Mattig's formulae for the redshift-distance relation.

Recent observations on the distribution of high redshift galaxies indicate, however, that the Universe has a large scale structure extending over ~ 50[Mpc]. We should therefore reanalyze Loh and Spillar's data by taking into account such inhomogeneities in the Universe.

The light propagation in the inhomogeneous universe and the effect of local inhomogeneities on the observed data have been discussed by several authors (Dyer & Roeder 1972, 1973, 1974, Weinberg 1976, Schneider 1987, Dyer & Oattes 1988, and Futamase & Sasaki 1989). In their discussions local inhomogeneities are regarded as the gravitationally lensing objects, and are assumed to be uniformly distributed. Thus the effect of some local inhomogeneities is investigated by statistically dealing with the gravitational lens effect.

III. Our results

The results of the present thesis on multiple-image system are as follows: When interpreting the multiple quasar 1115+080 as a multiple-image system, we find the possibility that this system has further images than those that have so far been observed. In our analysis the travel time differences between the images are estimated. We have also proposed a new method to calculate the deflector mass. By combining our estimation with our method and the one with the method proposed by Borgeest (1986) we find that some limits are imposed on the Hubble constant.

We further suggest that apparent superluminal motion may appear in the gravitationally lensed system. In particular, 1115+080 is claimed to be the most promising candidate for such motion to be observable.

Next the rotation of polarization plane is discussed which is induced by a rotating object (gravitational Faraday effect). We find that, in the general case of dark lens, no differences between the rotation angles of the polarization planes of images arise when estimated up to the lowest order in G. For the twin quasar 0957+561, which is also interpreted as a multiple-image system, there is a possibility that a part of the rotation is attributed to the gravitational Faraday effect.

Our result on the statistical gravitational lens effect is as follows: We have investigated, in the redshift-volume measurement, the influence of the gravitational lens effect on the density parameter Ω_0. It is then found that this effect caused by local inhomogeneities should not be neglected and decreases the value of Ω_0.

IV. Outline of this thesis

The present thesis is organized as follows. We will start, in Chapter 2, with a general formulation of the gravitational lens effect. In Chapter 3, we review the observed results of some candidates for multiple images, giant arcs and an Einstein ring. In Chapter 4, we will analyze observed data concerning the multiple quasar 1115+080, interpreting this as a multiple-image system in our sense. Next, in Chapter 5, apparent superluminal motions of images are discussed, which are induced by the gravitational lens effect. In Chapter 6, we investigate the gravitational Faraday effect induced by a rotating nonspherical deflector. Chapter 7 is devoted to a statistical investigation into the influence of the local inhomogeneities on the density parameter Ω_0. Finally, in Chapter 8, we will summarize the results of this thesis.

2. General Formulation of the Gravitational Lens Effects

In 1919 Eddington observed the deflection of the light passing near the sun during an eclipse. This observation is famous as a test of general relativity. In those times, however, it was not known that the source object of the gravitational field acts as a lens. Einstein (1936) was the first to suggest the possibility of the gravitational lens effects, showing that a star acts as a lens. Further, Zwicky (1937) showed that the probability of observing the gravitationally lensed object would be higher in the case by extranebulae than in the case by stars.

In 1960s, many authors investigated various aspects of the gravitational lens effect: the lens effect in a spherically symmetric gravitational field (Liebes 1964), the travel time difference between images and its applications to cosmology (Refsdal 1964a,1964b,1966 *etc.*). In 1970s fundamental studies of the gravitational lens effects were made by a number of authors (Press & Gunn 1973, Bourassa, Kantowski & Norton 1973 hereafter BKN, Bourassa & Kantowski 1975 hereafter BK, and Cooke & Kantowski 1975, *etc.*).

Theoretical as well as observational studies have been more extensively carried out after the discovery of the twin quasar "0957+561"(Walsh *et al.* 1979).

In this chapter we briefly review the general formulation of the gravitational lens effect. First the lens equation, which is the most fundamental equation for the gravitational lens effects, is derived in §2.1. Next, various kinds of information obtainable from the lens equation are discussed (§2.2). Finally, we review the travel time differences between images (§2.3).

2.1 Lens Equations

In this section the derivation of the lens equation is briefly described. First we present the general form of the deflection angle α from the geodesic equation.

A gravitational lens system is illustrated in Fig.2.1. The object which causes the gravitational lens effect is located at the origin of the coordinate system $\{x^1, x^2, x^3\}$. We call this object the "deflector". We assume that the observer is standing on the x^3 axis. The plane $\{x^3 = 0\}$ is called the "deflector plane". The photon emitted from the source is assumed to pass through the image position $(x_{\rm I}, y_{\rm I}, 0)$ on the deflector plane ($x = x^1$, $y = x^2$). And the source position on the deflector plane, when the deflector is assumed not to be present, is denoted by $(x_{\rm S}, y_{\rm S}, 0)$.

We assume that the gravitational field is so weak that the Newtonian approximation is valid, that is, we can deal with the linearized general relativity in our analyses.

The deflection angle $\vec{\alpha}$ in Fig.2.1 is defined as

$$\vec{\alpha} = \left.\frac{\vec{u}}{|\vec{u}|}\right|_{\rm obs.} - \left.\frac{\vec{u}}{|\vec{u}|}\right|_{\rm source}, \tag{2.1}$$

where $\vec{u}$ is the velocity of light *i.e.*, $d\vec{x}/dt$. The metric in this system is given by

$$g_{\mu\nu} = \eta_{\mu\nu} + h_{\mu\nu}, \tag{2.2}$$

$$\eta_{\mu\nu} = diag(+1, -1, -1, -1), \tag{2.3}$$

$$h_{\mu\mu} = \tfrac{2}{c^2}\varphi \qquad (\mu = 0, \ldots, 3), \tag{2.4}$$

$$h_{0i} = \psi_i \qquad (i = 1, 2, 3), \tag{2.5}$$

$$others = 0, \tag{2.6}$$

up to the lowest order in G, where φ and ψ_i are given by

$$\varphi(\vec{x}) = -G \int \frac{\rho(\vec{x}')}{|\vec{x} - \vec{x}'|} d^3x', \tag{2.7}$$

$$\psi_i(\vec{x}) = \frac{4G}{c^3}\int \frac{\rho(\vec{x}')\frac{dx_i'}{dt}}{|\vec{x}-\vec{x}'|}d^3x', \tag{2.8}$$

and $\rho(\vec{x}')$ is the mass distribution of the deflector. From eq.(2.1),

$$\begin{aligned}\vec{\alpha} = & \int_{t_S}^{t_{obs.}} dt \frac{d}{dt}\Big(\frac{\vec{u}}{|\vec{u}|}\Big) \\ = & -\frac{2}{c}\int_{t_S}^{t_{obs.}} \vec{\nabla}\varphi dt - \int_{t_S}^{t_{obs.}} \vec{u}\times(\vec{\nabla}\times\vec{\psi})dt.\end{aligned} \tag{2.9}$$

In estimating the deflection angle under the Newtonian approximation, we can express the path of the light by $\vec{x}(t) = (x_I, y_I, ct + x_0^3)$. Then $\vec{\alpha}$ is dependent on the image position (x_I, y_I) on the deflector plane. For the sake of simplicity, positions (x, y) on the deflector plane are denoted by complex variables $z = x+iy$ (BKN). From eq.(2.9) we can define the complex deflection angle, $\alpha = \alpha_x + i\alpha_y$. Then eq.(2.9) is expressed as

$$\begin{aligned}\alpha(z_I, \overline{z}_I) = & \int_{-\infty}^{\infty} dt\Big[-\frac{2}{c}(\partial_x\varphi + i\partial_y\varphi) \\ & - \big\{\partial_x(u\cdot\psi) + i\partial_y(u\cdot\psi)\big\}\Big]_{z=z_I}.\end{aligned} \tag{2.10}$$

Our next task is to derive the lens equation. There are two methods to do so. The first makes use of the geometrical relation in Fig.2.1 (BKN), and the second makes use of Fermat's principle (Schneider 1985, Blandford & Narayan 1986). We shall discuss the latter after describing travel time differences.

Since $|\alpha| \ll 1$ is assumed, it is clear that the relation between z_S, z_I and α is given by

$$\frac{D_s}{D_d}z_S = \frac{D_s}{D_d}z_I + D_{ds}\alpha, \tag{2.11}$$

where D_d, D_s and D_{ds} are angular diameter distances between the observer and

the deflector, between the observer and the source, and between the deflector and the source, respectively. The above relation is called the "lens equation".

There are some difficulties in evaluating the angular diameter distance. One of them is that the distance depends on the cosmological fluctuation of the density of those matters in which the light passes through (Dyer & Roeder 1973, Alcock & Anderson 1985,1986). Another is the problem of the Hubble constant $H_0(\sim 50$ or ~ 100[km/sMpc]).

It is convenient to adopt the dimensionless form to the lens equation given by:

$$\theta_S = \theta_I + \frac{D_{ds}}{D_s}\alpha(\theta_I, \overline{\theta}_I), \tag{2.12}$$

where $\theta = z/D_d$, being the angle over the celestial sphere, is an observable quantity. This equation contains the parameters which characterize the deflector model employed, D_{ds}/D_s, and θ_S. On the other hand, H_0 does not appear in eq.(2.12). Then we have only to fix these parameters for constructing the deflector model by observations.

On the other hand, the image positions are obtained by solving the lens equation with respect to θ_I for a given deflector model. In particular, we must solve the lens equation numerically by using the computer in most cases. We have two methods for numerical investigation: i) the Newton-Raphson method, ii) the Schramm-Kayser method (Schramm and Kayser 1988). The advantage of method ii) is that solutions converge rapidly. There is a disadvantage, however, such that it needs huge memories on the machine. Moreover when we adopt an extended source in order to investigate the morphology of images, the physical meaning of the image shapes becomes ambiguous in method ii). We thus adopt method i) for analyses of the configuration of images (see Chapter 4).

2.2 Properties of images

In this section the properties of images obtainable from the lens equation (2.12) will be described. Considering that the source has a small extended area $\delta\vec{\theta}_{\rm S}$, we expect its image also to have an extended area $\delta\vec{\theta}_{\rm I}$. The relation between $\delta\vec{\theta}_{\rm S}$ and $\delta\vec{\theta}_{\rm I}$, which is given by the so-called magnification matrix, tells us some important information on the deflector, on the source and on the images. Now we have only to investigate information from the magnification matrix.

From eq.(2.12), shifting the source position by $\delta\vec{\theta}_{\rm S}$: $\vec{\theta}_{\rm S} \rightarrow \vec{\theta}_{\rm S} + \delta\vec{\theta}_{\rm S}$, we get the relation between $\delta\vec{\theta}_{\rm S}$ and $\delta\vec{\theta}_{\rm I}$ given by

$$\delta\vec{\theta}_{\rm S} = \delta\vec{\theta}_{\rm I} + [\,{\rm A}\,]\delta\vec{\theta}_{\rm I}, \tag{2.13}$$

where the 2×2 matrix $[\,{\rm A}\,]$ is given by

$$[\,{\rm A}\,] = \frac{D_{\rm ds}}{D_{\rm s}}\frac{\delta\vec{\alpha}}{\delta\vec{\theta}_{\rm I}}. \tag{2.14}$$

If the metric of the local gravitational fields is static, *i.e.*, $g_{\mu\nu,0} = 0$ and $g_{0i} = 0$, $[\,{\rm A}\,]$ is symmetric in general. Moreover there is a function Φ of $\vec{\theta}_{\rm I}$ such that

$$\frac{\delta\Phi}{\delta\vec{\theta}_{\rm I}} = \frac{D_{\rm ds}}{D_{\rm s}}\vec{\alpha}(\vec{\theta}_{\rm I}), \qquad [\,{\rm A}\,] = \frac{\delta^2\Phi}{\delta\vec{\theta}_{\rm I}\delta\vec{\theta}_{\rm I}}, \tag{2.15}$$

(Kovner 1987a). When the deflector consists of a single thin object, Φ is explicitly expressed by

$$\Phi = -\frac{4G}{c^2}\frac{D_{\rm ds}}{D_{\rm d}D_{\rm s}}\int d^2\theta'\sigma(\vec{\theta}')\ln|\vec{\theta} - \vec{\theta}'|, \tag{2.16}$$

where σ is called the "projected surface mass density" per steradian, for which

$$\int d^2\theta\sigma(\vec{\theta}) = M_{\rm d} \quad (= \textit{mass of deflector}). \tag{2.17}$$

Rather than $[\,{\rm A}\,]$, we prefer to use another 2×2 matrix $[\,{\rm M}\,]$ which is defined

by

$$[\,\mathrm{M}\,] = \Big([\,\mathrm{I}\,] + [\,\mathrm{A}\,]\Big)^{-1}, \tag{2.18}$$

where $[\,\mathrm{M}\,]$ is called the "magnification matrix" or "amplification matrix". By using this matrix, we can rewrite eq.(2.13) as

$$\delta\vec{\theta}_{\mathrm{I}} = [\,\mathrm{M}\,]\delta\vec{\theta}_{\mathrm{S}}. \tag{2.19}$$

In BK's notation, $[\,\mathrm{M}\,]$ is explicitly given by

$$[\,\mathrm{M}\,] = \frac{1}{\mathcal{G}^2 - |\mathcal{F}|^2}\begin{pmatrix} \mathcal{G} + Re\mathcal{F} & -Im\mathcal{F} \\ -Im\mathcal{F} & \mathcal{G} - Re\mathcal{F} \end{pmatrix}. \tag{2.20}$$

In eq.(2.20), $\mathcal{G}$ and $\mathcal{F}$ are given by

$$\mathcal{G} = 1 + \frac{D_{\mathrm{ds}}}{D_{\mathrm{s}}}\frac{\partial\overline{\alpha}}{\partial\overline{\theta}_{\mathrm{I}}}, \tag{2.21}$$

$$\mathcal{F} = -\frac{D_{\mathrm{ds}}}{D_{\mathrm{s}}}\frac{\partial\overline{\alpha}}{\partial\overline{\theta}_{\mathrm{I}}}, \tag{2.22}$$

where $\mathcal{G}$ in general is real and is expressed by

$$\mathcal{G} = 1 - \frac{4\pi G}{c^2}\frac{D_{\mathrm{ds}}}{D_{\mathrm{d}}D_{\mathrm{s}}}\sigma(\theta_{\mathrm{I}}, \overline{\theta}_{\mathrm{I}}). \tag{2.23}$$

In the "dark lens" case when the light cannot pass through the interior of the deflector, $\mathcal{G} = 1$ and $\mathcal{F}$ is an analytic function only of θ_{I}.

Now the eigenvalues $\lambda_{\pm}$ of $[\,\mathrm{M}\,]$ are given by

$$\lambda_{\pm} = \frac{1}{\mathcal{G} \mp |\mathcal{F}|}. \tag{2.24}$$

Let I be the observed apparent luminosity of an image, and I_0 be the imaginary apparent luminosity of the source in the case with no deflection. The ratio I/I_0

is equal to the ratio of the image area to the source area on the deflector plane, and given by

$$\begin{aligned} \frac{I}{I_0} &= \left| det\left(\frac{\delta\vec{\theta}_{\rm I}}{\delta\vec{\theta}_{\rm S}}\right) \right| \\ &= \left| \frac{1}{\mathcal{G}^2 - |\mathcal{F}|^2} \right|. \end{aligned} \tag{2.25}$$

This ratio is called the "amplification factor" (see Chapter 7).

The lines $\mathcal{G}^2 - |\mathcal{F}|^2 = 0$ on the deflector plane are called the "critical lines" (Kovner 1987a). When an image is on this line, the amplification factor becomes infinite. The number of images changes when an image crosses the critical line, because the linear mapping given in eq.(2.19) is broken down on this line.

If the source-profile on the deflector plane has an eccentricity $\tilde{\rm e}$ and the semi-major axis declines to the right ascension with the angle $\chi_{\rm S}$, then the image-profile also has the eccentricity ϵ given by

$$\epsilon = \sqrt{\frac{2|(1-\tilde{\rm e}^2)(\mathcal{G}-\mathcal{F}e^{2i\chi_{\rm S}})^2 - (\mathcal{G}+\mathcal{F}e^{2i\chi_{\rm S}})^2|}{\left\{(1-\tilde{\rm e}^2)|\mathcal{G}-\mathcal{F}e^{2i\chi_{\rm S}}|^2 - |\mathcal{G}+\mathcal{F}e^{2i\chi_{\rm S}}|^2\right\} + |(1-\tilde{\rm e}^2)(\mathcal{G}-\mathcal{F}e^{2i\chi_{\rm S}})^2 - (\mathcal{G}+\mathcal{F}e^{2i\chi_{\rm S}})^2|}}, \tag{2.26}$$

and the semi-major axis of the image profile also declines to the right ascension with the angle $\chi_{\rm I}$ given by

$$\exp(2i\chi_{\rm I}) = \frac{4\mathcal{G}\mathcal{F} + \tilde{\rm e}^2\left(\mathcal{G}e^{-i\chi_{\rm S}} - \mathcal{F}e^{i\chi_{\rm S}}\right)^2}{|4\mathcal{G}\mathcal{F} + \tilde{\rm e}^2\left(\mathcal{G}e^{-i\chi_{\rm S}} - \mathcal{F}e^{i\chi_{\rm S}}\right)^2|}, \tag{2.27}$$

(Yoshida & Omote 1988). These expressions (2.26) and (2.27) agree with those derived by BKN in the limit $\tilde{\rm e} \to 0$.

If the shapes of images $A, B, \ldots$ are known, we can obtain the mapping between images, namely, we can decide the relative magnification matrix given

by

$$\begin{aligned}[\,\mathrm{M}_{AB}\,] &\equiv [\,\mathrm{M}_A\,][\,\mathrm{M}_B\,]^{-1} \\ &= [\,\frac{\delta\vec{\theta}_A}{\delta\vec{\theta}_B}\,],\end{aligned} \tag{2.28}$$

which is a mapping from $\delta\vec{\theta}_B$ to $\delta\vec{\theta}_A$. Moreover, from these quantities the relative amplification factor I_A/I_B and the relative orientation angle *i.e.* $\Delta\chi_{AB} = \chi_A - \chi_B$ are obtained. These observable quantities are necessary for investigating the structure of the deflector.

However the image configuration obtained by eqs.(2.26) and (2.27) can hardly correspond to giant arcs or to Einstein rings because the mapping given by eqs.(2.19), (2.26) and (2.27) is, at most, a linear transformation. This mapping yields an ellipse for the image shape. As stated by Narasimha and Chitre (1988), and by Kovner and Paczyński (1988), the lens equation must be solved for every points on the source contour.

The following property of the gravitational lens effect is noteworthy: any non-singular transparent lens produces an odd number of images. This property was suggested by many authors (Young *et al.* 1980, Dyer & Roeder 1980, *etc.*), and was confirmed by Burke (1981), McKenzie (1985), and Blandford and Narayan (1986). A simple example was given by Dyer and Roeder as follows. We consider a transparent lens with spherical symmetry. The deflection angle is given by

$$\frac{D_{\rm ds}}{D_{\rm s}}\vec{\alpha} = -\frac{4GD_{\rm ds}}{c^2 D_{\rm d} D_{\rm s}}\mathcal{M}(|\vec{\theta}|)\frac{\vec{\theta}}{|\vec{\theta}|^2}, \tag{2.29}$$

where

$$\mathcal{M}(|\vec{\theta}|) = 2\pi\int_0^{|\vec{\theta}|}\sigma(r)r\,dr, \tag{2.30}$$

with σ being the projected surface mass density per steradian. In this case the

lens equation is expressed as

$$\vec{\theta}_{\rm S} = \vec{\theta}\Big(1 - \frac{4GD_{\rm ds}}{c^2 D_{\rm d} D_{\rm s}} \mathcal{M}(|\vec{\theta}|) \frac{1}{|\vec{\theta}|^2}\Big). \tag{2.31}$$

We can thus reduce this equation to one-dimensional equation, by making a change of variables $\vec{\theta}_{\rm S} \to s, \quad \vec{\theta} \to x$ without loss of generality, because of $\vec{\theta}_{\rm S} /\!\!/ \vec{\theta}$. The lens equation then becomes

$$s = x - \frac{4GD_{\rm ds}}{c^2 D_{\rm d} D_{\rm s}} \mathcal{M}(|x|) \frac{1}{x}. \tag{2.32}$$

Since σ is non-singular in the limit $x \to 0$, the deflection angle becomes zero as x goes to zero. It is now clear that $\mathcal{M}(|x|)$ is an even function of x. The deflection angle α then has odd parity with respect to x. The lens equation (2.32) thus has an odd number of images.

Burke and McKenzie proved that the system has an odd number of images in any non-singular transparent lens system.

2.3 Travel Time Differences Between Images

If the lights emitted from a source at time $t_{\rm S}$ propagate along different paths, to be observed as images A and B, the times when these lights are received by an observer are generally different from each other. This difference between the arrival times is called the "travel time difference between images", and is briefly described in this section (Refsdal 1964b,1966, Cooke & Kantowski 1975, Kayser & Refsdal 1983, and Borgeest 1983).

Since the light propagates along a null geodesic,*i.e.*, $ds^2 = 0$, we can solve the equation

$$c^2\big(1 + \frac{2}{c^2}\varphi\big)dt^2 - \big(1 - \frac{2}{c^2}\varphi\big)d\ell^2 + 2c\psi_i dx^i dt = 0, \tag{2.33}$$

with respect to cdt. Up to the lowest order in G, we have

$$cdt = d\ell - \frac{2}{c^2}\varphi d\ell - \psi_i dx^i, \tag{2.34}$$

where $d\ell^2 = dx^2 + dy^2 + dz^2$. Then the travel time of the light emitted at $t_{\rm S}$ and observed at $t_{\rm obs.}$ is given as

$$c\int_{t_{\rm S}}^{t_{\rm obs.}} dt = \int_{t_{\rm S}}^{t_{\rm obs.}} d\ell - \frac{2}{c^2}\int_{t_{\rm S}}^{t_{\rm obs.}} \varphi d\ell - \int_{t_{\rm S}}^{t_{\rm obs.}} \psi_i dx^i. \tag{2.35}$$

Therefore the travel time difference $\triangle t_{AB}$ between images A and B is given by

$$c\triangle t_{AB} = \int_{t_{\rm S}}^{t_{\rm obs.}} (d\ell_A - d\ell_B) - \int_{t_{\rm S}}^{t_{\rm obs.}} \Big\{ (\psi_i dx^i{}_A + \frac{2}{c^2}\varphi d\ell_A) - (\psi_i dx^i{}_B + \frac{2}{c^2}\varphi d\ell_B) \Big\}. \tag{2.36}$$

The first term in (2.36) is called the "geometrical term" and the second is called the "potential term". We denote the geometrical and the potential terms as $\triangle t_g$ and $\triangle t_p$, respectively. The former is the difference between path lengths of the images, and the latter arises from the difference between the light velocities.

Consider the forward and the backward wavefronts of lights which are tangential to each other at $D_{\rm d}\vec{\theta}_{\rm S}$ on the deflector plane. The geometrical term is expressed as the difference between the distances along each path of the light from the forward to the backward wavefronts:

$$c\triangle t_{gAB} = \frac{1}{2}(1+{\rm z_d})(K_f + K_b) D_{\rm d}^2 \{ |\vec{\theta}_A - \vec{\theta}_{\rm S}|^2 - |\vec{\theta}_B - \vec{\theta}_{\rm S}|^2 \}, \tag{2.37}$$

where K_f and K_b are principal curvatures of the forward and the backward wavefronts. The sum of K_f and K_b is given by

$$K_f + K_b = \frac{D_{\rm s}}{D_{\rm d} D_{\rm ds}}, \tag{2.38}$$

(Cooke & Kantowski 1975). Thus, $c\triangle t_{gAB}$ is expressed as

$$c\triangle t_{gAB} = \frac{1}{2}(1+{\rm z_d})\frac{D_{\rm d} D_{\rm s}}{D_{\rm ds}} (|\vec{\theta}_A - \vec{\theta}_{\rm S}|^2 - |\vec{\theta}_B - \vec{\theta}_{\rm S}|^2), \tag{2.39}$$

where $\rm z_d$ is the redshift of the deflector and the factor $(1+{\rm z_d})$ comes from the

renormalization to the present scale which is necessary owing to the expansion of the Universe. From eq.(2.12), moreover, (2.39) is rewritten as follows

$$c\,\triangle t_{gAB} = \frac{1}{2}(1+\mathrm{z_d})\frac{D_\mathrm{d}D_\mathrm{ds}}{D_\mathrm{s}}\left(|\alpha(\theta_A,\overline{\theta}_A)|^2 - |\alpha(\theta_B,\overline{\theta}_B)|^2\right). \tag{2.40}$$

Next we derive the potential term. From eqs.(2.7), (2.8) and (2.35), it follows that

$$\frac{2}{c^2}\int_{t_\mathrm{S}}^{t_\mathrm{obs.}}\varphi d\ell_A - \frac{2}{c^2}\int_{t_\mathrm{S}}^{t_\mathrm{obs.}}\varphi d\ell_B \simeq \frac{2G}{c^2}\int d^3x'\rho(\vec{x}')\ln\frac{(x_A-x')^2+(y_A-y')^2}{(x_B-x')^2+(y_B-y')^2}, \tag{2.41}$$

and

$$\int_{t_\mathrm{S}}^{t_\mathrm{obs.}}\psi_i dx^i{}_A - \int_{t_\mathrm{S}}^{t_\mathrm{obs.}}\psi_i dx^i{}_B \simeq -\frac{4G}{c^3}\int d^3x'\rho(\vec{x}')(\vec{v}(\vec{x}')\cdot\vec{u})\ln\frac{(x_A-x')^2+(y_A-y')^2}{(x_B-x')^2+(y_B-y')^2}, \tag{2.42}$$

where $\vec{v} = d\vec{x}'/dt$, $t_\mathrm{S}\to-\infty$ and $t_\mathrm{obs.}\to\infty$. Since $x'(y') = D_\mathrm{d}\theta'_x(D_\mathrm{d}\theta'_y)$, the potential term is written in terms of θ, by use of eqs.(2.41) and (2.42), as follows

$$\begin{aligned} c\,\triangle t_{pAB} =& -\frac{4G}{c^2}(1+\mathrm{z_d})\int d^2\theta'\sigma(\vec{\theta}')\ln\frac{|\vec{\theta}_A-\vec{\theta}'|}{|\vec{\theta}_B-\vec{\theta}'|} \\ &+\frac{8G}{c^4}(1+\mathrm{z_d})\int d^2\theta' d\theta'_{||}\tilde{\rho}(\vec{\theta}',\theta'_{||})\{\vec{u}\cdot\vec{v}'(\vec{\theta}',\theta'_{||})\}\ln\frac{|\vec{\theta}_A-\vec{\theta}'|}{|\vec{\theta}_B-\vec{\theta}'|}, \end{aligned} \tag{2.43}$$

where

$$\begin{aligned} \rho(\vec{x}')d^3x' &= \tilde{\rho}(\vec{\theta}')d^2\theta d\theta_{||}, \\ \vec{v}(\vec{x}') &= \vec{v}'(\vec{\theta}',\theta'_{||}), \\ \theta_{||} &= x^3/D_\mathrm{d}. \end{aligned}$$

If we choose the path from $\vec{\theta}_B$ to $\vec{\theta}_A$ on which the deflection angle $\vec{\alpha}(\vec{\theta})$ is not singular, eq.(2.43) can be expressed as an integral of $\vec{\alpha}(\vec{\theta})$ with respect to $\vec{\theta}$, such

that

$$c \triangle t_{pAB} = (1 + z_d) D_d \int_{\vec{\theta}_B}^{\vec{\theta}_A} \vec{\alpha}(\vec{\theta}) d\vec{\theta}, \tag{2.44}$$

(Gorenstein, Falco & Shapiro 1988).

The total travel time difference between images A and B is given by

$$\begin{aligned} c \triangle t_{AB} = & \frac{1}{2}(1 + z_d) \frac{D_d D_s}{D_{ds}} (|\vec{\theta}_A - \vec{\theta}_S|^2 - |\vec{\theta}_B - \vec{\theta}_S|^2) \\ & + (1 + z_d) D_d \int_{\vec{\theta}_B}^{\vec{\theta}_A} \vec{\alpha}(\vec{\theta}) d\vec{\theta}, \end{aligned} \tag{2.45}$$

which can further be rewritten by use of eq.(2.12) as

$$c \triangle t_{AB} = (1 + z_d) D_d \int_{\vec{\theta}_B}^{\vec{\theta}_A} \{\vec{\alpha}(\vec{\theta}) - \frac{\vec{\alpha}_A + \vec{\alpha}_B}{2}\} d\vec{\theta}, \tag{2.46}$$

where $\vec{\alpha}_{A,B} = \vec{\alpha}(\vec{\theta}_{A,B})$. This form is useful for investigating properties of the travel time differences. It is clear that any constant part $\vec{\alpha}_{\text{const.}}$ of the deflection angle does not contribute to the travel time differences. This means that even if the source position is shifted by some angle, the travel time difference will remain unchanged, that is, the travel time difference depends only on the structure of the deflector and on the image positions. The symmetric linear part $\vec{\alpha}_{\text{linear}}$ of the deflection angle does not contribute to the travel time difference either. This fact means that the circularly symmetric and constant part of the surface mass distribution of the deflector does not contribute to the travel time difference. It follows from this fact that the dark matter which are distributed homogeneously does not contribute to travel time differences at all (Gorenstein, Falco & Shapiro 1985,1988, Borgeest 1986, and Kovner 1987b).

As mentioned above, we describe the relation between the lens equation and Fermat's principle. The latter states that the light propagates along the path whose length becomes stationary, *i.e.*,

$$\delta \int dt = 0. \tag{2.47}$$

This form can be extended to the case of gravitationally lensed lights (Schneider 1985). For a given source the propagation time τ of the light is given by eqs.(2.39) and (2.44) as

$$c\tau = \frac{1}{2}(1+\mathrm{z_d})\frac{D_\mathrm{d}D_\mathrm{s}}{D_\mathrm{ds}}|\vec{\theta}-\vec{\theta}_\mathrm{s}|^2 + (1+\mathrm{z_d})D_\mathrm{d}\int^{\vec{\theta}} \vec{\alpha}(\vec{\theta})\cdot d\vec{\theta}. \tag{2.48}$$

By using eq.(2.16), we can rewrite eq.(2.48) in the form:

$$c\tau = (1+\mathrm{z_d})\frac{D_\mathrm{d}D_\mathrm{s}}{D_\mathrm{ds}}\Big(\frac{1}{2}|\vec{\theta}-\vec{\theta}_\mathrm{s}|^2 + \Phi(\vec{\theta})\Big). \tag{2.49}$$

The lens equation can then be derived from Fermat's principle $\delta\tau = 0$. That is, τ forms the propagation time surface on the deflector plane and its extreme points yield the image positions.

The investigation of the propagation time surface leads to some important properties of the gravitational lens system; i) any nonsingular transparent deflector generates an odd number of images, ii) when all the travel time differences are observed, the image which arrives at the earth earliest has the positive partial parity and the positive total parity, iii) images with the positive partial parity are brighter than the original source, iv) images with the negative partial parity pass through a region with $\sigma > c^2 D_\mathrm{d}D_\mathrm{s}/4\pi G D_\mathrm{ds}$. Here the partial parity is the sign of $\mathrm{tr}[\,\mathrm{M}\,]$ and the total parity is the one of $\det[\,\mathrm{M}\,]$ (Schneider 1985, Blandford & Narayan 1986).

Before closing this section, we have to notice that the travel time difference is the only dimensionful observable of systems such as multiple-image systems, and that it enables us to determine the Hubble constant H_0, when a cosmological model and a mass distribution of the deflector are assumed. In eq.(2.49), while $[\frac{1}{2}|\vec{\theta} - \vec{\theta}_S|^2 + \Phi(\vec{\theta})]$ depends on types of deflector models adopted and on the observational data of images, the factor $(1+z_d)\frac{D_d D_s}{D_{ds}}H_0$ depends on cosmological models employed and on the redshifts of the deflector and the source, but not on H_0. We can thus obtain the relation of the Hubble constant to the cosmological model employed*.

$\star$ We will apply this relation to the multiple quasar 1115+080 in Chapter 4.

3. Review of Observations of Multiple Images, Giant Arcs and Einstein Rings

Since the first discovery of the twin quasar 0957+561, a number of candidates for multiple images, giant arcs and Einstein rings have been discovered during this decade. While early candidates for multiple-image systems were observed by chance, recent ones have been discovered by virtue of systematic optical/radio observations. Moreover many objects which have distorted shapes due to the gravitational lens effect have been in the last few years.

The necessary conditions for identifying the distinct images as lights from one and the same source are:

i) similarity of spectra of images,

ii) coincidence of redshifts of images,

iii) small separation between images.

On the other hand, the sufficient conditions for an event being due to the gravitational lens effect have not been established yet. However some criteria for this are stated as follows:

i) a bright galaxy with a low redshift exists close to the line of sight of images,

ii) emission lines with a high redshift exist in a spectrum of a near-by galaxy.

Some multiple quasars were discovered systematically based on the first criterion, whereas Huchra *et al.* (1985) discovered the multiple quasar 2237+0305, to be interpreted as a multiple-image system, with the second criterion. Other criteria were proposed by Turner *et al.* (see their paper 1988).

In this chapter we briefly review observational data of multiple images (§3.1), giant arcs and an Einstein ring (§3.2).

Table 3.1 Candidates for multiple-image systems

system	redshift of QSO	# of images	separation	lens object	redshift of lens object
0957+561	1.41	2	6.15″	G_1 + cluster	0.36
1115+080	1.722	≥ 4	$< 2.4''$	galaxy	0.4∼ 0.5
2345+007	2.15	≥ 3	7.1″	—	1.48 ∼ 1.49
2016+112	3.2733	3	3.4″	C + D (galaxies)	C : — D :1.01
1635+267	1.961	2	3.72″	—	∼ 0.57
2237+0305	1.695	4	1.81″	Sb-galaxy	0.0394
1042+178	0.921	4	2.″	—	—
3C324	1.206	≥ 2	2.″	A (radio-galaxy)	0.845
0023+171	0.9461	2 or 3	$< 5.9''$	—	—
UM673 (=0142−100)	2.719	2	2.22″	galaxy	0.493
1413+117	2.551	4	1.10″	—	2.071 or 1.660 or 1.438
UM425 (=1120+019)	1.465	2	6.3″	galaxy	∼ 0.6
1429−008	1.5	2	5.14″	—	—
0537+441	0.849	2	—	—	—
3C194	1.779	3	—	galaxy	0.312
0414+0534	1.2(?)	4	—	—	—

3.1 Multiple-Image Systems

Sixteen or more candidates for multiple-image systems are known at present, as listed in Table 3.1. Here let us briefly explain some of them, one by one, in order of their discoveries.

a) 0957+561

The discovery of the twin quasar 0957+561 to be a candidate for multiple-image system (Walsh *et al.* 1979) stimulated theoretical investigation of the

gravitational lens effect as well as observations of quasars. Theoretical studies made so far for this system are as follows: analyses of this system by using deflector models to reproduce the image configuration (Chang & Refsdal 1979, *etc.*), estimation of the travel time difference between images (Dyer & Roeder 1981, *etc.*), estimation of the Hubble constant from the observed travel time difference between images (Borgeest & Refsdal 1984, *etc.*), evaluation of the deflector mass (Borgeest 1986, *etc.*) and others. On the other hand, the geometry of 0957+561 was investigated in relation to optical observations (Stockton 1981, *etc.*) and also to radio observations (Porcas *et al.* 1981, *etc.*).

The deflectors in this system are both the cD-galaxy (hereafter G_1) which is located nearest to images A and B and the cluster of the galaxies surrounding this cD-galaxy (Young *et al.* 1980). An elliptical King model was applied to both G_1 and the cluster (Young *et al.* 1981a, *etc.*). The masses of G_1 and of the cluster are obtained to be $\sim 10^{12}M_\odot$ and $\sim 10^{15}M_\odot$, respectively.

The remaining problems about this system are: how luminous the third image is and where it is located. It may be unnatural if the system has only two images, because the lens with a non-singular mass distribution produces an odd number of images in general (see §2.2). Therefore the third image (or more images) must exist somewhere. Young *et al.* (1980) indicated two possibilities for the third image (to be referred to hereafter as B_2): i) if B_2 is close to B, the apparent luminosity of B_2 would be nearly equal to that of B, ii) if B_2 is located close to the core of G_1, B_2 would be much fainter than B. Moreover, Roberts *et al.* (1985) showed the third possibility: iii) B_2 may consist of three or more images and would be close to the nucleus of G_1.

Possibility i) was denied by both VLBI and VLA observations (Porcas *et al.*, Gorenstein *et al.* 1984). Possibility ii) appears at present not to be inconsistent with optical observations and also with radio observations. Possibility iii) would be acceptable if the total luminosity of the components of B_2 becomes fainter, by passing through G_1, than Stockton's limit on the luminosity of B by 1.6[mag.].

Table 3.2 a) Geometry and Magnitudes of 0957+561[1)]

component	$\Delta\alpha$	$\Delta\delta$	magnitude(R)
A	$-1.123''$	$6.047''$	17.33
B	$0.00''$	$0.00''$	17.62
G_1	$0.18''$	$0.98''$	$\sim$18.5

1) Young *et al.* (1981a).

Table 3.2 b) Core-Jet geometry of images A and B[2)]

	A		B	
	core	jet	core	jet
flux density [mJy]	22.8 ± 0.9	30 ± 2	17.5 ± 0.5	23.2 ± 2
major axis [m.a.s.]	1.37 ± 0.06	13 ± 2	1.55 ± 0.05	15 ± 1
minor axis [m.a.s.]	0.81 ± 0.09	12 ± 1	0.55 ± 0.07	9 ± 1
position angle [deg.]	$18. \pm 3$	77 ± 30	15 ± 1	8 ± 11
separation from core [m.a.s.]	—	49 ± 2	—	55 ± 2
position angle core-jet axis [deg.]	—	16 ± 2	—	15 ± 2

2) Gorenstein *et al.* (1988b).

Table 3.2 c) Polarization $\cdots \Psi = \Psi^0 + \mathrm{RM} \times \lambda^2$ fit[3)]

component	Ψ^0[deg.]	RM [rad/m^2]
A	94.0 ± 5.54	-61.8 ± 3.1
B	93.8 ± 5.5	-161.8 ± 3.1
difference	0.2 ± 4	~ 100

3) Greenfield *et al.* (1985a).

Narashima *et al.* (1986) supported this third possibility, and showed that if there is the nucleus with $\sim 10^{10}\mathrm{M}_\odot$ within ~ 50[pc] in G_1, the images close to the nucleus would be fainter than other images by 10[mag.].

The following properties are noteworthy of this system: i) each image has core-jet structure. This property is important in determining the components of the amplification matrix relating one image to another (Gorenstein *et al.* 1985, 1988). ii) The polarization plane of each image rotates (Greenfield *et al.* 1985). iii) This system has a faint radio source with 0.014 multiple intensity of that of B, being located close to B. iv) The travel time difference between images has been observed (Florentin-Nielson 1985, Vanderriest *et al.* 1989). Dyer and Roeder (1981) estimated this travel time difference between images to be $1 \sim 1.5$[years], this being consistent with the observed value.

The observed data for this system 0957+561 are listed in Table 3.2a, b and c.

b) 1115+080

The multiple quasar 1115+080, discovered by Weymann *et al.* (1980), is the first candidate for multiple-image system with three or more images. Owing to poor resolution ($\sim 2.5''$) of their observation, they were able to determine only the spectra of images A, B and C, but not the morphology of the images.

Hege *et al.* (1980) were the first to study the morphology of the images of this system. According to their observation, image A seems to be more elongated than other images and to have a position angle of the major axis is $\sim 20°$. This structure of A was confirmed by Young *et al.*'s observation (1981b) and also by Hege *et al.*'s (1981). A theoretical analysis by Young *et al.*, moreover, showed that, in order to reproduce the geometry of this system, A should be separated further into two images A_1 and A_2, its position angle being $\sim 20°$. Later the duplicity of A was confirmed by more accurate observations (Foy *et al.* 1985, Shaklan & Hege 1985, Henry & Heasley 1986 and Christian *et al.* 1987). The fifth image, A_{22}, was suggested to be located close to $A_{21}(= A_2)$ with the same magnitude as A_2 by Foy *et al.*.

While the difference, $\Delta m_{A_1-A_2}$, between the apparent magnitude of A_1 and that of A_2 was found to be nearly equal to zero by Hege *et al. etc.*, it was reported

Table 3.3 a) Geometry and Magnitude of 1115+080[1)]

component	$\Delta\alpha$[2)]	$\Delta\delta$[2)]	magnitude(V)
A_1	-1.27″	-2.08″	16.99
A_2	-1.44″	-1.62″	17.27
B	0.39″	-1.95″	18.74
C	0.00″	0.00″	18.26
lens galaxy	0.18″	-1.67″	20.96±0.05

1) Christian *et al.* (1987)

2) $\Delta\alpha$, $\Delta\delta$ = coordinates measured with respect to image C

$+\Delta\alpha$ = west, $+\Delta\delta$ = north.

Table 3.3 b) Travel Time Differences between Images of 1115+080[3)]

$\Delta t_{A_1-A_2}$	Δt_{A-B}	Δt_{A-C}
> 4[days]	< 2.5[months]	< 2.5[months]

3) Vanderriest *et al.* (1986)

to be nearly equal to unity by Foy *et al.*. The latter regarded this difference as one due to the variation of parameters of the lens object or to the time evolution in intrinsic luminosity of the source. Vanderriest *et al.* (1986) justified Foy *et al.*'s interpretation. Moreover it was found that the luminosity of the original source may have varied by 0.3[mag.] during years 1981 – 1985. From this fact, they obtained the constraints on the travel time differences between A_1 and A_2, between A and B and between A and C.

In this system separations between the images are quite small. And the lens object cannot be observed by means of radio observations because the lens object is not a radio-source. Therefore no information has been obtained on this deflector. There were some suggestion on the location of the deflector before 1987: i) the lens object should be located between A and B, close to B because

the color of B is redder than other images (Young *et al.*, Shaklan & Hege); ii) the lens galaxy should be located between A_1 and A_2 (suggested by Henry and Heasley 1986).

It is Christian *et al.* (1987) who settled this problem. They succeeded in directly detecting the lens object by observing the images through some color filters. According to their observation, the lens galaxy is very red and is located close to B between A and B. The lens galaxy, moreover, is completely separated from the images in their observation. Christian *et al.*thus suggested that it is very compact. In their observation the redshift of the lens object, however, was not found. They guessed its redshift to be in the range from 0.4 to 0.5 both from the separation-redshift relation and from the mass-brightness relation.

Some models have been applied to this system. Adopting a transparent spiral galaxy model, Young *et al.* (1981b) located the deflector inside the triangle of the images, and predicted that image A consists of two images. Narasimha *et al.* (1982), moreover, analyzed this system by adopting a King model. Their analysis, however, was incomplete in some sense since they had no information on the lens object such as the location and redshift of the lens object in that time. On the other hand, in view of the fact that the lens galaxy is very compact as pointed out by Christian *et al.*, we analyzed this system by adopting a dark lens model (Yoshida & Omote 1988). We then estimated the mass of the lens galaxy as $\sim 10^{11}\mathrm{M}_{\odot}$. Our analysis will be discussed in Chapter 4.

The observational data are listed in Table 3.3 a and b.

c) 2345+007

The twin quasar 2345+007 was discovered by Weedman *et al.* (1982) as the third candidate for multiple-image system. The separation between images of this system is the largest among those multiple-image system known up to date except for the QSO pair 1146+111. For the above system, two images A and B are observed, and the missing image(s) should exist somewhere. Sol *et al.* (1984)

Table 3.4 Geometry and Magnitude of 2345+007

	data	reference
magnification of A	18.82 ± 0.03	Sol *et al.* (1984)
magnification of B	20.25 ± 0.04	Sol *et al.* (1984)
separation between A and B	$7.03'' \pm 0.08''$	Nieto *et al.* (1988)
position angle of $A - B$	$57° \pm 1°$	Nieto *et al.* (1988)
separation between B_1 and B_2	$0.36''$	Nieto *et al.* (1988)
position angle of $B_1 - B_2$	$69° \pm 1°$	Nieto *et al.*(1988)

suggested that image B has a double-image-structure. Tyson *et al.* (1988), moreover, showed that the missing image brighter than 25.0±0.3[mag.] is not seen outside $1''$ from B, $2''$ from A, and inside a search radius of $30''$. Therefore, if the missing image exists in this region, its brightness must be 6[mag.] fainter than those of the other images. Nieto *et al.* (1988) justified Sol *et al.*'s suggestion by their own observation with a high resolution. They, moreover, found that image B has a structure and can be separated into two images B_1 and B_2. The separation between B_1 and B_2 is $\sim 0.36''$ and this satisfies the constraint on the structure of B imposed by Sol *et al.*.

The problem here is that the deflector has not been detected. Some suspect that these images are not gravitationally lensed (Canizares 1987, Bahcall*et al.* 1986). The failure in detecting the deflector gives a constraint on the apparent magnitude 'm' of the deflector: $m_V \geq 22.2$[mag.], $m_R \geq 21.5$[mag.] (Sol *et al.*). Tyson *et al.*, moreover, suggested that some galaxies seen only in I-band (7800-10000 Å) might be acting as lenses. There is spectroscopic evidence for Sol *et al.*'s suggestion, such that absorption lines with redshifts $1.483 \sim 1.491$ appear in spectra of both images, thereby indicating a large amount of the dark matter. Tyson *et al.* found that the deflector mass necessary to produce the separation $\sim 7''$ is $\sim 10^{13} M_\odot$. They thus suggested that the object with a high M/L value is dominant in this system. We list the data of 2345+007 in Table 3.4.

Table 3.5 Geometry and Magnitude of 2016+112 [1)]

component	$\Delta\alpha$	$\Delta\delta$	magnitude
A	$0.00''$	$0.00''$	20.95
B	$-3.02''$	$-1.49''$	21.48
C'	$-2.03''$	$-3.37''$	22.85

1) Schneider *et al.* (1986).

d) 2016+112

The multiple quasar 2016+112 was discovered by Lawrence *et al.* (1984) as the fourth candidate for multiple-image system. Radio sources A, B and C were discovered by VLA observations. Separation between A and B is $3.4''$, and C is located south-west of B. From the spectra of the radio sources, it was found that the spectra of A and B are similar to each other except in the red and infrared region, while the spectrum of C is flatter than those of A and B. They thus concluded that A and B can be regarded as gravitationally lensed images and that C is interpreted as a deflector. We can interpret that the difference between the spectra of A and B in the red and infrared regions is due to the contamination in B made by the foreground galaxy, C.

There are, however, some serious problems in the gravitational lens interpretation: i) the image configuration $\angle ACB \sim 60°$, for which it is unnatural that such a configuration is produced only by C (Lawrence *et al.*, Narasimha *et al.* 1984), ii) the lack of the third image and iii) the difference between the ratio I_A/I_B in the radio flux (~ 0.93) and that in intensities of the emission lines *e.g.* Lyα (~ 1.64).

Problems i) and ii) were settled by a series of observations by Schneider *et al.* (1986, 1987). They found that galaxy C is secondary rather than primary and that the primary lens object is galaxy D located at $1.2''$ from image B. By the discovery that the strong and narrow emission line (Lyα) seen in the spectra of

A and B exist also in the spectrum of the vicinity of galaxy C, the source with this emission line being identified with the third image, C'. They discovered extended sources A_1 and B_1 westward of A and B, respectively. Later A_1 and B_1 were confirmed to be two separate clouds of ionized gas which lie within a few killopersec of the primary A/B QSO, not to be the images of the same source (Narasimha *et al.* 1987, Schneider *et al.* 1988).

The constraints on construction of the model to reproduce this lens system are listed as follows:

a) The model must reproduce the image configuration: A, B and C'.
b) There are no other images.
c) The role of galaxies C and D must be taken into account.
d) The difference between the radio flux ratio and the intensity ratio of the emission lines must be explained.

Moreover the constraint on the deflector mass necessary to produce the image configuration in this system is given by

$$\mathrm{M} \geq 9.25 \times 10^{12} h^{-1} \mathrm{M}_{\odot} \quad \left(\mathrm{H}_0 = 100 h_{[\mathrm{km/sMpc}]}\right).$$

Narasimha *et al.* (1987) reproduced this system by adopting two King galaxies with nuclei and a King cluster of galaxies. According to their analysis C' consists of two images C_1 and C_2, and another faint image exists in galaxy D. They, moreover, predicted travel time differences such that $\Delta t_{B-A} \approx 0.7 \sim 0.9_{[\mathrm{years}]}$, $\Delta t_{C_1-A} \approx 0.6 \sim 0.9_{[\mathrm{years}]}$ and $\Delta t_{C_1-C_2} \approx 0.05_{[\mathrm{years}]}$.

We list the data of this system in Table 3.5.

Table 3.6 Geometry and Magnitude of 1635+267[1)]

component	$\Delta\alpha$[2)]	$\Delta\delta$[2)]	magnitude(mag.)
A	0.00″	0.00″	19.15
B	-0.63″	3.74″	20.75

1) Turner *et al.* (1988)

2) $\Delta\alpha, \Delta\delta$ = coordinates measured with respect to image C

$+\Delta\alpha$ = west, $+\Delta\delta$ = north.

e) 1635+267

The QSO pair 1635+267A, B was discovered by Weedman in 1978 (Sramek & Weedman 1978). However they regarded this QSO pair as two separate quasars with slightly different redshifts. Djorgovski and Spinrad (1984) re-examined this QSO pair, to claim that these quasars are gravitationally lensed images.

According to their observation, spectra of images A, B are similar to one another and their redshifts are both 1.961 ± 0.03. They, moreover, found that there is an absorption line at $\lambda = 5930$Å in image A, and suggested that, if the absorption line is due to the contamination from a deflector, the redshift of the deflector is 1.118.

Since the deflector of this system has not been detected yet, some doubt whether $1635 + 267A/B$ are indeed gravitationally lensed (Canizares 1987, and Blandford & Kochaneck 1987).

In contrast to the pessimistic viewpoint, there is some evidence for the gravitational lens interpretation. Djorgovski and Spinrad pointed out that i) this angular separation is very small as in the cases of known other multiple-image systems, ii) the spectra of A and B have the same emission line, and iii) the difference between the redshift of A and that of B is very small. Turner *et al.* (1988) further showed that iv) the emission lines at C_{III}, Mg_{II} exist in each spectrum of the image, and that v) there is a certain evidence for the lens galaxy,

etc.. Turner *et al.* suggested that the redshift of the lens galaxy is ~ 0.57 on the basis of the fact that the spectrum obtained by subtracting the spectrum of A from 2.82 (= the value of the intensity of the spectrum of A / that of B) multiple of the spectrum of B is similar to that of known galaxies with redshift $\sim$0.57. The observed data are listed in Table 3.6.

Narasimha and Chitre (1988) analyzed this system by assuming that the lens galaxy is located at $0.71''$ from A and that its mass is $\sim 10^{12}\mathrm{M}_{\odot}$ with the mass-to-light ratio being 16.

f) 2237+0305

This candidate for multiple-image system, 2237+0305, was discovered on the basis of the fact that emission lines with a high redshift exist in the spectrum at the center of a galaxy with a small redshift (Huchra *et al.* 1985). Clearly the object which is emitting lights with a high redshift ($\mathrm{z_s} = 1.695$) is not a galaxy. Huchra *et al.* then pointed out that these lights are gravitationally lensed by the galaxy close to us ($\mathrm{z_d} = 0.0394$). Because of poor resolution ($\sim 2''$) of their observation, however, they could not separate the images from the nucleus of the galaxy. Thus in those times only one QSO image was found. Later observations made it clear that four images A, B, C and D actually exist in this system (Tyson & Gorenstein 1985, Yee 1988, Schneider *et al.* 1988).

For this system the lens galaxy, rather than the lensed images, has been investigated in detail. According to Huchra *et al.*'s observation, this lens galaxy is very bright, possibly an early type belonging to Sa or Sb type in Hubble's classification. It follows from the galaxy brightness distribution that a nucleus + disc model is applicable to this lens galaxy. They also found that, when the disc is fitted by the exponential law (*i.e.* $\mathrm{I} = \mathrm{I}_0 \exp(-x/x_0)$) the scale length x_0 is $\sim 5''$ ($\sim$ 3.4[kpc]) and that the ellipticity ϵ of the disc is ~ 0.47. The observations with high resolution, furthermore, led to the result that this spiral galaxy has two bars, two arms and one bulge. While the disc (bar + arm) obeys the exponential

Table 3.7a) Galaxy parameters for 2237+0305

redshift (distance)[1)]	ellipticity[1)]	position angle of major axis[2)]	position angle of bar[2)]
0.0394 (118Mpc)	0.57	77°	38°

1) Huchra *et al.* (1985). 2) Yee (1988).

Table 3.7b) Geometry and Magnitude of 2237+0305[1)]

component	$\Delta\alpha$[2)]	$\Delta\delta$[2)]	magnitude(V)	(dereddening)
A	$0.08'' \pm 0.01''$	$-0.94'' \pm 0.01''$	17.25	16.89
B	$-0.60'' \pm 0.02''$	$0.74'' \pm 0.01''$	17.38	16.95
C	$0.76'' \pm 0.01''$	$0.26'' \pm 0.01''$	17.61	16.94
D	$-0.77'' \pm 0.02''$	$-0.41'' \pm 0.02''$	17.98	17.44
lens galaxy	$0.00'' \pm 0.02''$	$0.00'' \pm 0.02''$	14.5±0.05	—

1) Yee (1988)

2) $\Delta\alpha, \Delta\delta$ = coordinates measured with respect to image C

$+\Delta\alpha$ = east, $+\Delta\delta$ = north.

law, the bulge follows the de Vaucouleurs law. Properties of this galaxy are listed in Table 3.7a.

The four QSO images are located close to the nucleus of the galaxy, forming a cross (Yee). While the colors of images A and B are much bluer than that of the galaxy, the colors of images C and D are slightly redder than those of other images. Such a result is very critical for the gravitational lens interpretation, because all images must have the same color according to the gravitational lens hypothesis. Yee and Schneider *et al.* interpreted that the differences are due to the differential reddening effect occurring when the lights pass through the different regions in the nucleus of the galaxy. Taking into account this effect arising from the bulge of the galaxy, Yee estimated the brightness of images in the case when the reddening effect does not operate. On the other hand, Kent

and Falco (1988) concluded that only with Yee's dereddening it is not possible to estimate the true brightness of the images, because the differential reddening effect exists not only in the bulge but also in the direction of the bar and because the microlensing effect due to individual stars in this galaxy must be also taken into account. The observed data of this system are listed in Table 3.7b.

The models that reproduce this system were investigated by Schneider *et al.* and by Kent and Falco. Schneider *et al.* assumed the constant mass-to-light ratio for this galaxy and analyzed this system by adopting 6724 spherical deflectors whose distribution is the same as the brightness distribution of the galaxy. On the other hand, Kent and Falco assumed that the mass distribution is the same as that of a King galaxy or obeys the de Vaucouleurs law. They then fixed parameters of each model by using the least square method. According to Kent and Falco's analysis, their models produce almost the same image configuration and the galaxies fixed by the least square method are similar to those other spiral galaxies of similar morphological type which exist in our neighborhood. From naive estimations (Yee, Kent & Falco) it follows that the mass of the galaxy is $9.0 \times 10^9 M_\odot \sim 1.2 \times 10^{10} M_\odot$.

g) 1042+178

This candidate for multiple-image system, which is identified with system 1042+178, was discovered by Hewitt *et al.* (1987a). The system has four images. From the VLA observation, they found that the images form a parallelogram. If these radio sources are taken to be lensed images, the geometry shows that the deflector is a single object located close to the center of the parallelogram.

They observed only one image in optical observations, but found that the optical image has a structure and that its strong emission line indicates $z_S = 0.921$. Since the redshift of the radio source is small, cosmological uncertainties (*e.g.* effect of the intergalactic matter) in this system would be smaller than that in other multiple-image systems. This is therefore the best system for determining the Hubble constant *etc.* by using the travel time differences between

images. At present it is premature to decide that the above radio sources are gravitationally lensed because Hewitt *et al.* did not obtain spectra of all the images and did not detect four images separately in optical observations. We must wait for more detailed and accurate observations.

h) 3C324

This radio galaxy was discovered by Spinrad and Djorgovski (1984). They found that this object exhibits magnitude of 21 $\sim$ 22[mag.] with a redshift z = 1.206. Hammer, Le févre and Nottale (1987) are the first to emphasize that this radio galaxy system is a candidate for multiple-image system. They found that its spectrum has the absorption line which indicates z = 0.845, besides the emission line which indicates z = 1.206. According to their observation (seeing $\leq$0.7, magnitude-limit=25.5[mag.]), at least, five components A, B, C, D and E exist within 15 [arcsec^2] at the center of 3C324. Its geometry is as follows: the separation between A and B is $1.1''$; the faintest component C is located at $0.8''$ east of A; faint component D is located at $1''$ north-west of A; and components E and F are at $2.2''$ west of B and at $3''$ south-west of A, respectively. From their observation using some filters they found further that A is a foreground galaxy with redshift z = 0.845 and that B and C are background objects with redshift z = 1.206. Thus components B and C may be interpreted to be deflected by component A. With the above data only, however, it is premature at present to conclude that these component are gravitationally lensed images.

i) 0023+171

This candidate for multiple-image system was discovered by Hewitt *et al.*'s systematic VLA survey (Hewitt *et al.* 1987b). Making VLA observations they found three components A, B and C. The separation between A and B is $\sim 3.0''$, and the separation between A and C is $5.9''$. Images A and B, moreover, have some structures and jets are emitted from both images but in the opposite directions. The jet from A appears to be emitted with position angle 60°.
Hewitt *et al.* guessed that this jet might be the fourth component.

In optical observations, they found images C_{opt} (brighter) and AB_{opt} (fainter) as the counter-components of the radio sources. The separation between AB_{opt} and C_{opt} is $4.8'' \pm 0.1''$ and AB_{opt} could not be resolved. While in the radio observation A and B were found to have some structures, in the optical observation there was an extended object located at about $1.0''$ south of C_{opt}. It is not clear whether these components are gravitationally lensed images or not.

Hewitt *et al.* obtained the spectra of AB_{opt} and C_{opt}, and pointed out that these spectra were similar to each other excepting some uncertain parts. From each emission line it is deduced that the redshift of the source is $z = 0.9641 \pm 0.0005$. Although the necessary conditions for this system to be gravitationally lensed images are satisfied in this candidate, we cannot still support this interpretation because the deflector of this system, which could be a galaxy and/or a cluster of galaxies, has not been detected yet. If the components of 0027+171 are indeed gravitationally lensed images, high M/L value ($\geq 10^3$) is needed.

j) UM673(=0142−100)

This candidate for multiple-image system was discovered by Surdej *et al.* (1987). They found that UM673 is separated into two images A and B. Subtraction of a picture with the Gaussian fits of images A and B from the original picture shows that there is another object (maybe a lensing object) located between A and B (Surdej *et al.* 1988).

The spectroscopic observation leads us to the following properties: i) both images A and B have very similar spectra, which have broad emission lines at the same wavelength indicating that the redshifts for A and B are $z_A = 2.719 \pm 0.009$ and $z_B = 2.719 \pm 0.0119$, respectively, ii) each spectrum has some absorption lines leading to some redshifts: $z = 0.493, z = 1.898, z = 2.356$ and $z = 2.736$. The absorption line with redshift $z = 0.493$ may be of the lensing object since the residual spectrum obtained by subtracting a numerical multiple of the spectrum of B from that of A is comparable with what is expected of galaxies in the cluster with $z = 0.493 \pm 0.01$. While the absorption lines with redshifts $z = 1.898$ and

Table 3.8 Geometry and Magnitude of UM673[1)]

component	separation[2)]	P.A.[2)]	magnitude(V)[mag.]
A	$2.22'' \pm 0.03''$	$106.3° \pm 0.5°$	17.0±0.2
B	—	—	19.1±0.2
galaxy[3)]	$0.8'' \pm 0.2''$	$106.3° \pm 0.5°$	~ 19.0

1) Surdej *et al.* (1988)

2) The separations and position angles (P.A.) are measured with respect to B

3) The galaxy size is 3.2″(E-W) and 1.8″(N-S).

z = 2.356 may be those due to higher ionization, we do not yet know what produces the absorption line with z = 2.736.

Surdej *et al.* analyzed this system by adopting an axially symmetric deflector model. They found that the mass of the galaxy is $\sim 2.4 \times 10^{11} M_{\odot}$, and that the travel time difference between A and B would be $\sim$ 7[weeks]. Their observed data are listed in Table 3.8.

k) 1413+117

This is known as one of the brightest members among broad absorption line quasars (BAL-QSOs). The BAL-QSO has a very broad and deep absorption line close to an emission line in the shorter range (Weynmann, Carswell & Smith 1981). Magain *et al.* (1988) found that QSO1413+117 consists of four components A, B, C and D. The mean separation between images is $\sim 1.0''$. They were able to obtain the spectroscopic data of B and C only. Both spectra are very similar to each other, and have an emission line which indicates $z = 2.551$. These spectra, moreover, have the absorption lines that indicate $z = 1.6603 \pm 0.003$ and $z = 1.4382 \pm 0.002$. Magain *et al.* claimed that the above lines are due to some isolated and mutually independent gas clouds.

Table 3.9 Geometry and Magnitude of 1413+117[1)]

component	$\Delta\alpha$[2)]	$\Delta\delta$[2)]	magnitude(V)[3)]
A	0.00″	0.00″	0.00
B	0.75″	0.17″	0.15
C	-0.50″	0.71″	0.30
D	0.35″	1.04″	0.40

1) Magain *et al.* (1988)

2) $\Delta\alpha, \Delta\delta$ = coordinates measured with respect to image C
$+\Delta\alpha$ = west, $+\Delta\delta$ = north.

3) Δm = magnitude differences with respect to image A,
the magnitude of A is 18.3[mag.]

We believe that this system can be a multiple-image system because both B and C have the same broad absorption line with intensities being nearly zero. If some of the four components are distinct objects, these components can hardly have broad and deep absorption lines at the same wavelength.

Assuming the deflector to be an axially symmetric galaxy with an asymmetric disturbance, Magain *et al.* analyzed this system, with the following conclusions: the deflector mass is $1.0 \times 10^{11} M_{\odot} \sim 1.53 \times 10^{12} M_{\odot}$, although, as suggested by them, the deflector is very compact because of the small separations between the images.

l) UM425(=1120+019)

The candidate for multiple-image system, UM425, was discovered by Meylan and Djorgovski(1989). The geometry of this system and the magnitudes of components are listed in Table 3.10 under seeing condition $\approx 1.4''$.

This system has four components A, B, C and D. Meylan and Djorgovski, however, reported that C and D are somewhat diffuse (nonstellar) in appear-

Table 3.10 Geometry and Magnitudes of UM425[1)]

component	separation[2)]	P.A.[2)]	magnitude(V)[mag.]
A	—	—	16.2±0.1
B	$6.5'' \pm 0.1''$	-29°	20.6±0.1
C	$6.8'' \pm 0.1''$	105°	21.8±0.1
D	$4'' \sim 5''$	$\sim 150°$	—

1) Meylan and Djorgovski (1989)

2) The separations and the position angles (P.A.) are measured with respect to A

ance, in particular, D is too faint and too close to A to make any reliable measurements, and that C is redder in color $(B-V)_C$ and bluer in $(V-R)_C$ than A and B. They concluded that C could be considered as a member of the foreground cluster of galaxies (maybe a deflector). On the other hand, B is slightly redder than A in $(V-R)_B$. This fact may indicate the existence of the lensing galaxy.

The spectroscopy in their observation shows that spectra of A and B are similar to each other and that they have the same strong emission lines which give the same redshift z=1.465. The ratio of the spectrum of B to that of A is fairly constant in the blue region, and has a slight but significant increase in the red region, being equivalent to a slight difference in color, as noted above.

The quantity (spectrum of B) - (spectrum of A)/100 suggests the early-type galaxy spectrum at redshift $z \sim 0.6$. Meylan and Djorgovski roughly estimated the R magnitude of this component as $m_R \sim 23 \pm 0.5$[mag.], and concluded that the spectrum of this component is comparable to the spectra of luminous elliptical galaxies at redshift $z \sim 0.6$.

Finally we note that there is evidence for the system to be the gravitationally lensed system: although A is ~ 100 times as bright as B, their spectra are very

similar and have the same strong emission lines which give the same redshift.

3.2 Giant Arcs and Einstein Ring

Lynds and Petrosian (1987) and Soucail *et al.* (1987) reported that there were arc-like objects close to the center of clusters CL 2244−02 and A370. Although these arcs were discovered ten years ago, no definite comments about them had been made since then for lack of sufficient data (Lynds & Petrosian 1989). It is only ten years after the first discoveries of these arcs that sufficient data were collected. Moreover other objects which have similar structures to those of CL 2244−02 and of A370 were discovered in other clusters A963, A2218 and CL 0500−24 (Lavery & Henry 1988, Pello-Descayre *et al.* 1988 and Giraud 1988). These arcs have common features such that i) they are bluer than any other members of their clusters, ii) they have long and narrow structures and iii) these arcs point towards the direction of the center of each cluster. These arcs each should be considered to be associated with clusters in some way.

Many astronomers and physicists have given various interpretations for the origin of these arcs (Miller & Goodrich 1988 and Braun & Dekel 1988). These could be classified roughly into two types: the first is that the arc itself belongs to a cluster, and the second is that the source of the arc is a background object, which appears to be arc-like due to the gravitational lens effect (Paczyński 1987). There are more than four theories in the former type which are based on: i) the gravitational interaction for a galaxy, ii) the light echo (Katz 1987), iii) the optical jet due to the synchrotron radiation, iv) the shock wave from the center of the cluster.

The first type of interpretations, however, has some difficulties. Theory i) cannot explain why similar actions do not appear in other objects near the arc. In theory ii) the upper limit of the polarization induced by the light echo is inconsistent with the observational data, and it is unnatural that they are arc-like. In theory iii) the counter component of the arc-like image, which is naturally

expected, are not seen in the radio observation. The arc itself is not so bright as expected in this theory. In theory iv) gas surrounding the arc should be cooled sufficiently, but negative evidence on this point was given by Braun and Dekel and Lynds and Petrosian (1989) in the X-ray observations.

On the other hand, since the gravitational lens effect in the second type of interpretations is not directly associated with the cluster, this effect which may be responsible for the arc do not suffer from the difficulties mentioned above. Kovner (1987) showed that the probability for occurrence of an arc-like image due to the gravitational lens effect is ~ 0.01.

It is the arc redshift that decides whether the first type of interpretations is right or not, because, if the arc redshift z_{Arc} is as small as the cluster redshift z_{CL}, then the arc should be directly associated with the cluster.

a) A370

This arc was claimed by Soucail *et al.* (1987a) as a gravitational lens system. The redshift of cluster A370 surrounding the arc is $z_{CL} = 0.373$ (Kristian *et al.* 1978), and this cluster is one of the brightest, having a cD-galaxy in its center.

Properties of the arc in this cluster are that i) the arc is bluer than any other member of the cluster, ii) the central intensity peak of the arc, which characterizes bright galaxies, does not appear, iii) the brightness distribution of the arc is very flat (Soucail *et al.* 1987b), and that iv) the arc is reasonably circular (Lynds & Petrosian 1989).

Moreover an object at the eastern end of the arc (#62 in Soucail *et al.*'s identification) has also a blue and featureless structure. Soucail *et al.* (1987b) suggested that #62 is associated with the arc in some way. The spectroscopic observation of Soucail *et al.* (1988) shows that the spectrum of #62 has continuum and emission lines similar to those of the arc. The emission line indicates redshift $z_{Arc} = 0.724$ (Soucail *et al.* 1988, Miller & Goodrich 1988 and Lynds & Petrosian 1989).

Table 3.11.a) Arc[1] in A370

	curvature radius ([kpc])	length ([kpc])	substanding angle	arc redshift
Primary Arc[2]	$15.1''$ $(103h_{50}^{-1})$	$21''$ $(143h_{50}^{-1})$	$\sim 80°$	0.724[3]
Secondary Arcs[4]				
A_1	$\sim 48''$	$3''$		
A_2	$(A_1 - A_2)$	$4''$		
A_3	$\sim 37''$	$3''$		$0.6 \sim 1.2$
A_4	$(A_3 - A_4)$	$2.5''$		
A_5		$9.3''$		

Table 3.11 b) Variation of the Arc width with colors[2]

	U	B	V	R	I
Width	$1.92''$	$1.42''$	$0.89''$	$0.66''$	$0.42''$

1) This cluster ($z_{CL} = 0.373$) has a cD-galaxy near its center (Kristian *et al.* 1978).

2) Lynds and Petrosian (1989). No polarization is detected from this Arc.

3) Soucial *et al.* (1988).

4) There are other images A_6, B_1, B_2 and B_3. A_5 and A_6 lie on the same circle (Fort *et al.* 1988).

It is questionable, however, whether #62 is indeed a part of the arc, because it breaks away from the primary arc with a sharp angle in the polar coordinate system (Lynds & Petrosian).

In the observation by Lynds and Petrosian, the spectrum of the arc seems to have BALs. Since no BAL appears in the spectra of the other members of cluster A370, the arc is confirmed to be a gravitationally lensed image.

In explaining the arc by the gravitational lens effect, the main problem is to explain why those counterparts of the arc do not appear which are expected in a simple gravitational lens model. Fort *et al.* (1988) surveyed in order to discover the necessary counterparts, but in vain. On the other hand, it was pointed out that a single arc could be well produced if the extended source was located near one of the caustics on the source plane (Grossman & Narayan 1988, Narasimha

& Chitre 1988 and Blandford & Kovner 1988). Therefore the problem of no counterpart is not severe.

As a by-product in Fort *et al.*'s observation, they found other arc-like systems. These arc systems have the same properties as the primary arc, and their redshifts are nearly equal to 1. They are believed not to be a physically isolated object.

Here we must notice other features: i) the width of the primary arc varies in color (Lynds & Petrosian), ii) there is no polarization
(Miller & Goodrich, Lynds & Petrosian), and iii) by means of the VLA observation some radio sources were found near the primary arc, but not in the arc itself.

b) CL 2244−02

This arc was discovered by Lynds and Petrosian, but was not analyzed just as the arc in A370 discovered at that time was not. The cluster of galaxies (CL 2244−02) has the redshift $z_{CL} = 0.327$. Its brightness distribution is well in accord with de Vaucouleurs' law. The cluster has a giant arc near two large clumps (Hammer *et al.* 1989).

We show the morphology of the arc in Table 3.12. The special feature to be noticed is that the arc is completely circular. A remarkable difference between this arc and the one in A370 is that the former has a patchy brightness distribution. It is known that this arc has, at least, six brightness peaks, and its color is much bluer than other members of CL 2244−02 as in the case of A370. The spectroscopic observation shows no emission and absorption lines, and the spectrum is rather featureless. The arc redshift has not been determined yet unlike the arc in A370.

Despite the absence of knowledge on the redshift of the arc in CL 2244−02, important evidence for the arc to be gravitationally distorted images was given by Hammer *et al.*: they found additional images near the center of the curvature of the arc, which have photometric properties similar to that of the arc.

Table 3.12 a) Arc[1] in CL 2244−02

	curvature radius ([kpc])	length ([kpc])	substanding angle	width ([kpc])
Primary Arc[2]	$10.6''$ $(63.6h_{50}^{-1})$	$19''$ $(114h_{50}^{-1})$	$\sim 102°$	$0.74''$ $4.4h_{50}^{-1}$

Table 3.12 b) Magnitudes and colors of this system[3]

	B	V	R	$B-R$
Primary Arc	21.51	20.87	20.40	1.11
T	24.25	20.6	23.06	1.19
S	24.75	23.88	23.64	1.11

1) There are two clumps near the center of this cluster $z_{CL} = 0.329$ (Kristian *et al.* 1978). There are secondary arcs T and S. Their photometric properties are similar to the primary arc (Hammer *et al.* 1989).

2) Lynds and Petrosian (1989).

3) Hammer *et al.* (1989).

As in A370, the arc in CL 2244−02 reveals no polarization: the upper limit of the polarization is $4\% \pm 2\%$, as is given by Miller and Goodrich (1988). It was also shown by Lynds and Petrosian (1989) that there are two radio sources near the arc.

c) A2218

This arc was discovered by Pello-Descayre *et al.* (1988). The redshift of cluster A2218 is $z_{CL} = 0.171$. A2218 has a large cD-galaxy near its center, and is well-known as one of the largest clusters in the Abell catalogue.

Pello-Descayre *et al.* found that this cluster has three arcs: $A-A'$, H and $L-L'$, but the redshifts of these arcs have not been determined because of their complexity and their faintness.

The color of $A-A'$ is bluer than any other members of A2218, whereas the colors of H and $L-L'$ are redder. Therefore H and $L-L'$ may probably belong

Table 3.13 Arc[1] in A2218

	curvature radius ([kpc])	length ([kpc])	substanding angle	magnitude
Primary Arc[2]	$41''$ $(160h_{50}^{-1})$	$25''$ $(100h_{50}^{-1})$	$\sim 90°$	22.5

1) A cD-galaxy lies on the center of this cluster $z_{CL} = 0.171$ (Kristian *et al.* 1978).

It has an extended envelope $\sim 46''(\sim 180h_{50}^{-1}\text{kpc})$ and it is axially symmetric[2].

2) Pello-Descayre *et al.* (1988).

Table 3.14 a) Arc[1] in A963

	curvature radius ([kpc])	length ([kpc])	substanding angle
Southern Arc	$18.6''$ $(80h_{50}^{-1})$	$22.7''$ $(98h_{50}^{-1})$	$\sim 70°$
Northern Arc	$26.7''$ $(114h_{50}^{-1})$	$9.7''$ $(41h_{50}^{-1})$	$\sim 30°$

Table 3.14 b) Magnitudes and colors of these Arcs[1]

	B	R	$B-R$
Southern Arc	22.3	21.6	0.7
Northern Arc	23.6	23.1	0.5

1) This cluster ($z_{CL} = 0.206$) has a cD-galaxy with ellipticity ~ 0.5 and major axis $\sim 51''$ (Lavery and Henry 1988).

to this cluster. On the other hand, $A - A'$ could be an image produced by the gravitational lens effect, since this arc has the same photometric properties as those in A370, CL 2244−02. We feel, however, that it is too early to regard this system as a gravitationally lensed system.

d) A963

This arc system was found by Lavery and Henry (1988). Cluster A963 has the redshift $z_{CL} = 0.206$ and has, near its center, a large cD-galaxy with ellipticity $\epsilon \approx 0.5$ and major axis $\approx 50''$.

It is a remarkable difference from other arc systems that this system has two arcs on each side of the cD-galaxy. Both arcs are extended in the direction orthogonal to the major axis of the cD-galaxy. These arcs, evidently, are consistent with those images that are produced by the gravitational lens effect. Lavery and Henry analyzed this system by adopting the constant surface density model (cluster) with a point mass (cD-galaxy). The photometric properties of this arc system are similar to those of other arc systems. In particular, the brightness distribution is as patchy as that in CL 2244−02. The lensed object (source) may therefore be considered to be a LMC type galaxy. We, however, hesitate to say that these arcs are gravitationally lensed images because of insufficient data on this arc system.

e) CL 0500−24

This arc was discovered by Giraud (1988). The cluster of galaxies CL 0500−24 in which this arc is observed is known to have redshift $z_{CL} \approx 0.32$ and to consist of many galaxies, that is to say, this cluster is known to be a rich cluster of galaxies (Wambsganss *et al.* 1989).

The remarkable difference of this arc system from other arc systems, in particular from A370, is that the shape of this arc is rather straight than circular. It is not clear even whether the concave of the arc points towards the direction of the center of the cluster. Since the arc appears to be superposed on galaxies of the members of the cluster, the problem remains to be as to settle whether the elongated feature is a disrupted tail of the interacting pair or due to the gravitational lens effect.

Wambsganss *et al.* constructed a gravitational lens model for this arc by using their data and showed that this model is a very natural one in explaining this arc-like structure.

For this arc also, we believe that detailed spectroscopic observations (sufficient to determine its redshift) are needed for clarifying the nature of the arc.

Table Arc[1] in CL 0500−24

	curvature radius ([kpc])	length ([kpc])	substanding angle	color $(B-R)$
Arc	$26''$ $(69 \sim 80h_{50}^{-1})$	$14''$ $(37 \sim 43h_{50}^{-1})$	$\sim 30°$	$0.9 \sim 1.0$

1) Giraud (1988).

f) MG1131+0456 "Einstein Ring"

Besides giant arcs, a ring-like object was also discovered in VLA observation (Hewitt *et al.* 1988). This ring is elliptical and has two compact sources on the opposite sides of the ring. From the VLA mapping, Hewitt *et al.* found a clear difference between the ring itself and its interior part. Unlike the ring itself, its interior part shows no emission.

The compact sources exist in the north and south of the ring. The northern component is separated into two sources A_1 and A_2. The southern component, B, is accompanied by component C, which is located south-west of B.

It was shown by observing polarization along the ring that the polarization is in north-south direction at the positions of the compact sources, and that the all other parts of the ring appear to be polarized at angles that vary quite smoothly around the ring. It is very likely that this kind of polarization is due to the Faraday effect. It is not possible, however, to make any definite comment on the polarization, since data on polarization have been obtained only for one frequency.

A very faint object, on the other hand, was optically observed near the radio source, but the ring redshift has not been determined yet because of poor condition of their spectroscopic observation.

Two interpretations are possible for this ring: i) the remnant of an explosion in a supernova, ii) the Einstein ring due to the gravitational lens effect. We feel that the latter interpretation (i) is more desirable than the former (ii) because the optical and infrared properties of this ring appear to be inconsistent with

Table 3.16 Einstein Ring MG1131+0456[1)]

	major axis	minor axis	ellipticity	P.A.
Radio observation	$2.2''$	$1.6''$	0.27	70°
Optical observation	$2.5''$	$2.6''$	0.16	45°

1) This system is located at $\alpha = 11^{h}31^{m}56^{s}.44$, $\delta = 04°55'49''.4$.

Compact components were discovered by the radio observation, .

Northern components: doublet A_1&A_2, Southern components: B&C.

those of the supernova remnant (Hewitt *et al.*). However the reasons why we cannot definitely say that this ring is due to the gravitational lens effect are that there have been no spectroscopic observations of this ring sufficient to determine its redshift, and the deflector has not been detected. More accurate observations on this ring are thus required.

4. Analysis of Multiple Quasar "1115+080"

Since the discovery of the multiple quasar 1115+080 (Weymann *et al.* 1980), many deflector models have been adopted for explaining the image configuration of this system by regarding this as the multiple-image system. Young *et al.* (1980) adopted a transparent spiral galaxy model in order to reproduce their observational fact that image A has a slightly elongated structure. In their analysis they suggested that image A should be separated into double images A_1 and A_2. Narasimha *et al.* (1982) adopted a transparent King model. Assuming the apparent magnitude of the deflector to be less than 21 [mag.] and its redshift to be greater than 0.8, they estimated its mass to be $\sim 6 \times 10^{11} M_{\odot}$. The above analyses, however, contained a number of unknown parameters and many ambiguities because the deflector had not been detected at that time. Young *et al.* and Narasimha *et al.* assumed the deflector to be located inside the triangle of images A, B and C.

Table 4.1 Observed data of 1115+080 (Christian *et al.* 1987)

component	$\Delta\alpha$ a)	$\Delta\delta$ a)	magnitude(V)
A_1	-1.27″	-2.08″	16.99
A_2	-1.44″	-1.62″	17.27
B	0.39″	-1.95″	18.74
C	0.00″	0.00″	18.26
lens galaxy	0.18″	-1.67″	20.96±0.05

a) $\Delta\alpha, \Delta\delta$ = coordinates measured with respect to image C

$+\Delta\alpha$ = west, $+\Delta\delta$ = north.

Apart from these theoretical approaches, search for the deflector was made by many authors (Shaklan & Hege 1985, Henry & Heasley 1986, *etc.*), but the lens galaxy was not directly detected until 1987 when Christian *et al.* (1987) succeeded in directly detecting the deflector. Their observational data are listed in Table 4.1. Before Christian *et al.*'s observation, image B had been believed

to be contaminated by a putative lens galaxy. According to Christian *et al.*'s observation, however, image B and the deflector are completely separated from each other. It reveals that we need not adopt a transparent lens model to this system.

In what follows we adopt a dark lens model to the deflector of this system (in §4.1). We will estimate travel time differences between the images and give the relation between these differences and relative luminosities in §4.2. In the next section §4.3 the effect of inhomogeneities in the Universe on estimation of cosmological distances is discussed. In §4.4 the mass of the deflector is estimated by Borgeest's method (Borgeest 1986). We will further propose another method to estimate the mass of the deflector only from the parameter fixing of the lens model. It is shown how the constraint on the Hubble constant H_0 is imposed by combining our mass estimations with the two methods. Finally, §4.5 will be devoted to discussion of our results.

4.1 Gravitational Lens Model

We apply a dark lens model with dipole and quadrupole moments to the multiple-image system in question. The deflection angle α is given by the following form in the complex representation (Bourassa, Kantowski and Norton 1973)

$$\alpha = -\frac{2}{c}\int_{-\infty}^{+\infty}\Big(\partial_{x_{\rm I}}\phi_N(x_{\rm I}, y_{\rm I}, ct) + i\partial_{y_{\rm I}}\phi_N(x_{\rm I}, y_{\rm I}, ct)\Big)dt, \tag{4.1}$$

where ϕ_N is the Newtonian potential expanded up to the quadrupole moment term, and ($x_{\rm I}$, $y_{\rm I}$) is an image position on the deflector plane. Eq.(4.1) can be transformed to the following form;

$$\alpha^* = -\frac{4G}{c^2}\Big(\frac{M_G}{z_{\rm I}} + \frac{d_G e^{i(\chi_d+\chi_G)}}{z_{\rm I}^2} + \frac{q_G e^{2i\chi_G}}{z_{\rm I}^3}\Big), \tag{4.2}$$

where M_G is the deflector mass , d_G and χ_d are the dipole moment of the deflector and its projected direction onto the deflector plane, respectively; q_G and χ_G are

the quadrupole moment of the deflector and the direction of the principal axis projected onto the same plane; $z_{\rm I}$ is the image position on the deflector plane in the complex coordinate, *i.e.* $z_{\rm I} = x_{\rm I} + iy_{\rm I}$. The complex angular coordinate $\theta(= \frac{z}{D_{\rm d}})$ is often more convenient than the complex coordinate z (see §2.1). We then express eq.(4.2) in the following form

$$\alpha^* = -\frac{D_{\rm s}}{D_{\rm ds}}\frac{\mu}{\theta_{\rm I}}\Big(1 + \frac{\delta e^{i(\chi_G+\chi_d)}}{\theta_{\rm I}} + \frac{\xi e^{2i\chi_G}}{\theta_{\rm I}^2}\Big), \tag{4.3}$$

where

$$\mu = \frac{4GM_G}{c^2}\frac{D_{\rm ds}}{D_{\rm d}D_{\rm s}}, \tag{4.4a}$$

$$\delta = \frac{d_G}{M_G D_{\rm d}}, \tag{4.4b}$$

$$\xi = \frac{q_G}{M_G D_{\rm d}^2}. \tag{4.4c}$$

The lens equation is given by

$$\theta_s = \theta - \frac{\mu}{\theta^*}\Big(1 + \frac{\delta e^{-i(\chi_G+\chi_d)}}{\theta^*} + \frac{\xi e^{-2i\chi_G}}{\theta^{2*}}\Big). \tag{4.5}$$

Since the number of parameters in this model is seven and the number of images is four, we can fix these parameters so that the image positions $\theta_{A_1}, \theta_{A_2}, \theta_B$ and θ_C are the solutions of eq.(4.5). The conditions for fixing these parameters are: i) μ is real and positive, ii) the above parameters are constant with respect to $\theta_{\rm I}(\theta_{\rm I} = \theta_{A_1}, \theta_{A_2}, \theta_B$ and θ_C). We can fix these parameters by means of the numerical method. Fixed parameters are listed in Table 4.2. Substituting them into the lens equation (4.5) and solving it again, we obtain the results listed in Table 4.3. In order to reproduce the observed image positions with our model, we shifted the location of the lens galaxy to $0.01''$ south and $0.05''$ west of the observed deflector position. Because of $0.6''$ seeing in Christian *et al.*'s observation, we believe that we can regard the above shift as insignificant one. So far

Table 4.2 Fixed values of the parameter

μ	δ	ξ	χ_G	χ_d
3.402×10^{-11}	-9.402×10^{-7}	-5.715×10^{-12}	$-22.99°$	$-63.77°$

Table 4.3 Numerical results[a)]

component	$\Delta\alpha$ [b)]	$\Delta\delta$ [b)]	relative intensity [c)]
≪ observed components ≫			
A_1	-1.27″	-2.08″	4.23
A_2	-1.46″	-1.61″	3.53
B	0.39″	-1.95″	0.87
C	0.00″	0.00″	1.0
≪ additional components ≫			
D	0.18″	-1.67″	0.08
E	-0.80″	-1.21″	0.008

a) Numerical or observational error is ±0.05″

b) $\Delta\alpha, \Delta\delta$ = coordinates measured with respect to image C

$+\Delta\alpha$ = west, $+\Delta\delta$ = north.

c) Relative luminosities of the images to image C

as observed positions of images A_1, A_2, B and C are concerned, the numerical results are consistent with observed ones.

Next we estimate ratios of apparent luminosities between images. The ratio of apparent luminosity I of an image to that of original source I_s is, as mentioned in §2.2, given by

$$\frac{I}{I_s} = \left|\frac{1}{\mathcal{G}^2 - |\mathcal{F}|^2}\right|. \tag{4.6}$$

Since we are adopting the dark lens model, we have

$$\mathcal{G} = 1,$$

$$\mathcal{F} = -\frac{\mu}{\theta_{\mathrm{I}}^2}\left(1 + \frac{2\delta e^{i(\chi_G+\chi_d)}}{\theta_{\mathrm{I}}} + \frac{3\xi e^{2i\chi_G}}{\theta_{\mathrm{I}}^2}\right), \tag{4.7}$$

Having fixed the parameters, we can calculate the ratios I/I_s. However, since I_s is not observable, we write down the relative luminosities of all the images to that of image C in Table 4.3. It is to be noted that these relative luminosities differ from Christian *et al.*'s data. We will discuss these differences in the next section.

From the parameters in Table 4.2 the position of the original source is fixed to be

$$\vec{\theta}_S - \vec{\theta}_{LG} = (-0.011'', -0.018''). \tag{4.8}$$

We then find that the original source is located very close to the lens galaxy.

Besides these observed images, our numerical analysis suggests that there are two more images D and E (see Table 4.3). Image D is located at $0.35''$ north-west of image B, and is fainter than B by 2.6[mag.]. We do not think that it is easy to distinguish image D from image B. Moreover, image E is fainter than the lens galaxy by 2.5[mag.]. It is very difficult, therefore, to detect image E. We might think of a possibility that this image is A_{22} (see in §3.1-(b)). The feature of E, however, is not consistent with constraints imposed on A_{22} such that: i) $\Delta\theta_{A_{21}-A_{22}} \approx 0.03''$, ii) $\mathrm{m}_{\mathrm{A}_{21}} \approx \mathrm{m}_{\mathrm{A}_{22}}$. The above possibility is therefore considered to be very small. Furthermore, since $|\xi|/|\theta_E|^2 \geq 1$ in eq.(4.5) for image E, this solution is beyond the capacity of our approximation.

We plot the positions of the reproduced images, new additional images, original source and the lens galaxy in Fig.4.1. The ×-marks in this figure are positions of images reproduced by assuming the source to be point-like. Ratios of the image areas show those of the apparent luminosities of the images to that of the original source. Fig. 4.1 is obtained by assuming that the source is extended.

4.2 Travel Time Differences and Relative luminosities

As seen in §2.3, the travel time difference between any two images is expressed as the sum of the geometrical term Δt_g and the potential term Δt_p. According to Cooke and Kantowski (1975), the travel time difference between images 1 and 2 is given as:

$$\Delta t_{1-2} = \frac{1+\mathrm{z_d}}{c}\frac{D_\mathrm{d}D_\mathrm{s}}{D_\mathrm{ds}}\Big[\frac{1}{2}(|\theta_s-\theta_1|^2-|\theta_s-\theta_2|^2)+\frac{D_\mathrm{ds}}{D_\mathrm{s}}Re\Big(\int_{\theta_2}^{\theta_1}\alpha^*\cdot d\theta\Big)\Big]. \quad (4.9)$$

Let us now define the quantities T and f_{1-2} as follows:

$$\mathrm{T} = \frac{1+\mathrm{z_d}}{c}\frac{D_\mathrm{d}D_\mathrm{s}}{D_\mathrm{ds}}\mathrm{H_0}, \quad (4.10)$$

$$f_{1-2} = \frac{1}{2}(|\theta_s-\theta_1|^2-|\theta_s-\theta_2|^2)+\frac{D_\mathrm{ds}}{D_\mathrm{s}}Re\Big(\int_{\theta_2}^{\theta_1}\alpha^*\cdot d\theta\Big). \quad (4.11)$$

Then T is independent of the type of lens models employed and of the Hubble constant $\mathrm{H_0}$. It depends, however, on the redshifts of the source and the deflector, the deceleration parameter q_0 and the density parameter Ω_0. On the other hand, f_{1-2} is dependent on the type of deflector models employed and on the positions of observed images, and is independent of both redshifts and the above cosmological parameters. Originally, T and f_{1-2} were introduced by Refsdal (1966), and the former is called the "cosmological factor" (Yoshida & Omote 1988). The form of f_{1-2} contains a factor $D_\mathrm{ds}/D_\mathrm{s}$. Substituting the explicit form of α (eq.[4.3]) into eq.(4.11), however, we can write f_{1-2} as follows:

$$f_{1-2} = \frac{1}{2}(|\theta_s-\theta_1|^2-|\theta_s-\theta_2|^2)-\mu Re\Big[\ln\frac{\theta_1}{\theta_2}-\delta e^{i(\chi_G+\chi_d)}\Big(\frac{1}{\theta_1}-\frac{1}{\theta_2}\Big)-\frac{\xi}{2}e^{2i\chi_G}\Big(\frac{1}{\theta_1^2}-\frac{1}{\theta_2^2}\Big)\Big].$$

Therefore f_{1-2} does not depend on the cosmological parameters at all. The parameters μ, δ, ξ, χ_G and χ_d fixed numerically are given in Table 4.2. Substituting

these values into f_{1-2}, we then find

$$\begin{aligned} f_{C-A_1} &= 7.97 \times 10^{-11}, \\ f_{C-A_2} &= 5.97 \times 10^{-11}, \\ f_{C-B} &= 9.83 \times 10^{-11}. \end{aligned} \tag{4.12}$$

Using eqs.(4.10) and (4.11), we can write down the travel time difference Δt_{1-2} in the following form:

$$\mathrm{H}_0 \, \Delta \, t_{1-2} = \mathrm{T} f_{1-2}. \tag{4.13}$$

Thus, if the travel time differences are observed, we can relate the Hubble constant H_0 to T, namely, to q_0 (assuming the cosmological constant Λ_0 to vanish). If other observations of H_0 determine its value, then the relation (4.13) fixes the value of q_0 (Kayser & Refsdal 1983).

In the homogeneous Friedmann-Robertson-Walker universe (to be referred to hereafter as FRW), the angular distances D_d, D_s and D_ds are given by the following (Weinberg 1972):

$$D_\mathrm{d} = \frac{c}{\mathrm{H}_0} \frac{1}{(1+\mathrm{z_d})^2} \frac{1}{q_0^2} \left[q_0 \mathrm{z_d} + (q_0 - 1)(\sqrt{1 + 2q_0 \mathrm{z_d}} - 1) \right], \tag{4.14a}$$

$$D_\mathrm{s} = \frac{c}{\mathrm{H}_0} \frac{1}{(1+\mathrm{z_s})^2} \frac{1}{q_0^2} \left[q_0 \mathrm{z_s} + (q_0 - 1)(\sqrt{1 + 2q_0 \mathrm{z_s}} - 1) \right], \tag{4.14b}$$

$$\begin{aligned} D_\mathrm{ds} = \frac{c}{\mathrm{H}_0} \frac{1}{(1+\mathrm{z_s})^2(1+\mathrm{z_d})} \frac{1}{q_0^2} \Big[& q_0 (\mathrm{z_s} \sqrt{1 + 2q_0 \mathrm{z_d}} - \mathrm{z_d} \sqrt{1 + 2q_0 \mathrm{z_s}}) \\ & + (q_0 - 1)(\sqrt{1 + 2q_0 \mathrm{z_s}} - \sqrt{1 + 2q_0 \mathrm{z_d}}) \Big]. \end{aligned} \tag{4.14c}$$

The cosmological factor is given by eqs.(4.14 a-c) as:

$$\mathrm{T} = \frac{\left[q_0 \mathrm{z_d} + (q_0 - 1)(\sqrt{1 + 2q_0 \mathrm{z_d}} - 1) \right] \left[q_0 \mathrm{z_s} + (q_0 - 1)(\sqrt{1 + 2q_0 \mathrm{z_s}} - 1) \right]}{q_0^2 \left[q_0 (\mathrm{z_s} \sqrt{1 + 2q_0 \mathrm{z_d}} - \mathrm{z_d} \sqrt{1 + 2q_0 \mathrm{z_s}}) + (q_0 - 1)(\sqrt{1 + 2q_0 \mathrm{z_s}} - \sqrt{1 + 2q_0 \mathrm{z_d}}) \right]}. \tag{4.15}$$

The relation between T and q_0 for various values of redshifts $\mathrm{z_d}$ is shown in Fig.4.2. As can be seen there, the q_0-dependence of T seems to be much weaker

than the z_d-dependence. Given H_0 and observed travel time differences Δt_{ob}, we find it difficult to fix q_0 by use of $T = \frac{H_0 \Delta t_{ob}}{f}$.

Although the redshift of the lens galaxy is not known up to the present, Christian *et al.* estimated it as $0.4 \lesssim z_d \lesssim 0.45$ both from the separation-redshift relation and from the luminosity-mass relation. Then, assuming that $H_0 = 100$[km/sMpc], $q_0 = 0.5$ and $0.4 \lesssim z_d \lesssim 0.45$, we obtain the following results for the travel time differences:

$$\begin{aligned} 4.8 &\lesssim \Delta t_{C-A_1} \lesssim 5.6\text{[months]}, \\ 3.6 &\lesssim \Delta t_{C-A_2} \lesssim 4.2\text{[months]}, \\ 6.0 &\lesssim \Delta t_{C-B} \lesssim 6.9\text{[months]}. \end{aligned} \tag{4.16}$$

It is thus found that the images are to be observed in the order of B, A_1, A_2 and C.

As has been seen in the previous section, it is clear that the calculated relative luminosities differ from observed ones, and they are listed in Table 4.4, where the calculated values are normalized to the luminosity of C.

If the intensity of the photon flux from the original source varies, the observed relative luminosity of any image must also vary, but differently. In estimating the relative luminosities, we must, therefore, take into account the evolutionary effect as well as the gravitational amplification effect. Let us regard $t_{ob} = 19/\text{Feb}/1986$ as the standard time, and suppose that image C is observed with an apparent luminosity I_C at t_{ob}. The pure gravitational amplification factors of the luminosities of other images, *e.g.*, A_1, are:

$$\frac{I(A_1; t_{ob} - \Delta t_{C-A_1})}{I(C; t_{ob})}, \ldots. \tag{4.17}$$

Comparison of the above values with the calculated relative luminosities provides a criterion for whether the lens model employed is valid or not.

Table 4.4 Observed and calculated relative luminosities

	A_1	A_2	B
observation[a)]	3.22	2.49	0.64
calculation	4.23	3.53	0.87

a) Christian *et al.* (1987).

Assuming that the differences between the observed and calculated relative luminosities listed in Table 4.4 are due only to the time evolution of the intrinsic luminosity of the source,[⋆] we can identify the calculated values with those given in eq (4.17). The variation Δm of the magnitude of the original source during Δt is given by:

$$\begin{aligned}\Delta \mathrm{m}_X &= \mathrm{m}(t_{ob}) - \mathrm{m}(t_{ob} - \Delta t_{C-X}) \\ &= 2.5 \log_{10} \frac{I(X; t_{ob} - \Delta t_{C-X})}{I(X; t_{ob})} \\ &= 2.5 \log_{10} [\frac{I(X; t_{ob} - \Delta t_{C-X})}{I(C; t_{ob})} \frac{I(C; t_{ob})}{I(X; t_{ob})}] \\ &= 2.5 \log_{10} \frac{I_{cal.}(X)}{I_{obs.}(X)}.\end{aligned} \tag{4.18}$$

Thus, Δm varies during Δt as follows:

$$\begin{aligned}\Delta \mathrm{m}_{\mathrm{A}_1} &= 0.296 \pm 0.05[\mathrm{mag.}], \\ \Delta \mathrm{m}_{\mathrm{A}_2} &= 0.378 \pm 0.05[\mathrm{mag.}], \\ \Delta \mathrm{m}_{\mathrm{B}} &= 0.343 \pm 0.05[\mathrm{mag.}].\end{aligned} \tag{4.19}$$

These errors are estimated on the basis of Christian *et al.*'s observation. The above Δm's seem to be consistent with each other within the error. Since there are few published data of the travel time differences, we cannot proceed any further. It is hoped that more detailed observation will be made of this system over long duration.

⋆ This is a very crude assumption because the distribution of matter, such as intergalactic matters, along each light path is not necessarily the same.

4.3 Geometrical Optics in 1115+080

In the above discussion we have assumed that the Universe is described by the FRW universe. It is not clear, however, whether we can assume that the Universe is homogeneous in a scale such that the gravitational lens effect affects light-propagation. In fact, the matter density in a lens object such as a galaxy or a cluster of galaxies is more condensed than the mean density of the whole Universe. We should, therefore, take into account inhomogeneities in the Universe. In this section we discuss the effects on estimation of cosmological distances ($D_{\rm d}, D_{\rm s}$ and $D_{\rm ds}$) due to inhomogeneities in the Universe .

The geometrical term Δt_g of the travel time difference given by Cooke and Kantowski (1975) is the difference between the path-lengths of images. Fig.2 in Cooke and Kantowski's paper shows that the wavefront emanated from the source (forward wavefront) and the wavefront converging into the observer (backward wavefront) are tangential at the point $\vec{z}_s$, onto the deflector plane. Then Δt_g is expressed in terms of the distances from these wavefronts to the image positions $\vec{z}_A$ and $\vec{z}_B$ on the deflector plane. That is to say, if both wavefronts are locally spherical (shear free $|\sigma| = 0$), the path length ΔL along the light path from the forward to the backward wavefronts is given by

$$\begin{aligned}\Delta L_A &= \Delta L_{fA} + \Delta L_{bA} \\ &= \frac{1}{2}K_f|z_s - z_A|^2 + \frac{1}{2}K_b|z_s - z_A|^2,\end{aligned}$$

where K_f and K_b are the principal curvatures of the forward wavefront and of the backward wavefront, respectively. Thus the contribution of the geometrical term to the travel time difference becomes

$$\Delta t_g = \frac{1+z_{\rm d}}{2c}(K_f + K_b)\left(|z_s - z_A|^2 - |z_s - z_B|^2\right). \tag{4.20}$$

Our problem now is how $(K_f + K_b)$ can be expressed in terms of cosmological quantities.

According to the geometrical optics (Sachs 1961, Pirani 1964), the optical scalars (the expansion θ and the shear $|\sigma|$) are given by

$$\theta \equiv \frac{\sqrt{\mathcal{A}}'}{\sqrt{\mathcal{A}}} = \frac{1}{2} k^{\mu}_{;\mu}, \tag{4.21}$$

$$|\sigma| = \sqrt{\frac{1}{2} k_{(\mu;\nu)} k^{\mu;\nu} - \theta^2}, \tag{4.22}$$

where $\mathcal{A}$ is the cross-sectional area of the light bundle, k^{μ} is a tangent vector to the null geodesic (light ray) and the prime denotes the derivative with respect to an affine parameter λ, which characterizes the null geodesic. Kantowski (1968) showed the following relation between the above two optical scalars and two principal curvatures $K_{\pm}$:

$$\theta \pm |\sigma| + (k \cdot v) K_{\pm} = 0, \tag{4.23}$$

where v^{μ} is the observer four velocity. The optical scalar equations (identities) are given by

$$\theta' + \theta^2 + |\sigma|^2 = -\frac{1}{2} R_{\mu\nu} k^{\mu} k^{\nu} \equiv \Re, \tag{4.24}$$

$$\left(|\sigma| e^{i\phi}\right)' + 2\theta |\sigma| e^{i\phi} = C_{\mu\alpha\nu\beta} k^{\mu} k^{\nu} \overline{e}^{\alpha} \overline{e}^{\beta} \equiv F e^{i\beta}, \tag{4.25}$$

where $\overline{e}^{\alpha}$ is the complex space-like vector which constructs a tetrad together with k^{μ} (see in §5.1). $R_{\mu\nu}$ and $C_{\mu\alpha\nu\beta}$ are the Ricci tensor and the Weyl tensor, respectively, and $\Re$ and F are called the "Ricci term" and the "Weyl term", respectively. While the Ricci term depends on the distribution of matter inside the light bundle, the Weyl term depends on the distribution of matter, such as clumps, outside the light bundle.

As already mentioned above, if $|\sigma| = 0$, one principal curvature of the wave-front is equal to another. Therefore so that

$$K_{\pm} \equiv K = -\frac{\theta}{(k \cdot v)} = -\frac{\sqrt{\mathcal{A}}'}{(k \cdot v)\sqrt{\mathcal{A}}}. \tag{4.26}$$

Since $\sqrt{\mathcal{A}}$ is proportional to angular diameter distances, we have

$$K_f(\lambda_d) + K_b(\lambda_d) = \frac{D_{\rm s}}{D_{\rm d} D_{\rm ds}}.$$

The geometrical term Δt_g is then given by eq.(2.40).

The Ricci term in eq.(4.24) is given by virtue of the Einstein field equations as

$$\Re = -\frac{3}{2}\Omega u^5, \tag{4.27}$$

where $u \equiv 1 + {\rm z}$ (z is the source redshift), Ω is the density parameter. Since Ω is the density parameter in the light bundle rather than that in the whole Universe (*i.e.*, Ω_0), it is doubtful whether we can identify Ω with Ω_0. Taking into account the cosmological fluctuation on the density parameter, we introduce a parameter γ_R such as:

$$\Omega = \gamma_R \Omega_0, \qquad (0 \leq \gamma_R \leq 1), \tag{4.28}$$

(Dyer & Roeder 1973). If the Universe is homogeneous, *i.e.*, $\gamma_R = 1$ in the scale where the gravitational lens effect becomes important, the angular diameter distances in eqs.(4.14a-c) satisfy the optical scalar equations. On the other hand, assuming that the light ray passes through an empty space, *i.e.*, $\gamma_R = 0$, Dyer and Roeder (1972) obtained such angular distances . For the general value of γ_R, the solutions of eq. (4.24) are expressed in terms of the hypergeometrical series.

In general, the shear $|\sigma|$ of the wavefront does not vanish. In the calculation of angular diameter distances, the contribution of the Weyl term is important. This term depending considerably on the distribution of clumps in the vicinity of the light bundle, cannot be determined unless the above distribution is known. We thus assume that the Weyl term can be expressed as:

$$F = \frac{3}{2}\gamma_F \Omega_0 u^5, \tag{4.29}$$

like the Ricci term (Alcock & Anderson 1985,1986). We now define the effective distance $\mathrm{L}_\pm$ by

$$\frac{\mathrm{L}'_\pm}{\mathrm{L}_\pm} = \theta \pm |\sigma|. \tag{4.30}$$

The optical scalar equations can then be separated into three equations:

$$\frac{\mathrm{L}''_\pm}{\mathrm{L}_\pm} = -\frac{3}{2}[\gamma_R \mp \gamma_F \cos(\beta - \phi)]\Omega_0 u^5, \tag{4.31}$$

$$\phi' = 3\gamma_F \mathrm{L}_+ \mathrm{L}_- \Omega_0 u^5 \frac{\sin(\beta - \phi)}{\mathrm{L}'_+ \mathrm{L}_- - \mathrm{L}_+ \mathrm{L}'_-}. \tag{4.32}$$

The relation of the affine parameter λ to $u = 1 + \mathrm{z}$ is given by

$$u' = u^2 \sqrt{\frac{1}{2}\Omega_0 - q_0 - (\frac{3}{2}\Omega_0 - q_0 - 1)u^2 + \Omega_0 u^3}. \tag{4.33}$$

The initial conditions of $L_\pm$ are set for initial redshift u_i as:

$$\mathrm{L}_\pm(u_i) = 0, \qquad \mathrm{L}'_\pm(u_i) = u_i. \tag{4.34}$$

The second condition indicates that $\mathrm{L}_\pm$ becomes the proper distance in the vicinity of $u = u_i$.

Assuming that β =const., we find that the solution of eq.(4.32) is given by $\phi = \beta =$ const.. Eq.(4.31) is then rewritten as:

$$\frac{L''_{\pm}}{L_{\pm}} = -\frac{3}{2}(\gamma_R \mp \gamma_F)\Omega_0 u^5, \tag{4.35}$$

The relation of the effective distance to the principal curvature at $\lambda = \lambda_d$ is obtained by the method of Cooke and Kantowski as:

$$K_{\pm f}(\lambda_d) + K_{\pm b}(\lambda_d) = \frac{H_0}{c}\frac{L_{\pm s}}{L_{\pm d}L_{\pm ds}}. \tag{4.35}$$

We show in Fig.4.3 numerical solutions of eq.(4.35), assuming that $\Omega_0 = 2q_0 = 1$ and $-3 \leq \gamma \equiv \gamma_R \pm \gamma_F \leq 3$. The cosmological factor,

$$T = (1 + z_d)\frac{L_d L_s}{L_{ds}},$$

depends considerably on our choice of the parameter γ. Taking into account the influence of inhomogeneities, we have only to investigate the γ-dependence of T in the case of 1115+080. In Fig.4.4, we show the γ-dependence of L_d, L_s, L_{ds} and $L_d L_s / L_{ds}$ in the range $-3 \leq \gamma \leq 3$, where $\Omega_0 = 2q_0 = 1$ is assumed. We find that $L_d L_s / L_{ds}$ varies within a factor ~ 2 compared to the case of $\gamma = 1$.

4.4 Mass of the Lens Galaxy in 1115+080

Borgeest (1986) estimated the mass of the lens object of 0957+561 on the basis of the observed travel time differences. He expressed the travel time difference as a product of two terms: the first term is the deflector mass, and the second depends only on the type of the lens models employed. In his method the deflector mass is calculated by use of the observed travel time differences and by the parameter fixing of the lens model. His method, however, has a disadvantage such that travel time differences can not be theoretically estimated. Thus other

methods are preferable with which to determine the deflector mass only by the parameter fixing of the lens model. In this section we present such a method. Furthermore, we will find that a certain constraint on the Hubble constant H_0 can be imposed by combining our mass estimations with the two methods (Borgeest's method and ours).

The deflection angle α depends, in general, on many parameters besides the deflector mass M_G. If the deflector is a single thin object, M_G can be factorized in the expression for the deflection angle α. The lens equation is then written as

$$\theta_s = \theta + \mu\tilde{\alpha}, \tag{4.37}$$

where

$$\mu = \frac{4GM_G}{c^2}\frac{D}{D_{\rm d}^2}, \tag{4.38}$$

$$\tilde{\alpha} = \frac{D_{\rm ds}}{D_{\rm s}}\frac{\alpha}{\mu}. \tag{4.39}$$

For a given multiple-image system, we can express μ in eq.(4.38) as

$$\mu = \frac{\theta_2 - \theta_1}{\tilde{\alpha}_1 - \tilde{\alpha}_2}, \cdots, \tag{4.40}$$

by using the lens equation (4.37), and can calculate $\mu_{numerical}$ numerically so that the deflector model employed reproduces the observed image configuration. Using the value of $\mu_{numerical}$ thus obtained and eq.(4.38), we can relate $\mu_{numerical}$ to the Hubble constant and to the cosmological factor T, to find

$$\mu_{numerical} = \frac{4GM_G}{c^3}\frac{\mathrm{H}_0(1+\mathrm{z}_d)}{\mathrm{T}}.$$

The deflector mass is then given as

$$\frac{M_G}{M_\odot} = \frac{\mu_{numerical}}{2(1+\mathrm{z}_d)}\frac{c\mathrm{T}}{\mathrm{H}_0 m_\odot}, \tag{4.41}$$

where $M_\odot$ and $m_\odot$ are the solar mass and the Schwarzschild radius of the Sun, respectively. From eq.(4.41) we can estimate the deflector mass in the FRW

universe

$$2.6 \times 10^{11} h^{-1} \leq \frac{M_G}{M_\odot} \leq 2.9 \times 10^{11} h^{-1}, \tag{4.42}$$

where $\Omega_0 = 2q_0 = 1$ and $\mathrm{H}_0 = 100h$[km/sMpc].

As mentioned above, however, since the space in which the light ray passes through is not homogeneous, we must take into account the cosmological fluctuation in the mean density, thereby finding,

$$1.8 \times 10^{11} h^{-1} \leq \frac{M_G}{M_\odot} \leq 5.3 \times 10^{11} h^{-1}, \tag{4.43}$$

where $-3 \leq \gamma \leq 3$.

Moreover, given an observed travel time difference Δt, we can calculate, by using the relation: $\frac{\mathrm{T}}{\mathrm{H}_0} = \frac{\Delta t}{f}$, the deflector mass quite independently both of T and of H_0 (Borgeest 1986).

$$\frac{M_G}{M_\odot} = \frac{\mu_{numerical}}{2(1+\mathrm{z}_d)} \frac{c\,\Delta\, t}{f m_\odot}.$$

Vanderriest *et al.* (1986) obtained, for the present system, the lower limit of $\Delta t_{A_1-A_2}$ and the upper limit of Δt_{A-B}. Using their data and eq.(4.12), we find that the deflector mass is to be in the following range:

$$6.1 \times 10^{10} \leq \frac{M_G}{M_\odot} \leq 2.5 \times 10^{11}. \tag{4.45}$$

In the case of $h = 1$, (4.43) is consistent with (4.45). The condition that these two ranges (4.43) and (4.45) should overlap imposes a constraint on h such as

$$0.74 \leq h \leq 8.7.$$

Thus, the range allowed for the Hubble constant is:

$$74[\mathrm{km/sMpc}] \leq \mathrm{H}_0 \leq 870[\mathrm{km/sMpc}]. \tag{4.46}$$

The upper limit of H_0 in (4.46) is too large to put restraints on the value of H_0. itself. However it is to be noted that our method puts a lower limit on the Hubble

constant. It is expected that more detailed data of the travel time differences will provide more definite lower limit on the Hubble constant. It is interesting that the above range of H_0 is consistent with the value obtained from the observation of the travel time difference in 0957+561 (Florentin-Nielsen 1985, Vanderriest *et al.* 1989).

4.5 Discussion

In this chapter we have fixed the parameters of the lens model in which the deflector potential is expanded up to quadrupole moment. We found that even such a simple model could well reproduce the geometry of 1115+080. However, the approximation of the multipole expansion up to the quadrupole moment term may not be valid for some new images to be expected in this model. At any rate careful attention must be paid to the problem of whether such a new image is really a physical image or a ghost image.

Bearing in mind the above situation, we expect that the number of images we can observe in this system is five: A_1, A_2, B, C and D. We find that the magnitude of image D is $m_V \simeq 20.98 \pm 0.05$[mag.] and is nearly equal to that of the lens galaxy. Unfortunately, however, it is very difficult to observe image D for the following reasons: i) It is difficult to determine the subarcsecond structure of the images since 1115+080 is not a radio-source, ii) image D will not be seen in the residual picture obtained by subtracting image B from the original picture, since all images have the same color, iii) image D is located close to image B.

Assuming that $H_0 = 75$[km/sMpc], M_G obtained with our model is in the following range: $(2.5 \sim 7.1) \times 10^{11} M_\odot$. Our result shows that the deflector should be as weighty as any typical galaxy. This fact seems to be inconsistent with the observation by Christian *et al.* (1986). We can say, however, that the existence of much fainter or dark matters may be responsible for this apparent inconsistency. Furthermore, by combining our mass estimations with the above two methods, the constraint is found to be imposed on the Hubble constant H_0.

In order to obtain definite results, we certainly need more detailed observations of travel time differences over long duration as well as observations with accurate resolution such as in the case of the Hubble Telescope.

5. Apparent Superluminal Motions of Images by a Gravitational Lens

Through analyses of relative positions of some pairs of radio sources for several years, it has been found that these sources appear to have been moving away from each other with velocities several times greater than that of light. These sources are called the "superluminal sources". Many sources of this kind have been discovered, *e.g.*, the radio source 3C120, some BL Lac objects, *etc.*.

Since, of course, motions with velocities greater than the light velocity are prohibited, these phenomena must be explained as illusionary motions. Most popular models for these are: the relativistic jet model and the screen model. In the former, plasma jets with a relativistic velocity are emitted from the core of a quasar. If this jet is emitted with a very small angle α with respect to the line-of-sight, its apparent velocity w is

$$w = \frac{v \sin \alpha}{(1 - \frac{v}{c} \cos \alpha)},$$

where v is the physical velocity of the jet relative to the core. If $\alpha = \cos^{-1}(\frac{v}{c})$, then w has a maximum value, given by

$$w_{max} = \frac{v}{\sqrt{1 - (\frac{v}{c})^2}}.$$

For a relativistic speed v, w can then be greater than the light velocity. In the latter model, on the other hand, relativistic signals are emitted from the core of a quasar, and they brighten the foreground gas-screen. This brightened screen may be observed as superluminal emission.

In this section we propose that such a motion may also appear in a gravitationally lensed system. The apparent velocity of the image due to the gravitational lens effect is equal to the physical velocity of the source multiplied by the amplification factor of the image (Omote & Yoshida 1989).

5.1 Apparent Superluminal Motion in Gravitationally Lensed System

The lens equation is given by eq.(2.12),*i.e.*,

$$\vec{\theta}_{\rm S} = \vec{\theta} + \frac{D}{D_{\rm d}}\vec{\alpha}(\vec{\theta}), \tag{5.1}$$

where $D = D_{\rm d}D_{\rm ds}/D_{\rm s}$; $D_{\rm d}$, $D_{\rm s}$ and $D_{\rm ds}$ are the angular diameter distances between the observer and the deflector, the observer and the source, and the deflector and the source, respectively. As mentioned in Chapter 2, solutions of the lens equation provide us with the positions of images which are multiply produced by the gravitational lens effect. Now let us suppose that the relative position of the source to the deflector varies in time owing to a transverse motion of either the source or the deflector. Then the image positions also move to the deflector. The velocity $\vec{v}_{\rm I}$ of an image is given by

$$\vec{v}_{\rm I} = \frac{1}{(1+{\rm z_S})}[{\rm M}]\vec{v}_{\rm S}, \tag{5.2}$$

or

$$\vec{v}_{\rm I} = \frac{1}{(1+{\rm z_d})}\frac{D_{\rm d}}{D_{\rm s}}[{\rm M}]\vec{v}_{\rm D}, \tag{5.3}$$

where $\vec{v}_{\rm S}$ ($\vec{v}_{\rm D}$) and ${\rm z_S}$ (${\rm z_d}$) are the source (deflector) velocity and the redshift of the source (deflector), respectively (Bourassa & Kantowski 1975), and [M] is the magnification matrix given in eq.(2.20),*i.e.*,

$$[{\rm M}] = \frac{1}{\mathcal{G}^2 - |\mathcal{F}|^2}\begin{pmatrix} \mathcal{G} + Re\mathcal{F} & -Im\mathcal{F} \\ -Im\mathcal{F} & \mathcal{G} - Re\mathcal{F} \end{pmatrix}, \tag{5.4}$$

where $\mathcal{G}$ and $\mathcal{F}$ are defined in eqs.(2.21), (2.22).

Near one of the critical lines in which $\mathcal{G}^2 - |\mathcal{F}|^2 = 0$, the velocity of the image is expected to be infinitely large although the velocity of the source or of

the deflector is finite (smaller, of course, than the light velocity). In order to discuss this case in detail, we consider below the gravitational lens effect induced by an object with spherical symmetry.

In this case, the deflection angle $\vec{\alpha}$ with respect to the image position $\vec{\theta}$ is given by

$$\vec{\alpha}(\vec{\theta}) = -\frac{4GM}{c^2 D_{\rm d}} \frac{\vec{\theta}}{|\vec{\theta}|^2} f(|\vec{\theta}|^2), \tag{5.5}$$

where f is the function of $|\vec{\theta}|^2$ given by

$$f(|\vec{\theta}|^2) = 1 - \Theta(\theta_m - |\vec{\theta}|) \frac{4\pi}{M} \int_{|\vec{\theta}|}^{\theta_m} dr \rho(r) r \sqrt{r^2 - |\vec{\theta}|^2}. \tag{5.6}$$

In the above equation, M, $\rho(r)$ and θ_m are the total mass, mass distribution and maximum radius of the deflector under consideration. In this case the source, multiple images and the deflector are aligned in a line on the deflector plane because of $\vec{\theta}_{\rm S} /\!/ \vec{\theta}$. Thus the lens equation is now reduced to the following form:

$$\theta_{\rm S} = \left[\theta \left\{ 1 - \frac{\mu}{|\vec{\theta}|^2} f(|\vec{\theta}|^2) \right\} \right], \tag{5.7}$$

where $\theta_{\rm s}$ and θ are positive and $\mu = 4GMD/c^2 D_{\rm d}^2$. The critical lines are given by

$$1 + \frac{\mu}{\theta_{\rm cri}^2} f(\theta_{\rm cri}^2) - 2\mu f'(\theta_{\rm cri}^2) = 0, \tag{5.8}$$

where the prime denotes the derivative with respect to θ^2 and $\theta_{\rm S} \neq 0$ is assumed.

The locus of the source when some images are on one of the critical lines is called the "caustic" (Kovner 1987a). Suppose that the source moves with velocity $\vec{v}_{\rm S}$, and it crosses over one of the caustics. Then it so happens that two or more images near a critical line approach each other and are annihilated on the critical line. Similarly, a pair of images may be created on a critical line and be separated from each other.

From eq.(5.2) the velocity of an image located at $\vec{\theta} = (\theta\cos\phi, \theta\sin\phi)$ is given by

$$\vec{v}_{\rm I} = \frac{1}{(1+\frac{\mu}{\theta^2}f - 2\mu f')}\left\{\frac{\vec{v}_{\rm S}\cdot\vec{n}_+}{1+z_{\rm S}}\right\}\vec{n}_+ + \frac{1}{(1-\frac{\mu}{\theta^2}f)}\left\{\frac{\vec{v}_{\rm S}\cdot\vec{n}_-}{1+z_{\rm S}}\right\}\vec{n}_-, \tag{5.9}$$

where

$$\vec{n}_+ = \begin{pmatrix}\cos\phi\\ \sin\phi\end{pmatrix}, \quad \vec{n}_- = \begin{pmatrix}-\sin\phi\\ \cos\phi\end{pmatrix}, \tag{5.10}$$

are eigen-directions of $[\,\mathrm{M}\,]$. Thus the velocity of the image near one of the critical lines is given by

$$|\vec{v}_{\rm I}| \sim \left|\frac{(\vec{v}_{\rm S}\cdot\vec{n}_+)}{(1+z_{\rm S})(1+\frac{\mu}{\theta^2}f - 2\mu f')}\right| \equiv \left|\frac{(\vec{v}_{\rm S}\cdot\vec{n}_+)}{(1+z_{\rm S})\varepsilon}\right|, \tag{5.11}$$

where ε is nearly equal to zero. Then it becomes possible that $|\vec{v}_{\rm I}|$ becomes greater than the light velocity, that is to say, here the apparent superluminal motion is generated as a result of the gravitational lens effect.

Images with superluminal motion are brighter than any other images produced by the gravitational lens effect because the amplification factor of the former becomes infinitely large as they approach the critical line. We can thus expect that the apparent superluminal motion appears in a very bright pair of images with small separation. Among many candidates for multiple-image system, we know that the second candidate, *i.e.*, the multiple quasar 1115+080, has such a pair: A_1 and A_2 (see Chapter 4). 1115+080 is therefore the most promising candidate for apparent superluminal motion.

6. Rotation of Polarization Plane during Propagation in a Weak Gravitational Field

By adopting the harmonic coordinate gauge condition and making the post-Newtonian approximation, Plebanski (1960) pointed out the possibility that the polarization plane is rotated by the gravitational field with metric $g_{\mu\nu} = \eta_{\mu\nu} + h_{\mu\nu}$ (the gravitational Faraday effect). Plebanski found that, when a spherical deflector rotates rigidly, the polarization plane does not rotate for the light passing outside the deflector (*dark lens*), but does so for the light passing through the deflector (*transparent lens*). In the case of Kerr metric, it has been known that the rotation of the polarization plane is absent in the approximation up to $O(m_g/r_0, a/r_0)$ (Lawrence 1973, Su & Malott 1980 and Fayos & Llosa 1982). Here m_g, a and r_0 are the Schwarzschild radius, angular momentum of the Kerr black hole and the impact parameter, respectively. On the other hand, Ishihara, Takahashi and Tomimatsu (1988) showed that the rotation appears in the case of Kerr metric in the approximation up to the third order in m_g/r_0 or in a/r_0.

In this chapter we discuss the gravitational Faraday effect in a weak gravitational field. First we construct the parallel propagator for the polarization vector (Synge 1960) in terms of a null tetrad and investigate the path-dependence of the parallel propagator in §6.1. In the next section (§6.2) a formulation, without gauge fixing, for the rotation of the polarization plane up to $O(h)$ are presented. Our evaluation is carried out under the post-Newtonian approximation with the harmonic coordinate gauge condition. In the last section (§6.3), we then show that the rotation does not take place in the dark lens case, and discuss the reason for this.

6.1 Parallel Propagator for polarization vector

We define the null tetrad $\{e_{(i)\mu} : i = 0, \ldots, 3, \mu = 0, \ldots, 3\}$ on a null geodesic $\{C\}$ by

$$\eta^{(i)\,(j)} e_{(i)\mu} e_{(j)\nu} = g_{\mu\nu}, \tag{6.1}$$

$$g^{\mu\nu} e_{(i)\mu} e_{(j)\nu} = \eta_{(i)\,(j)}, \tag{6.2}$$

$$\left[\eta_{(i)\,(j)}\right] = \left[\eta^{(i)\,(j)}\right] = \begin{pmatrix} 0 & 1 & 0 & 0 \\ 1 & 0 & 0 & 0 \\ 0 & 0 & 0 & 1 \\ 0 & 0 & 1 & 0 \end{pmatrix}, \tag{6.3}$$

where i's and μ's are indices for the null tetrad and for the coordinates, respectively. Here we define the components of the tetrad as follows: $e_{(0)\mu} \equiv k_\mu$ and $e_{(1)\mu} \equiv m_\mu$, both being real null vectors: k_μ is tangential to $\{C\}$; $e_{(2)\mu}$ and $e_{(3)\mu}$ are space-like complex vectors, and $e_{(3)\mu}$ is the complex conjugate of $e_{(2)\mu}$: $e_{(2)\mu} \equiv e_\mu = \overline{e}_{(3)\mu}$.

Following the geometrical optics we take the potential vector A_μ as follows:

$$A_\mu = a_\mu e^{i\theta}. \tag{6.4}$$

Maxwell's equations then lead to the following equations:

$$k^2 = 0, \qquad k^\lambda k_{\mu;\lambda} = 0, \tag{6.5}$$

$$f_\mu k^\mu = 0, \qquad k^\lambda f_{\mu;\lambda} = 0, \tag{6.6}$$

$$(\partial_\lambda a) k^\lambda + \frac{1}{2} a k^\lambda_{\ ;\lambda} = 0, \tag{6.7}$$

where $k_\mu \equiv \partial_\mu \theta$, $a \equiv \sqrt{a_\mu \overline{a}^\mu}$, $f_\mu \equiv a_\mu / a$ and $f_\mu \overline{f}^\mu = 1$. Eqs.(6.5), (6.6) and (6.7) are for the null geodesic, for the parallel displacement of the polarization vector,

and for the amplitude of light. By using an affine parameter λ, we can rewrite eqs.(6.5) and (6.6) in the following forms:

$$\frac{\delta}{\delta\lambda}k_\mu = 0, \qquad \frac{\delta}{\delta\lambda}f_\mu = 0. \tag{6.8}$$

Since the null tetrad spans the four-dimensional space-time, we can express f_μ as

$$f_\mu = c^{(0)}k_\mu + c^{(1)}m_\mu + c^{(2)}e_\mu + c^{(3)}\overline{e}_\mu. \tag{6.9}$$

From eq.(6.6) it immediately follows that $c^{(1)} = 0$. By rotating $\{e_{(i)\mu}\}$ around k_μ, we can always choose the coefficients in (6.9) so that $c^{(0)}$ vanishes (Sachs 1961 and Pirani 1965). Thus f_μ is reduced to the form:

$$f_\mu = \alpha e_\mu + \beta\overline{e}_\mu. \tag{6.10}$$

The normalization condition for the polarization vector requires $|\alpha|^2 + |\beta|^2 = 1$, and eq.(6.8) becomes

$$\frac{\delta}{\delta\lambda}\alpha = \frac{\delta}{\delta\lambda}\beta = 0. \tag{6.11}$$

Hence the coefficients α and β are constant along $\{C\}$: this is naturally understood from the fact that $e_{(i)\mu}$'s are parallel-transported along $\{C\}$.

When a vector V_μ is parallel-transported along a null geodesic curve, we can always define a two-point tensor for any two points S and O on this curve (Synge 1960):

$$V_{\mu'}(\mathrm{O}) = G_{\mu'}{}^{\nu}(\mathrm{O},\mathrm{S})V_\nu(\mathrm{S}). \tag{6.12}$$

Such $G_{\mu'}{}^{\nu}(\mathrm{O},\mathrm{S})$ is called the "parallel propagator" and satisfies the conditions,

$$\lim_{\mathrm{O}\to\mathrm{S}} G_{\mu'}{}^{\nu}(\mathrm{O},\mathrm{S}) = g_\mu{}^{\nu}(\mathrm{S}) = \delta_\mu{}^{\nu} \tag{6.13}$$

and

$$
\begin{aligned}
G^{\mu'}{}^{\nu}(\mathrm{O},\mathrm{S}) &= g^{\mu'\sigma'}(\mathrm{O})G_{\sigma'}{}^{\nu}(\mathrm{O},\mathrm{S}), \\
G_{\mu'\nu}(\mathrm{O},\mathrm{S}) &= G_{\mu'}{}^{\tau}(\mathrm{O},\mathrm{S})g_{\tau\nu}(\mathrm{S}).
\end{aligned}
\tag{6.14}
$$

$G_{\mu'}{}^{\nu}(\mathrm{O},\mathrm{S})$ can be expressed in terms of the tetrad $\{e_{(i)\mu}\}$. Since $\{e_{(i)\mu}\}$ generates arbitrary vectors, the parallel-transported vector V_μ also is expressed as

$$
V_\mu = c^{(i)}e_{(i)\mu}. \tag{6.15}
$$

Here the coefficient $c^{(i)}$ is constant along the geodesic because of $\frac{\delta}{\delta\lambda}V_\mu = 0$ and $\frac{\delta}{\delta\lambda}e_{(i)\mu} = 0$, and is given by virtue of eq.(6.2)

$$
c^{(i)} = V_\mu(\lambda)e^{(i)\mu}(\lambda), \tag{6.16}
$$

for any point on the geodesic. We thus obtain

$$
G_{\mu'}{}^{\nu}(\mathrm{O},\mathrm{S}) = e^{(i)}_{\mu'}(\mathrm{O})e^{\nu}_{(i)}(\mathrm{S}) \tag{6.17}
$$

It is clear that eq.(6.17) satisfies eq.(6.13).

For given two points S and O the null geodesic is not uniquely defined so far as the gravitational lens effect is concerned. The coefficient $c^{(i)}$ in eq.(6.15) on each geodesic curve is different from each other, and so is $G_{\mu'}{}^{\nu}(\mathrm{O},\mathrm{S})$. In dealing with $G_{\mu'}{}^{\nu}(\mathrm{O},\mathrm{S})$ affected by the gravitational lens effect, we must discuss its path-dependence.

In the following we restrict ourselves to the case of the polarization vector f_μ, where the full formulation leading to eq.(6.17) is not needed. In stead of $G_{\mu'}{}^{\nu}(\mathrm{O},\mathrm{S})$ we introduce the "partial parallel propagator" as

$$
\tilde{G}_{\mu'}{}^{\nu}(\mathrm{O},\mathrm{S}) = e_{\mu'}(\mathrm{O})\overline{e}^{\nu}(\mathrm{S}) + \overline{e}_{\mu'}(\mathrm{O})e^{\nu}(\mathrm{S}), \tag{6.18}
$$

because $f_\mu m^\mu = f_\mu k^\mu = 0$ holds in our cases. Let us thus discuss the propagations of k^μ, e_μ and $\overline{e}_\mu$.

We assume that the metric of space-time is given by

$$g_{\mu\nu} = \eta_{\mu\nu} + h_{\mu\nu}, \tag{6.19}$$

where $\eta_{\mu\nu}$ is the Minkowskian flat metric, and deal with the metric up to $O(h)$ only. Then $g^{\mu\nu}$ is given by

$$g^{\mu\nu} = \eta^{\mu\nu} - h^{\mu\nu}, \tag{6.20}$$

where

$$h^{\mu\nu} = \eta^{\mu\alpha}\eta^{\nu\beta}h_{\alpha\beta}.$$

Since k_μ is a tangent vector to $\{C\}$, we can express the vector as

$$k^\mu = \frac{d}{d\lambda}x^\mu.$$

Defining u^μ as $u^\mu = k^\mu/k^0 = dx^\mu/dx^0$, we obtain the equation for u^μ in our approximation as follows:

$$\begin{aligned}\frac{d}{dx^0}u^i = -u^\alpha\frac{d}{dx^0}h_{i\alpha}(x^0, x^a(x^0)) - \frac{1}{2}u^i\frac{d}{dx^0}h_{00}(x^0, x^a(x^0)) \\ + \frac{1}{2}u^i u^j u^k\frac{d}{dx^0}h_{jk}(x^0, x^a(x^0)) \\ + \frac{1}{2}(\delta^{ij} - u^i u^j)u^\alpha u^\beta\partial_j h_{\alpha\beta}(x^0, x^a(x^0)).\end{aligned} \tag{6.21}$$

We define further a unit vector t^i in the 3-dimensional Euclidean space $\mathcal{E}^3$ such that

$$t^i = (1 - \frac{1}{2}h_{00})u^i - \frac{1}{2}h_{ij}u^j - h_{i0}, \tag{6.22}$$

which satisfies the differential equation

$$\frac{d}{dx^0}t^i = -\frac{1}{2}(\delta^{ij} - t^i t^j)\left[\frac{d}{dx^0}h_{jk}t^k - t^\alpha t^\beta\partial_j h_{\alpha\beta}\right], \tag{6.23}$$

where $t^\mu = (1, t^i)$. We assume that the source of lights is far enough from the deflector and set, at the source of lights, $t^i = \overset{\circ}{t}{}^i$ as the initial condition ($x^0 = x^0_{\mathrm{S}}$).

Solving eq.(6.23) under this initial condition and in our approximation, we obtain

$$t^i = \mathring{t}^i + \triangle t^i + O(h^2), \tag{6.24}$$

$$\begin{aligned}\triangle t^i = -\frac{1}{2}\left(\delta^{ij} - t^{\circ i}t^{\circ j}\right)\Big[h_{jk}(x^0, r^a_\perp + \mathring{t}^a x^0)\mathring{t}^k \\ - \int_{x^0_S}^{x^0} dx^{0\prime}\partial_j h_{\alpha\beta}(x^{0\prime}, r^a_\perp + \mathring{t}^a x^{0\prime})\mathring{t}^\alpha\mathring{t}^\beta\Big],\end{aligned} \tag{6.25}$$

where $\vec{r}_\perp$ is the impact vector and $\mathring{\vec{t}}$ and $\vec{r}_\perp$ must be determined on each null geodesic curve. The quantity $\triangle t^i$ with $x^0 = -x^0_S \to \infty$ gives the deflection angle.

Next let us discuss the propagation of e_μ and $\overline{e}_\mu$. As e_μ is orthogonal to u^μ, we have only to discuss the propagation of $e_i (i = 1, 2, 3)$. The equation for e_i is given by

$$\begin{aligned}\frac{d}{dx^0}e_i = \frac{1}{2}\Big\{\frac{d}{dx^0}h_{ij}(x^0, x^a(x^0))\Big\}e_{\perp j} + \frac{1}{2}e_{/\!/}t^\alpha t^\beta\Big\{\partial_i h_{\alpha\beta}(x^0, x^a(x^0))\Big\} \\ + \frac{1}{2}\epsilon_{ijk}e_{\perp j}\epsilon_{klm}\Big\{\partial_l h_{m\alpha}(x^0, x^a(x^0))\Big\},\end{aligned} \tag{6.26}$$

where

$$e_{/\!/} = e_i t^i, \qquad e_{\perp i} = e_i - e_{/\!/}t^i.$$

We obtain, up to $O(h)$,

$$\begin{aligned}e_i = \mathring{e}_i + \frac{1}{2}h_{ij}(x^0, r^a_\perp + \mathring{t}^a x^0)\mathring{e}_j \\ + \frac{1}{2}\mathring{e}_{/\!/}\mathring{t}^\alpha\mathring{t}^\beta\int_{x^0_S}^{x^0} dx^{0\prime}\partial_i h_{\alpha\beta}(x^{0\prime}, r^a_\perp + \mathring{t}^a x^{0\prime}) \\ + \frac{1}{2}\epsilon_{ijk}\epsilon_{klm}\mathring{e}_{\perp j}\int_{x^0_S}^{x^0} dx^{0\prime}\partial_l h_{m\alpha}(x^{0\prime}, r^a_\perp + \mathring{t}^a x^{0\prime})\mathring{t}^\alpha.\end{aligned} \tag{6.27}$$

From eqs.(6.23) and (6.27), the explicit form of e_0 is given by

$$\begin{aligned} e_0 = &-\mathring{e}_{/\!/} + \frac{1}{2}\Big[h_{ij}(x^0, r^a_\perp + \mathring{t}^a x^0) + \delta^{ij} h_{00}(x^0, r^a_\perp + \mathring{t}^a x^0)\Big]\mathring{e}_j \mathring{t}^i \\ &+ \mathring{e}_i h_{i0}(x^0, r^a_\perp + \mathring{t}^a x^0) \\ &- \frac{1}{2}\mathring{e}_i \mathring{t}^\alpha \mathring{t}^\beta \int_{x^0_{\rm S}}^{x^0} dx^{0\prime} \partial_i h_{\alpha\beta}(x^{0\prime}, r^a_\perp + \mathring{t}^a x^{0\prime}) \\ &- \frac{1}{2}\epsilon_{ijk}\mathring{t}^i \mathring{e}_j \epsilon_{klm} \int_{x^0_{\rm S}}^{x^0} dx^{0\prime} \partial_l h_{m\alpha}(x^{0\prime}, r^a_\perp + \mathring{t}^a x^{0\prime}) \mathring{t}^\alpha. \end{aligned} \tag{6.28}$$

For the sake of notational simplicity, we introduce A_i and B_{ij} defined by

$$\begin{aligned} A_i &= \frac{1}{2}\mathring{t}^\alpha \mathring{t}^\beta \int_{x^0_{\rm S}}^{x^0} dx^{0\prime} \partial_i h_{\alpha\beta}(x^{0\prime}, r^a_\perp + \mathring{t}^a x^{0\prime}), \\ B_{ij} &= \frac{1}{2}\epsilon_{ijk}\epsilon_{klm} \int_{x^0_{\rm S}}^{x^0} dx^{0\prime} \partial_l h_{m\alpha}(x^{0\prime}, r^a_\perp + \mathring{t}^a x^{0\prime}) \mathring{t}^\alpha. \end{aligned} \tag{6.29}$$

It then follows from eq.(6.23) that A_i is related to the deflection angle. On the other hand, B_{ij} is related to the rotation of the polarization plane, as will be seen later.

Finally, let us express $\tilde{G}_{\mu'\nu}(\mathrm{O},\mathrm{S})$ in terms of e_i and e_0:

$$\begin{aligned} \tilde{G}_{0'0}(\mathrm{O},\mathrm{S}) =& e_{0'}(\mathrm{O})\mathring{\bar{e}}_0(\mathrm{S}) + \bar{e}_{0'}(\mathrm{O})\mathring{e}_0(\mathrm{S}), \\ =& 2|\mathring{e}_{/\!/}|^2 - \Big(\mathring{\bar{e}}_{/\!/}\mathring{e}_i + \mathring{e}_{/\!/}\mathring{\bar{e}}_i\Big)\Big[h_{i0}(x^0, r^a_\perp + \mathring{t}^a x^0) - A_i + \mathring{t}^j B_{ij} \\ &+ \frac{1}{2}\mathring{t}^j\big\{h_{ij}(x^0, r^a_\perp + \mathring{t}^a x^0) + \delta^{ij} h_{00}(x^0, r^a_\perp + \mathring{t}^a x^0)\big\}\Big], \end{aligned} \tag{6.30}$$

$$
\begin{aligned}
\tilde{G}_{0'i}(\mathrm{O},\mathrm{S}) =& e_{0'}(\mathrm{O})\overset{\circ}{\overline{e}}_i(\mathrm{S}) + \overline{e}_{0'}(\mathrm{O})\overset{\circ}{e}_i(\mathrm{S}),\\
=& -\left(\overset{\circ}{\overline{e}}_i\overset{\circ}{e}_j + \overset{\circ}{e}_i\overset{\circ}{\overline{e}}_j\right)\Big[\overset{\circ}{t}{}^j - h_{j0}(x^0, r^a_\perp + \overset{\circ}{t}{}^a x^0) + A_j - \overset{\circ}{t}{}^k B_{jk}\\
&+ \frac{1}{2}\overset{\circ}{t}{}^k\left\{h_{jk}(x^0, r^a_\perp + \overset{\circ}{t}{}^a x^0) + \delta^{jk}h_{00}(x^0, r^a_\perp + \overset{\circ}{t}{}^a x^0)\right\}\Big], \qquad (6.31)\\
\tilde{G}_{i'0}(\mathrm{O},\mathrm{S}) =& e_{i'}(\mathrm{O})\overset{\circ}{\overline{e}}_0(\mathrm{S}) + \overline{e}_{i'}(\mathrm{O})\overset{\circ}{e}_0(\mathrm{S}),\\
=& -\left(\overset{\circ}{\overline{e}}_l\overset{\circ}{e}_k + \overset{\circ}{e}_l\overset{\circ}{\overline{e}}_k\right)\Big[\delta_{ik}\overset{\circ}{t}{}^l + A_i\overset{\circ}{t}{}^k\overset{\circ}{t}{}^l + B_{ij}P_{jk}\overset{\circ}{t}{}^l\\
&+ \frac{1}{2}h_{ij}(x^0, r^a_\perp + \overset{\circ}{t}{}^a x^0)\overset{\circ}{t}{}^l P_{jk}\Big], \qquad (6.32)
\end{aligned}
$$

and

$$
\begin{aligned}
\tilde{G}_{i'j}(\mathrm{O},\mathrm{S}) =& e_{i'}(\mathrm{O})\overset{\circ}{\overline{e}}_j(\mathrm{S}) + \overline{e}_{i'}(\mathrm{O})\overset{\circ}{e}_j(\mathrm{S}),\\
=& -\left(\overset{\circ}{\overline{e}}_j\overset{\circ}{e}_k + \overset{\circ}{e}_j\overset{\circ}{\overline{e}}_k\right)\Big[\delta_{ik} + A_i\overset{\circ}{t}{}^k + B_{il}P_{lk} + \frac{1}{2}h_{il}(x^0, r^a_\perp + \overset{\circ}{t}{}^a x^0)\Big], \qquad (6.33)
\end{aligned}
$$

where $P_{ij} = \delta^{ij} - \overset{\circ}{t}{}^i\overset{\circ}{t}{}^j$ is the projection from $\mathcal{E}^3$ onto the plane orthogonal to $\overset{\circ}{\vec{t}}$. The above expressions satisfy

$$
\begin{aligned}
\tilde{G}_{\mu'}{}^{\nu}(\mathrm{O},\mathrm{S})\overset{\circ}{e}_\nu(\mathrm{S}) &= e_{\mu'}(\mathrm{O}),\\
\tilde{G}_{\mu'}{}^{\nu}(\mathrm{O},\mathrm{S})\overset{\circ}{\overline{e}}_\nu(\mathrm{S}) &= \overline{e}_{\mu'}(\mathrm{O}),\\
\tilde{G}^{\mu'}{}_{\nu}(\mathrm{O},\mathrm{S})e_{\mu'}(\mathrm{O}) &= \overset{\circ}{e}_\nu(\mathrm{S}),\\
\tilde{G}^{\mu'}{}_{\nu}(\mathrm{O},\mathrm{S})\overline{e}_{\mu'}(\mathrm{O}) &= \overset{\circ}{\overline{e}}_\nu(\mathrm{S}).
\end{aligned} \qquad (6.34)
$$

Clearly $\tilde{G}^{\mu'}{}_{\nu}(\mathrm{O},\mathrm{S})$ depends on the light path characterized by $\overset{\circ}{t}{}^i$ and $r^i_\perp$.

6.2 Rotation of the Polarization Plane Induced by a Rigidly Rotating Body

In this section we derive a formula for the observable rotation angle of the polarization plane which is good up to $O(h)$. Next we estimate the angle for simple cases of a spherical or spheroidal deflector which is rotating rigidly.

As in the cases of e_μ and $\overline{e}_\mu$, the equation for the polarization vector f_μ is given by eq.(6.8)

$$\begin{aligned}\frac{d}{dx^0}f_i = \frac{1}{2}\left(\frac{d}{dx^0}h_{ij}\right)f_{\perp j} + \frac{1}{2}f_{/\!/}t^\alpha t^\beta \partial_i h_{\alpha\beta} \\ + \frac{1}{2}\epsilon_{ijk}f_{\perp j}\epsilon_{klm}\left(\partial_l h_{m\alpha}\right)t^\alpha.\end{aligned} \tag{6.35}$$

On the basis of the relations $f_\mu \overline{f}^\mu = 1$ and $f_\mu u^\mu = 0$ we now define a unit vector $S_{\perp i}$ in $\mathcal{E}^3$ by

$$S_i = f_i - \frac{1}{2}h_{ij}f_j, \tag{6.36}$$

$$S_{\perp i} = P_{ij}S_j. \tag{6.37}$$

The equation for $S_{\perp i}$ is given by

$$\frac{d}{dx^0}S_{\perp i} = \epsilon_{jkl}\epsilon_{lmn}\left\{\frac{1}{2}P_{ij}\left(\partial_m h_{n\alpha}\right) - \delta_{ij}\mathring{t}^m\frac{d}{dx^0}t^n\right\}S_{\perp k}. \tag{6.38}$$

Introducing moreover two real unit vectors (v_i and w_i) which are independent of each other and which are orthogonal to t^i in $\mathcal{E}^3$, we can express $S_{\perp i}$ and $\overline{S}_{\perp i}$ as follows:

$$\begin{aligned}S_{\perp i} &= \frac{1}{\sqrt{2}}\left(e^{i\phi}v_i - ie^{-i\psi}w_i\right), \\ \overline{S}_{\perp i} &= \frac{1}{\sqrt{2}}\left(e^{-i\phi}v_i + ie^{i\psi}w_i\right),\end{aligned} \tag{6.39}$$

where ϕ and ψ are real constants and $v_i w_i = 0$. It is clear that $S_{\perp i}\overline{S}_{\perp i} = 1$ and $S_{\perp i}S_{\perp i}$, $\overline{S}_{\perp i}\overline{S}_{\perp i} = \text{const}$. Equations for v_i, w_i are given by eq.(6.38),

$$\begin{aligned}\frac{d}{dx^0}v_i &= \epsilon_{jkl}\epsilon_{lmn}\left\{\frac{1}{2}P_{ij}\left(\partial_m h_{n\alpha}\right) - \delta_{ij}\mathring{t}^m\frac{d}{dx^0}t^n\right\}v_k, \\ \frac{d}{dx^0}w_i &= \epsilon_{jkl}\epsilon_{lmn}\left\{\frac{1}{2}P_{ij}\left(\partial_m h_{n\alpha}\right) - \delta_{ij}\mathring{t}^m\frac{d}{dx^0}t^n\right\}w_k.\end{aligned} \tag{6.40}$$

Since $\{t^i, v_i, w_i\}$ constitutes a triad in $\mathcal{E}^3$, *i.e.*,

$$\begin{aligned} t^i t^i = v_i v_i = w_i w_i = 1, \\ t^i = \epsilon_{ijk} v_j w_k, \quad v_i = \epsilon_{ijk} w_j t^k, \quad w_i = \epsilon_{ijk} t^j u_k, \end{aligned} \tag{6.41}$$

dv_i/dx^0 is expressed as

$$\frac{d}{dx^0} v_i = \mathcal{P}_v w_i + \mathcal{Q}_v t^i, \tag{6.42}$$

where $\mathcal{P}_v$ and $\mathcal{Q}_v$ are given by

$$\begin{aligned} \mathcal{P}_v =& w_i \frac{d}{dx^0} v_i = -\frac{1}{2} \mathring{t}^a \epsilon_{abc} (\partial_b h_{c\alpha}) \mathring{t}^\alpha, \\ \mathcal{Q}_v =& t^i \frac{d}{dx^0} v_i = -v_a \frac{d}{dx^0} t^a. \end{aligned} \tag{6.43}$$

By virtue of eq.(6.41), dv_i/dx^0 is written as

$$\begin{aligned} \frac{d}{dx^0} v_i =& \epsilon_{ijk} \Big[-\frac{1}{2} \mathring{t}^a \epsilon_{abc} (\partial_b h_{c\alpha}) \mathring{t}^\alpha \mathring{t}^j + \epsilon_{jab} \mathring{t}^a \frac{d}{dx^0} t^b \Big] v_k \\ \equiv& \epsilon_{ijk} \Omega_j v_k. \end{aligned} \tag{6.44}$$

As in the case of v_i, the equation for w_i is given by

$$\frac{d}{dx^0} w_i = \epsilon_{ijk} \Omega_j w_k. \tag{6.45}$$

We thus obtain equations for $S_{\perp i}$ and $\overline{S}_{\perp i}$

$$\frac{d}{dx^0} S_{\perp i} = \epsilon_{ijk} \Omega_j S_{\perp k}, \quad \frac{d}{dx^0} \overline{S}_{\perp i} = \epsilon_{ijk} \Omega_j \overline{S}_{\perp k}, \tag{6.46}$$

which, when integrated, lead us to

$$S_{\perp i} = \mathring{S}_{\perp i} + \epsilon_{ijk} \omega_j \mathring{S}_{\perp k}, \quad \overline{S}_{\perp i} = \mathring{\overline{S}}_{\perp i} + \epsilon_{ijk} \omega_j \mathring{\overline{S}}_{\perp k}, \tag{6.47}$$

where

$$\begin{aligned} \omega_i =& \int_{x_S^0}^{x^0} dx^{0\prime} \Omega_i (x^{0\prime}, r_\perp^s + \mathring{t}^s x^{0\prime}) \\ \equiv& \epsilon_{iab} \mathring{t}^a \triangle t^b + P \mathring{t}^i. \end{aligned} \tag{6.48}$$

The first term of eq.(6.48) corresponds to the rotation of the polarization

plane induced by the deflection of $\{C\}$. It is not an observable quantity, however, because $\overset{\circ}{\vec{t}} \times \Delta\vec{t}$ is a rotation around the axis orthogonal to the line-of-sight.

On the other hand, the second term is an observable quantity*, because it is the rotation around $\overset{\circ}{\vec{t}}$. Thus, we have only to discuss P, regarding it as the observable rotation angle of the polarization plane. The explicit form of P is

$$P = -\frac{1}{2}\mathring{t}^a \epsilon_{abc} \int_{x_S^0}^{x^0} dx^{0\prime} \partial_b h_{c\alpha}(x^{0\prime}, r_\perp^s + \mathring{t}^s x^{0\prime}) \mathring{t}^\alpha, \tag{6.49}$$

which is gauge-invariant (Plebanski 1961).

By using eq.(6.49) we can now estimate the rotation angles of the polarization plane for some simple cases. In so doing we choose the harmonic coordinate gauge and use the post-Newtonian approximation (Weinberg 1972). The metric is given by

$$\begin{aligned} h_{00}(\vec{x}) &= -\frac{2G}{c^2}\int d^3x' \frac{\rho(\vec{x}')}{|\vec{x} - \vec{x}'|}, \\ h_{i0}(\vec{x}) &= \frac{4G}{c^3}\int d^3x' \frac{\epsilon_{ijk}\omega^j x^{k\prime} \rho(\vec{x}')}{|\vec{x} - \vec{x}'|}, \\ h_{ij}(\vec{x}) &= \delta_{ij} h_{00}(\vec{x}), \end{aligned} \tag{6.50}$$

where ω^i is the rotational angular velocity of the deflector. In the limit $x^0 \equiv x_O^0 = -x_S^0 \to \infty$, the rotation angle P is given by

$$P = -\frac{1}{2}\mathring{t}^a \epsilon_{abc} \int_{-\infty}^{\infty} dx^0 \partial_b h_{c\alpha}(x^0, r_\perp^s + \mathring{t}^s x^0) \mathring{t}^\alpha. \tag{6.51}$$

First let us consider the case when a spherical deflector is rotating rigidly. If,

---

* Strictly speaking, the second term is not observable, unless we know the initial direction of the polarization vector. However, if we have two or more gravitationally lensed images, this term becomes observable (see §6.3).

in particular, ω is constant, we find

$$P = \frac{16\pi G}{c^3}\omega_{/\!/}\int_{r_\perp}^{\ell} dr\rho(r)r\sqrt{r^2 - r_\perp^2}\Theta(\ell - r_\perp), \tag{6.52}$$

where $\omega_{/\!/} = \overset{\circ}{t}{}^i\omega_i$ and $\Theta(\ell - r_\perp)$ is the step function satisfying $\Theta(x) = 1$ for $x \geq 0$ and $\Theta(x) = 0$ for $x < 0$. Eq.(6.52) thus shows that P always vanishes in the case of a spherical dark lens (Plebanski).

As a concrete example, we first estimate eq.(6.52) for the case of a deflector with constant mass density, and find that

$$P = \frac{4GM}{c^3}\omega_{/\!/}\sqrt{(1 - \frac{r_\perp^2}{\ell^2})^3}\Theta(\ell - r_\perp).$$

Next we consider the case of a deflector with spheroidal symmetry. It is interesting to see whether the rotation angle of the polarization plane vanishes or not in the dark lens case.

First, integrating eq.(6.51) with respect to x^0, we obtain the following form

$$\begin{aligned} P = \frac{4GM}{c^3}\omega_{/\!/} - \frac{4G}{c^3}\omega_{/\!/}\int d^3y\rho(\vec{y})\frac{\vec{r}_\perp \cdot (\vec{r}_\perp - \vec{y}_\perp)}{|\vec{r}_\perp - \vec{y}_\perp|^2} \\ + \frac{4G}{c^3}\int d^3y\rho(\vec{y})y_{/\!/}\frac{\vec{\omega}_\perp \cdot (\vec{r}_\perp - \vec{y}_\perp)}{|\vec{r}_\perp - \vec{y}_\perp|^2}, \end{aligned} \tag{6.53}$$

where $y_{/\!/} = \overset{\circ}{t}{}^i y_i, y_\perp^i = y^i - y_{/\!/}\overset{\circ}{t}{}^i$. The first term is related to the total mass of the deflector, and the second term is given by $\omega_{/\!/}\vec{r}_\perp \cdot \vec{\alpha}_0/c$, where $\vec{\alpha}_0$ is the deflection angle for the case when the deflector is not rotating. The third term corresponds to what vanishes owing to symmetry in the spherical lens case. In our case we expect this term to give a non-zero contribution to P (because $\rho(\vec{y}_\perp, y_{/\!/}) \neq \rho(\vec{y}_\perp, -y_{/\!/})$ in general).

Let us denote the third term by

$$\frac{4G}{c^3}\vec{\omega}_\perp \vec{H}, \tag{6.54}$$

where we assume that $\vec{\omega}$ is a constant vector and that the direction of $\vec{\omega}$ coincides with the normal of the spheroid. In eq.(6.54), $\vec{H}$ is given by

$$\vec{H} = \int d^3y \rho(\vec{y}) y_{/\!/} \frac{(\vec{r}_\perp - \vec{y}_\perp)}{|\vec{r}_\perp - \vec{y}_\perp|^2}.$$

The center of the spheroid is assumed to be located at the origin of the coordinate system $\{y^1, y^2, y^3\}$, where the deflector has the mass distribution of spheroidal symmetry given by

$$\rho(\vec{y}) = \begin{cases} \rho(a), & a \leq a_{max}, \\ 0, & a > a_{max}, \end{cases} \tag{6.55}$$

$$a^2 = (y^1)^2 + (y^2)^2 + \frac{(y^3)^2}{1-e^2}. \tag{6.56}$$

Here we denote the maximum major axis of the deflector by a_{max} and the eccentricity by e. Further it is convenient to introduce another coordinate system $\{x_\perp, y_\perp, z_{/\!/}\}$, which is related to $\{y^1, y^2, y^3\}$ through

$$\begin{aligned} y^1 &= x_\perp, \\ y^2 &= y_\perp \cos\gamma - z_{/\!/} \sin\gamma, \\ y^3 &= y_\perp \sin\gamma + z_{/\!/} \cos\gamma. \end{aligned} \tag{6.57}$$

These relations indicate that the y^1-axis coincides with the $x_\perp$-axis on the deflector plane defined in Chapter 2, and that γ is the angle between the y^3-axis and the $y_{/\!/}$-axis. Using eq.(6.57) we can express eq.(6.56) in terms of $x_\perp, y_\perp$ and

$z_{/\!/}$ as follows

$$\begin{aligned} a^2 &= x_\perp^2 + \frac{1-e^2\cos^2\gamma}{1-e^2}\Big(y_\perp + \frac{e^2\sin\gamma\cos\gamma}{1-e^2\cos^2\gamma}z_{/\!/}\Big)^2 + \frac{z_{/\!/}^2}{1-e^2\cos^2\gamma} \\ &= w^2 + \frac{z_{/\!/}^2}{1-e^2\cos^2\gamma}. \end{aligned} \tag{6.58}$$

We now estimate $\vec{H}$ by using eqs.(6.55) and (6.58). Since $\vec{H}$ is a vector on the deflector plane, we can introduce complex parameters $\mathcal{H}, r_\perp$ and η such that

$$\mathcal{H} = H_x - iH_y, \quad r_\perp = r_{x_\perp} + ir_{y_\perp}, \quad \eta = x_\perp + iy_\perp.$$

Then, $\mathcal{H}$ is expressed as follows

$$\mathcal{H} = \int dz_{/\!/} z_{/\!/} \int dx_\perp dy_\perp \frac{\rho(a)}{r_\perp - \eta}, \tag{6.59}$$

evaluation of which can be carried out by the method of Bourassa, Kantowski and Norton (1973).

The spheroid is divided into a shell with the major axis $a(\leq a_{max})$, and the shell is further divided into an elliptical ring with $z_{/\!/}$ fixed. First, we evaluate the contribution $\mathcal{H}_r$ from the elliptical ring, and next integrate $\mathcal{H}_r$ with respect to $z_{/\!/}$ to obtain the contribution $\mathcal{H}_s$ from the shell. Finally we evaluate $\mathcal{H}$ by integrating $\mathcal{H}_s$ with respect to a.

a) *The contribution from the elliptical ring* $\mathcal{H}_r$

The elliptical ring is specified by

$$\begin{aligned} x_\perp &= w\cos\phi, \\ y_\perp &= \epsilon w\sin\phi - \frac{e^2\sin\gamma\cos\gamma}{1-e^2\cos^2\gamma}z_{/\!/}, \end{aligned}$$

where w is given in eq.(6.58) and ϵ is the ellipticity of the ring

$$\epsilon = \sqrt{\frac{1-e^2}{1-e^2\cos^2\gamma}}. \tag{6.60}$$

Thus $\mathcal{H}_r$ is expressed as

$$\mathcal{H}_r = \epsilon\rho(a)adadz_{/\!/}z_{/\!/} \int_0^{2\pi} \frac{d\phi}{r_\perp - \eta}, \tag{6.61}$$

where

$$\eta = w\cos\phi + i\epsilon\sin\phi - i\frac{e^2\sin\gamma\cos\gamma}{1-e^2\cos^2\gamma}z_{/\!/}.$$

The integral in eq.(6.61) is rewritten as

$$\int_0^{2\pi} \frac{d\phi}{r_\perp - \eta} = \frac{2i}{w(1+\epsilon)} \oint_{|\xi|=1} \frac{d\xi}{(\xi-\xi_+)(\xi-\xi_-)}, \tag{6.62}$$

where

$$\xi_\pm = \frac{r_\perp + i\frac{e^2\sin\gamma\cos\gamma}{1-e^2\cos^2\gamma}z_{/\!/} \pm \sqrt{\left(r_\perp + i\frac{e^2\sin\gamma\cos\gamma}{1-e^2\cos^2\gamma}z_{/\!/}\right)^2 - w^2(1-\epsilon^2)}}{w(1+\epsilon)}. \tag{6.63}$$

We separate the integration in eq.(6.62) into two cases: the dark lens case and the transparent lens case. In the dark lens case, $\mathcal{H}_r^{(dark)}$ is expressed as

$$\mathcal{H}_r^{(dark)} = \frac{2\pi\epsilon\rho(a)adaz_{/\!/}dz_{/\!/}}{\sqrt{r_\perp^2 - \frac{e^2\sin^2\gamma}{1-e^2\cos^2\gamma}a^2 + 2ir_\perp\frac{e^2\sin\gamma\cos\gamma}{1-e^2\cos^2\gamma} + \frac{e^2\sin^2\gamma}{1-e^2\cos^2\gamma}z_{/\!/}^2}}, \tag{6.64}$$

because $|\xi_-| \le 1 \le |\xi_+|$ (Appendix A-(a)). On the other hand, in the transparent lens case, since $|\xi_\pm| \le 1$ for some $z_{/\!/}$ (Appendix A-(b)), $\mathcal{H}_r^{(trans.)}$ is given as

$$\mathcal{H}_r^{(trans.)} = \begin{cases} \mathcal{H}_r^{(dark)}, & (z_- > z_{/\!/} \text{ or } z_{/\!/} < z_+), \\ 0, & (z_- \le z_{/\!/} \le z_+), \end{cases} \tag{6.65}$$

where

$$z_\pm = \frac{e\sin\gamma}{1-e^2\sin^2\gamma}\left[e\cos\gamma(r_{y_\perp}) \pm \sqrt{(1-e^2)\left(a^2 - B_\perp^2\right)}\right], \tag{6.66}$$

$$B_\perp^2 = r_{x_\perp}^2 + \frac{r_{y_\perp}^2}{1 - e^2 \sin^2 \gamma}. \tag{6.67}$$

b) The contribution from the shell $\mathcal{H}_s$

Next we integrate $\mathcal{H}_r$ with respect to $z_{/\!/}$ from $-a\sqrt{1 - e^2 \sin^2 \gamma}$ to $a\sqrt{1 - e^2 \sin^2 \gamma}$. In the dark lens case, we obtain

$$\mathcal{H}_s^{(dark)} = 2\pi i \sqrt{1 - e^2} \cot \gamma \rho(a) a da \Big[2a - \frac{r_\perp}{\sin \beta} \ln\big(\frac{r_\perp + a \sin \beta}{r_\perp - a \sin \beta}\big)\Big], \tag{6.68}$$

where

$$\sin \beta \equiv e \sin \gamma.$$

In the transparent lens case, $\mathcal{H}_s^{(trans.)}$ is given by

$$\begin{aligned}\mathcal{H}_s^{(trans.)} = \mathcal{H}_s^{(dark)} &- 4\pi i e \cos \gamma \sqrt{1 - e^2} \rho(a) a da \sqrt{a^2 - B_\perp^2}\, \Theta(a - B_\perp) \\ &+ 2\pi i \epsilon \cot \gamma r_\perp \rho(a) a da \ln\Big(\frac{A_\perp + \tan \beta \sqrt{a^2 - B_\perp^2}}{A_\perp - \tan \beta \sqrt{a^2 - B_\perp^2}}\Big) \Theta(a - B_\perp),\end{aligned} \tag{6.69}$$

where

$$A_\perp \equiv \cot \beta \big(r_{x_\perp} + \frac{r_{y_\perp}}{\cos^2 \beta}\big).$$

c) The total $\mathcal{H}$

Finally we integrate $\mathcal{H}_s$ with respect to a, thereby obtaining $\mathcal{H}$ for the two cases:
in the dark lens case,

$$\begin{aligned}\mathcal{H}^{(dark)} &= i \cot \gamma \Big[M - \frac{2\pi \sqrt{1 - e^2}}{\sin \beta} r_\perp \int_{B_\perp}^{a_{max}} da \rho(a) a \ln\Big(\frac{r_\perp + a \sin \beta}{r_\perp - a \sin \beta}\Big)\Big] \\ &= i \cot \gamma \Big[M + \frac{c^2}{4G} r_\perp \overline{\alpha}_0^{(dark)}\Big];\end{aligned} \tag{6.70}$$

in the transparent lens case we obtain $\mathcal{H}$

$$\mathcal{H}^{(trans.)} = \mathcal{H}^{(dark)} - 4\pi i e \cos\gamma\sqrt{1-e^2}\int_{B_\perp}^{a_{max}} \rho(a)ada\sqrt{a^2-B_\perp^2}\,\Theta(a_{max}-B_\perp)$$
$$+ 2\pi i\epsilon\cot\gamma r_\perp \int_{B_\perp}^{a_{max}} \rho(a)ada\ln\Big(\frac{A_\perp+\tan\beta\sqrt{a^2-B_\perp^2}}{A_\perp-\tan\beta\sqrt{a^2-B_\perp^2}}\Big)\Theta(a_{max}-B_\perp). \tag{6.71}$$

The contribution from $\mathcal{H}$ to the rotation angle of the polarization plane is thus given by eq.(6.54) in our complex representation as:

$$\begin{aligned}\frac{4G}{c^3}\vec{\omega}_\perp\vec{H} &= \frac{4G}{c^3}\big[\omega_{\perp_x}Re(\mathcal{H}) - \omega_{\perp_y}Im(\mathcal{H})\big] \\ &= \frac{4G}{c^3}Re\big(\omega_\perp\mathcal{H}\big),\end{aligned} \tag{6.72}$$

where $\vec{\omega}_\perp$ in our coordinate system $\{x_\perp, y_\perp, z_{/\!/}\}$ is expressed by

$$\vec{\omega}_\perp = (0, \omega\sin\gamma, 0), \quad \omega_\perp = i\omega\sin\gamma.$$

In the dark lens case eq.(6.72) is reduced to the form

$$\frac{4G}{c^3}\vec{\omega}_\perp\vec{H} = -\frac{\omega\cos\gamma}{c}\Big[\frac{4GM}{c^2} + Re\big(r_\perp\overline{\alpha}_0^{(dark)}\big)\Big]. \tag{6.73}$$

We thus find that in the dark lens case P vanishes.

In the transparent lens case, on the other hand, we obtain the following P:

$$\begin{aligned}P =& \frac{8\pi G}{c^3}\omega\cos\gamma\sqrt{1-e^2}\Big[\Big[2\sin\beta\int_{B_\perp}^{a_{max}} da\rho(a)a\sqrt{a^2-B_\perp^2} \\ &- Re\Big[r_\perp\int_{B_\perp}^{a_{max}} da\rho(a)a\Big\{\frac{1}{\sqrt{1-e^2\cos^2\gamma}}\ln\Big(\frac{A_\perp+\tan\beta\sqrt{a^2-B_\perp^2}}{A_\perp-\tan\beta\sqrt{a^2-B_\perp^2}}\Big) \\ &- \frac{1}{\sin\beta}\ln\Big(\frac{A_\perp+\sqrt{a^2-B_\perp^2}}{A_\perp-\sqrt{a^2-B_\perp^2}}\Big)\Big\}\Big]\Big]\Theta(a_{max}-B_\perp).\end{aligned} \tag{6.74}$$

It is clear, of course, that eq.(6.74) coincides with eq.(6.52) in the limit $e \to 0$.

In Appendix B, we give the results for two simple cases of mass distribution with spheroidal symmetry.

As mentioned above, the rotation angle of the polarization plane vanishes in the dark lens case not only with spherical symmetry but also with spheroidal symmetry. We have presented the extended formula eq.(6.74) for the case of a transparent lens with spheroidal symmetry.

It seems to us to be miraculous that P vanishes for the case of spheroidal dark lens, and makes us wonder whether this is indeed a miracle. In the next section, we discuss the problem of whether P for the cases of the general dark lens vanishes or not.

6.3 Discussion

The rotation angle of the polarization plane during light propagation with respect to an image (*e.g.* A) is given by eq.(6.51), *i.e.*,

$$P = -\frac{1}{2}\overset{\circ}{t}{}^a_A \epsilon_{abc} \int_{-\infty}^{\infty} dx^0 \partial_b h_{c\alpha}(x^0, r^s_{\perp A} + \overset{\circ}{t}{}^s_A x^0)\overset{\circ}{t}{}^\alpha_A.$$

where $\overset{\circ}{t}{}^s_A$ and $r^s_{\perp A}$ are characteristic parameters of a null geodesic $\{C_A\}$. In particular $\vec{r}_{\perp A}$ is the position of image A on the deflector plane. Since the direction of the initial polarization is not observable, P_A is not observable either so far as we are observing only one image A. However, the differences are observable between the rotation angles of the polarization planes of multiple images produced by the gravitational lens effect. In this section we discuss this difference between the rotation angle of the polarization plane of image A and the corresponding angle of image B.

To this end let us denote this difference by $\triangle P$,*i.e.*,

$$\begin{aligned}\triangle P &= P_A - P_B \\ &= -\frac{1}{2}\epsilon_{abc}\int_{-\infty}^{\infty} dx^0 \left[\mathring{t}^a_A \mathring{t}^\alpha_A \partial_b h_{c\alpha}(x^0, r^s_{\perp A} + \mathring{t}^s_A x^0) - \mathring{t}^a_B \mathring{t}^\alpha_B \partial_b h_{c\alpha}(x^0, r^s_{\perp B} + \mathring{t}^s_B x^0)\right].\end{aligned} \tag{6.75}$$

Here the gravitational fields are assumed to be static or stationary. Once we choose the harmonic coordinate gauge and use the post-Newtonian approximation, we can reduce eq.(6.75) to the following form:

$$\begin{aligned}\triangle P &= -\frac{1}{2}\epsilon_{abc}\int_{C_A} dx^a \partial_b h_{c0}(x^s(x^0)) + \frac{1}{2}\epsilon_{abc}\int_{C_B} dx^a \partial_b h_{c0}(x^s(x^0)) \\ &= \frac{1}{2}\epsilon_{abc}\oint_C dx^a \partial_b h_{c0}(x^s(x^0)),\end{aligned} \tag{6.76}$$

where $\{C\}$ is a closed loop such that $\{C\} = \{C_A\} - \{C_B\}$. From eq.(6.76) and Stokes' theorem, eq.(6.76) can be rewritten as

$$\begin{aligned}\triangle P &= -\frac{1}{2}\int_S d\sigma^a \left(\partial_a \partial_b h_{b0} - \Delta h_{a0}\right) \\ &= \int_S d\sigma^a R_{a0},\end{aligned} \tag{6.77}$$

where S is the surface with boundary $\{C\}$ and R_{a0} the Ricci tensor (Weinberg 1972). Then Einstein's field equation yields,

$$\begin{aligned}\triangle P &= \frac{8\pi G}{c^4}\int_S d\sigma^a T_{a0} \\ &\simeq \frac{8\pi G}{c^3}\int_S d\sigma^a (\rho v^a).\end{aligned} \tag{6.78}$$

Hereafter let us restrict ourselves to the dark lens case. If we can choose the surface S so that ρ vanishes everywhere on S, $\triangle P$ will always vanish. Now we

show that S can in fact be chosen quite freely. Consider two surfaces S_1 and S_2 sharing the same boundary $\{C\}$. The difference between $\triangle P$'s estimated on S_1 and on S_2 is given by

$$\triangle P_{S_1} - \triangle P_{S_2} = \frac{8\pi G}{c^3} \int_{\partial V} d\sigma^a (\rho v^a), \tag{6.79}$$

where $\partial V = S_1 - S_2$.

$$\triangle P_{S_1} - \triangle P_{S_2} = \frac{8\pi G}{c^3} \int_V dV \partial_a (\rho v^a), \tag{6.80}$$

with V being the volume surrounded by two surfaces S_1 and S_2. From the mass conservation law, we find

$$\partial_a (\rho v^a) = -\partial_0 \rho = 0,$$

whence $\triangle P_{S_1} = \triangle P_{S_2}$. This completes the proof that, in the dark lens case with static or stationary weak gravitational fields, the difference between the rotation angles of the polarization planes of the respective images vanishes in our approximation.

In this connection, we must notice, however, that in eq.(6.75) $\mathring{t}^a dx^0$ cannot be reduced to dx^a when the gravitational fields depend on x^0 explicitly as in the case of the gravitational fields induced by binary stars. In such cases we expect $\triangle P$ to be non-zero even for the dark lens case.

Finally let us evaluate the typical dimension of P. First we consider the case of a typical galaxy with rotational velocity $v_{gal} \sim 10^2$[km/s], radius $a_{gal} \sim 10^{17}$[km], and mass $M_{gal} \sim 10^{12} M_\odot$. From eq.(6.52), we find

$$P_{gal} \sim 10^{-3}[\text{arcsec}].$$

Next we evaluate the same quantity but for a typical cluster of galaxies with rotational velocity $v_{cl} \sim 10^3$[km/s], radius $a_{cl} \sim 10^{19}$[km], and mass $M_{cl} \sim 10^{15} M_\odot$,

to find that the rotation angle is

$$P_{cl} \sim 0.1_{[\text{arcsec}]}.$$

Besides the rotation of the polarization plane due to the gravitational lens effect, the rotation in question is caused also by magnetic fields in galaxies or in intergalactic matters (Faraday rotation). However, it is possible to distinguish the contribution from the two effects in view of the fact that the latter is proportional to λ^2 the square of the wavelength. Thus in the rotation angle-λ^2 diagram the rotation due only to the gravitational lens effect is exhibited at $\lambda = 0$.

The rotation at $\lambda = 0$ was in fact measured for the twin quasar $0957 + 561$ by VLA observation (Greenfield *et al.* 1985). In this observation, $\triangle P$ was estimated as

$$\triangle P = 0.2^\circ \pm 1.4^\circ.$$

This value coincides, within error, with the above estimation for the typical cluster of galaxies. On the other hand, in Greenfield *et al.*'s observation, their error is too large to decide whether $\triangle P$ is indeed due to the gravitational Faraday effect. We expect that more accurate observations of 0957+561 will indicate a non-zero value of $\triangle P$.

7. Gravitational Lens Effect on the Redshift-Volume Measurement

One of the long-standing problems in which many astronomer and physicists have been interested is whether the Universe is open, flat or closed, namely, what value the density parameter 'Ω_0' takes? This problem is associated with most of astrophysical or cosmophysical problems such as galaxy formation, non-uniform motions of galaxies *etc.*. Many people who accept the inflationary universe seem to prefer $\Omega_0 = 1$ to other values, while most observations of Ω_0 show lower values.

Recently Loh and Spillar (1986), however, obtained the redshifts of a thousand of galaxies not by the spectroscopic method but by the photometric method, their observed flux ℓ being greater than some threshold value ℓ_0. They then estimated the density parameter as $\Omega_0 \approx 1$. In their analysis they assumed that the number of galaxies are conserved and that all galaxies evolve by the same amount in luminosity

On the other hand, Bahcall and Tremaine (1988), Caditz and Petrosian (1989), and Yoshii and Takahara (1989) reanalyzed Loh and Spillar's data without making Loh and Spillar's second assumption. They found that the evolution of galaxies affects the value of the density parameter and showed that $\Omega_0 \approx 0.2$, which is comparable with the value determined by other observations.

In their arguments, the above authors assumed implicitly that the Universe in the scale of $z \sim 1$ is described by the Friedmann-Robertson-Walker universe (hereafter to be abbreviated as FRW universe) in which the Universe is filled with isotropic and homogeneous perfect fluid, and adopted Mattig's formula for the redshift-angular diameter distance relation.

Recently it has been found, however, that the Universe has large inhomogeneities in the scale $30 \sim 50$[Mpc] concerning galaxy-distribution, and moreover has voids extending over 50[Mpc]. Obviously, such a new situation does not permit us to adopt Mattig's formulae any longer.

That is to say, we have now to take into account inhomogeneities, which may cause the gravitational lens effect for propagating light beams. Hammer and Nottale (1986) investigated the gravitational amplification effect, due to foreground galaxies, on the Hubble diagram, with the conclusion that this effect decreases the value of the deceleration parameter q_0.

In our paper we adopt the clumpy universe model, proposed by Dyer and Roeder (1972), as a possibly more realistic universe model than the FRW universe. Thus in our case, all matters are supposed to be concentrated into clumps such as galaxies, while the global structure of the Universe is assumed to be described by the FRW universe. The light emitted from a source propagates in the empty space to be received by the observer. In the way of the propagation the light beams may suffer the gravitational amplification effect from the clumps. Since all the clumps are assumed to be uniformly distributed, we have to treat their gravitational amplification effect statistically.

In this chapter, we will discuss the gravitational amplification effect on the redshift-volume measurement, which is one of the geometrical tests of Ω_0. First in §7.1 we present a formulation of statistical gravitational lens effect on flux moments. In the next section (§7.2), on the basis of our formulation, we will investigate how deeply the gravitational amplification effect influences on the measurement of Ω_0. Our results are summarized in the last section.

7.1 General Formulation of the Flux Moments under the Gravitational Lens Effect

In this section we first introduce, following Caditz and Petrosian (1989), the kth flux moment in the FRW universe. Next we extend the flux moments thus obtained to those in our universe model mentioned above.

The kth flux moment obtainable from those observations of galaxies in which the observed flux is $\ell > \ell_0$ and the redshift is within the interval

$[z_0 - \Delta z/2, z_0 + \Delta z/2]$ is defined as:

$$M_k(z_0, \ell_0) = \int_{z_0-\Delta z/2}^{z_0+\Delta z/2} dz \int_{\ell_0}^{\infty} \left(\frac{\ell}{\ell_0}\right)^k n(z, \ell) d\ell \qquad (k = 0, 1, 2 \ldots). \tag{7.1}$$

It depends on the cosmological parameters and on the luminosity function which gives information about the brightness distribution of galaxies. If the kth flux moment has n unknown parameters such as the density parameter or the cosmological constant, we can determine the above parameters from the first n flux moments. For example, when we have two unknown parameters in the flux moment, we have only to consider the 0th moment (the number counts of galaxies: N) and the 1st moment (the total flux from observed galaxies brighter than the minimum flux ℓ_0: F/ℓ_0).

Before deriving the flux moments in our universe model we first review those in the FRW universe. The metric and the volume element of the FRW universe are given by

$$ds^2 = c^2 dt^2 - R^2(t)\Big[\frac{dr^2}{1 - kr^2} + r^2(d\theta^2 + \sin^2\theta d\phi^2)\Big], \tag{7.2}$$

and

$$\begin{aligned} dV &= \frac{R^3 r^2 dr}{\sqrt{1 - kr^2}} \sin\theta d\theta d\phi \\ &= \Big(\frac{c}{H_0}\Big)^3 \frac{D^2(z) dz \sin\theta d\theta d\phi}{(1 + z)\chi(z)}, \end{aligned} \tag{7.3}$$

where $D(z)$ is the angular diameter distance (see Appendix C-(a)) which is measured in units of $\left(\frac{c}{H_0}\right)$. The $\chi(z)$ in (7.3) is given by

$$\chi(z) = \sqrt{\Omega_0(1 + z)^3 + \lambda_0 - K(1 + z)^2},$$

where the Hubble constant is expressed as $H_0 = (\dot{R}/R)_0$, the cosmological constant as $\lambda_0 = \Lambda_0 c^2/3{H_0}^2$, the density parameter as $\Omega_0 = 8\pi G\rho_0/3{H_0}^2$, the effective curvature as $K = \Omega_0 + \lambda_0 - 1$ and the deceleration parameter as $q_0 = -(\ddot{R}R/\dot{R}^2)_0$.

In (7.1) the number of galaxies with the observed flux $[\ell, \ell + d\ell]$ at redshift $[\mathrm{z}, \mathrm{z} + dz]$ is expressed, in terms of the intrinsic luminosity L of the source, as

$$n(\mathrm{z}, \ell) dz d\ell = \left(\frac{c}{\mathrm{H}_0}\right)^3 \frac{\Phi(\mathrm{z}, L) D^2(\mathrm{z})}{(1+\mathrm{z})\chi(\mathrm{z})} dz d\omega dL, \tag{7.4}$$

where $\Phi(\mathrm{z}, L)$ is called the "luminosity function" which must be determined by observations and represents the number density of galaxies with redshift z and L. The luminosity relation between the observed flux and L is given by

$$\ell = \frac{L}{4\pi \left(\frac{c}{\mathrm{H}_0}\right)^2 D^2(\mathrm{z})(1+\mathrm{z})^3}. \tag{7.5}$$

With eqs.(7.3)-(7.5) we can express the kth flux moment (7.1) as

$$\mathrm{M}_k(\mathrm{z}_0, \ell_0) = \int_{\mathrm{z}_0 - \Delta \mathrm{z}/2}^{\mathrm{z}_0 + \Delta \mathrm{z}/2} dz \left(\frac{c}{\mathrm{H}_0}\right)^3 \frac{D^2(\mathrm{z})}{(1+\mathrm{z})\chi(\mathrm{z})} \int_{L_0}^{\infty} \left(\frac{L}{L_0}\right)^k \Phi(\mathrm{z}, L) dL, \tag{7.6}$$

where $L_0 = 4\pi \left(\frac{c}{\mathrm{H}_0}\right)^2 (1+\mathrm{z})^3 D^2(\mathrm{z}) \ell_0$.

The luminosity function $\Phi(\mathrm{z}, L)$ of galaxies can be determined from surveys for redshifts, luminosities and the number of galaxies with low redshifts $\mathrm{z} \ll 1$, and is shown to be fitted well with the Schechter form (Schechter 1976, Felten 1985, Efstathiou *et al.* 1988 and Lapparent *et al.* 1989) given by

$$\Phi(\mathrm{z}, L) dL = (1+\mathrm{z})^3 \phi^* \left(\frac{L}{L^*}\right)^{\alpha} \exp\left[-\frac{L}{L^*}\right] d\left(\frac{L}{L^*}\right), \tag{7.7}$$

where ϕ^*, α and L^* are to be observationally determined. Now let us assume, following Loh and Spillar (1986), that ϕ^*, α and L^* have negligible dependences both on redshifts and on galaxy-types.

Then the kth flux moment with the Schechter form (7.7) is given by

$$\mathrm{M}_k(\mathrm{z}_0, \ell_0) = (\frac{c}{\mathrm{H}_0})^3 \mathrm{z}_0^2 \triangle \mathrm{z} d\omega \phi^* \xi(\mathrm{z}_0) G_k(x_0) x_0^{-k}, \tag{7.8}$$

where

$$\xi(\mathrm{z}) = \frac{D^2(\mathrm{z})(1+\mathrm{z})^2}{\mathrm{z}^2 \chi(\mathrm{z})},$$

$$G_k(x_0) = \int_{\mathrm{z}_0-\triangle \mathrm{z}/2}^{\mathrm{z}_0+\triangle \mathrm{z}/2} \frac{dz}{\triangle \mathrm{z}} \frac{\chi(\mathrm{z}_0)}{\chi(\mathrm{z})} (\frac{1+\mathrm{z}_0}{1+\mathrm{z}})^{3k-2} \left\{ \frac{D(\mathrm{z}_0)}{D(\mathrm{z})} \right\}^{2k-2} \Gamma(\alpha + k + 1; \frac{D^2(\mathrm{z})(1+\mathrm{z})^3}{D^2(\mathrm{z}_0)(1+\mathrm{z}_0)^3} x_0),$$

$$x_0 = \frac{4\pi (\frac{c}{\mathrm{H}_0})^2 D^2(\mathrm{z}_0)(1+\mathrm{z}_0)^3 \ell_0}{L^*}.$$

In the above equations $\xi(\mathrm{z})$ represents the deviation of the volume element from $(\frac{c}{\mathrm{H}_0})^3 \mathrm{z}^2 \triangle \mathrm{z}$, and $\Gamma(a; x)$ is the incomplete gamma function defined by

$$\Gamma(a; x) = \int_x^\infty dt \exp(-t) t^{a-1}. \tag{7.9}$$

By determining the dependence of ξ on the cosmological parameters from observations, we can determine the geometry of the Universe.

Next we estimate the kth flux moment in the clumpy universe model (Dyer & Roeder 1972) which is possibly a realistic model of the inhomogeneous universe. In so doing we assume that the Universe is described globally by the FRW universe, and locally by the clumpy universe in which all matters are concentrated into clumps. The light which passes near a clump may suffer the gravitational amplification effect from the clump. We can therefore regard such a clump as a gravitational lens object. Most of the equations derived for the FRW universe, except the luminosity relation, can be used in our universe here well as.

In the clumpy universe the luminosity relation must be modified as follows: since the light mostly propagates not through the space with the mean density

of the Universe but in almost empty space, the angular diameter distance in the clumpy universe differs from that in the homogeneous universe. Dyer and Roeder showed that the angular diameter distance $\tilde{D}(\mathrm{z})$ in units of $\left(\frac{c}{\mathrm{H_0}}\right)$ is given by

$$\tilde{D}(\mathrm{z}) = \int_0^{\mathrm{z}} \frac{d\mathrm{z}}{(1+\mathrm{z})^2\chi(\mathrm{z})}, \tag{7.10}$$

(see Appendix C-(b)).

It is to be noticed here that we are concerned with two kinds of angular diameter distance — $D(\mathrm{z})$ and $\tilde{D}(\mathrm{z})$. The former appears in the volume element of the Universe, because the Universe is assumed to be globally homogeneous. On the other hand, the latter has to be used in the luminosity function because the light propagates through the space with sparse matters.

Suppose that the light passes near a clump, and is brightened by a factor μ owing to the gravitational amplification effect. The luminosity relation is then given by

$$\ell = \frac{\mu\tilde{L}}{4\pi\left(\frac{c}{\mathrm{H_0}}\right)^2\tilde{D}^2(\mathrm{z})(1+\mathrm{z})^3}, \tag{7.11}$$

where $\tilde{L}$ is the intrinsic luminosity of the source corresponding to the observed flux ℓ in the inhomogeneous universe.

With the luminosity relation (7.11), the number of galaxies with observed flux $[\ell, \ell + d\ell]$ within the redshift interval $[\mathrm{z}, \mathrm{z} + d\mathrm{z}]$ is given by

$$\tilde{n}(\mathrm{z},\ell)d\mathrm{z}d\ell = \left(\frac{c}{\mathrm{H_0}}\right)^3 \frac{D^2(\mathrm{z})d\omega d\mathrm{z}d\tilde{L}}{(1+\mathrm{z})\chi(\mathrm{z})} \int_{\mu_0}^{\infty} d\mu p(\mathrm{z},\mu)\Phi(\mathrm{z},\tilde{L}), \tag{7.12}$$

where $p(\mathrm{z},\mu)$ is the probability distribution for the case when lights are brightened by a factor μ owing to the gravitational amplification effect. In eq.(7.12) μ_0 is the minimum amplification factor, to be defined later.

Then the kth flux moment in the inhomogeneous universe is expressed as

$$\tilde{\mathrm{M}}_k(\mathrm{z}_0,\ell_0) = \int_{\mathrm{z}_0-\Delta\mathrm{z}/2}^{\mathrm{z}_0+\Delta\mathrm{z}/2} dz\Big(\frac{c}{\mathrm{H}_0}\Big)^3 \frac{D^2(\mathrm{z})}{(1+\mathrm{z})\chi(\mathrm{z})} \int_{\mu_0}^{\infty} d\mu p(\mathrm{z},\mu) \times \int_{\tilde{L}_0}^{\infty} d\tilde{L}\Big\{\frac{\mu\tilde{L}}{4\pi\big(\frac{c}{\mathrm{H}_0}\big)^2\tilde{D}^2(\mathrm{z})(1+\mathrm{z})^3\ell_0}\Big\}^k \Phi(\mathrm{z},\tilde{L}), \tag{7.13}$$

where $\mu\tilde{L}_0 = 4\pi(1+\mathrm{z})^3\tilde{D}^2(\mathrm{z})\ell_0$. We adopt the Schechter form (7.7) as the luminosity function, thereby obtaining $\tilde{\mathrm{M}}_k$ as follows,

$$\tilde{\mathrm{M}}_k(\mathrm{z}_0,\ell_0) = \Big(\frac{c}{\mathrm{H}_0}\Big)^3 \mathrm{z}_0^2 \,\Delta\, \mathrm{z} d\omega\phi^*\xi(\mathrm{z}_0)\tilde{G}_k(\tilde{x}_0)\tilde{x}_0^{-k}, \tag{7.14}$$

where

$$\tilde{G}_k(\mathrm{z}_0,\tilde{x}_0) = \int_{\mathrm{z}_0-\Delta\mathrm{z}/2}^{\mathrm{z}_0+\Delta\mathrm{z}/2} \frac{dz}{\Delta\mathrm{z}} \frac{\chi(\mathrm{z}_0)}{\chi(\mathrm{z})}\Big(\frac{1+\mathrm{z}_0}{1+\mathrm{z}}\Big)^{3k-2} \frac{D^2(\mathrm{z})}{D^2(\mathrm{z}_0)}\Big(\frac{\tilde{D}(\mathrm{z}_0)}{\tilde{D}(\mathrm{z})}\Big)^{2k} \times \int_{\mu_0}^{\infty} d\mu\mu^k p(\mathrm{z},\mu)\Gamma\Big(\alpha+k+1;\frac{1}{\mu}\Big(\frac{1+\mathrm{z}}{1+\mathrm{z}_0}\Big)^3\frac{\tilde{D}^2(\mathrm{z})}{\tilde{D}^2(\mathrm{z}_0)}\tilde{x}_0(\mathrm{z}_0)\Big), \tag{7.15}$$

and

$$\tilde{x}_0(\mathrm{z}_0) = \frac{4\pi\big(\frac{c}{\mathrm{H}_0}\big)^2\tilde{D}^2(\mathrm{z}_0)(1+\mathrm{z}_0)^3\ell_0}{L^*}. \tag{7.16}$$

Finally we have to define the probability distribution $p(\mathrm{z},\mu)$, which depends on the distribution of galaxies in the inhomogeneous universe and also on the type of clump models employed as gravitational lenses. The form of $p(\mathrm{z},\mu)$ has been discussed by many authors (Press & Gunn 1973, Weinberg 1976, Canizares 1981, Vietri & Ostriker 1983, Peacock 1986, Ehlers & Schneider 1986, and Issacson & Canizares 1989).

We review the derivation of the probability distribution in Appendix D. Let us assume that the clumps which act as gravitational lenses are uniformly distributed in the inhomogeneous universe, and that all the clumps have point-like structures. The probability distribution is then given by

$$p(z_S,\mu)=\frac{3\Omega_0}{\sqrt{(\mu^2-1)^3}}\frac{\tilde{D}(z_S)}{D^2(z_S)}\int_0^{z_S}dz_L\frac{(1+z_L)^2D^2(z_L)\tilde{D}_{SL}}{\chi(z_L)\tilde{D}(z_L)}, \tag{7.17}$$

(Ehlers & Schneider 1986), where z_L and z_S are the redshifts of the clump acting as a gravitational lens and of the galaxy (source) of the light, respectively. In (7.17) $\tilde{D}_{LS}$ is the angular diameter distance form the source to a clump and is given, in units of $\left(\frac{c}{H_0}\right)$, by

$$\tilde{D}_{SL}(z_L,z_S)=(1+z_L)\int_{z_L}^{z_S}\frac{dz}{(1+z)^2\chi(z)}. \tag{7.18}$$

From (7.15) and (7.18), we have

$$\begin{aligned}\tilde{G}_k(z_0,\tilde{x}_0)=&3\Omega_0\int_{z_0-\Delta z/2}^{z_0+\Delta z/2}\frac{dz_S}{\Delta z}\frac{\chi(z_0)}{\chi(z_S)}\left(\frac{1+z_0}{1+z_S}\right)^{3k-2}\frac{D^2(z_S)}{D^2(z_0)}\left(\frac{\tilde{D}(z_0)}{\tilde{D}(z_S)}\right)^{2k}\\&\times\int_0^{z_S}dz_L\frac{(1+z_L)^2D^2(z_L)\tilde{D}_{SL}(z_L,z_S)}{\chi(z_L)\tilde{D}(z_L)}\\&\times\int_{\mu_0}^{\infty}d\mu\frac{\mu^k}{\sqrt{(\mu^2-1)^3}}\Gamma\left(\alpha+k+1,\frac{1}{\mu}\left(\frac{1+z_S}{1+z_0}\right)^3\frac{\tilde{D}^2(z_S)}{\tilde{D}^2(z_0)}\tilde{x}_0(z_0)\right),\end{aligned} \tag{7.19}$$

Since the Universe is assumed to be described globally by the FRW universe, it is required that the luminosity relation of the present case, on average, must be the same as that in the case of the FRW universe. This imposes the following

constraint:

$$\int_{\mu_0}^{\infty} d\mu p(z,\mu)\frac{\mu L}{4\pi\left(\frac{c}{H_0}\right)^2\tilde{D}^2(z)(1+z)^3}=\frac{L}{4\pi\left(\frac{c}{H_0}\right)^2 D^2(z)(1+z)^3},$$

i.e.,

$$\frac{1}{\tilde{D}^2(z_S)}\int_{\mu_0}^{\infty}\mu p(z_S,\mu)d\mu=\frac{1}{D^2(z_S)}, \tag{7.20}$$

from which $\mu_0(z_S)$ is found to be

$$\mu_0^2(z_S)=1+\left[\frac{3\Omega_0}{\tilde{D}(z_S)}\int_0^{z_S}dz_L\frac{(1+z_L)^2D^2(z_L)\tilde{D}_{SL}(z_L,z_S)}{\chi(z_L)\tilde{D}(z_L)}\right]^2. \tag{7.21}$$

It is reasonable that the lower limit μ_0 of the amplification factor μ is larger than unity because μ is the total amplification factor of those two images produced by point-like lenses which are assumed to be too close to be separated.

Now, from (7.14), (7.19) and (7.21) we have the full formulation of $\tilde{M}_k$. In the next section we reanalyze Loh-Spillar's data by using $\tilde{M}_k$

7.2 Reanalysis of Loh-Spillar's Observational Data

According to Loh and Spillar (1986), and Caditz and Petrosian (1989), the ratios $C_k(z_0,\ell_0)$ in the inhomogeneous universe can be defined as

$$C_k(z_0,\ell_0)=\frac{\tilde{M}_k(z_0,\ell_0)}{\tilde{M}_{k-1}(z_0,\ell_0)}. \tag{7.22}$$

The above dimensionless quantities can be obtained from observations. From (7.14), C_k is rewritten as

$$C_k(z_0,\ell_0)=\frac{\tilde{G}_k(z_0,\tilde{x}_0,\varsigma_i)}{\tilde{x}_0\tilde{G}_{k-1}(z_0,\tilde{x}_0,\varsigma_i)}\qquad(i=1,2,\ldots), \tag{7.23}$$

where ς_i's $(i=1,2,\ldots)$ are the cosmological parameters and the parameters

which appear in the expression for the luminosity function. If we have a sufficient number of observed C_k's, we can determine these parameters from (7.23).

Loh and Spillar (1986) measured the first two flux moments within three redshift bins having width Δz centered at z_0 (= 0.25, 0.50 and 0.75). They found $\Omega_0 \sim 1$ assuming that the light propagates in the FRW universe without λ_0 and that the power-law index α in the luminosity function $\Phi(z, L)$ is independent of redshifts and galaxy-types. The first two flux moments determine the first ratio C_1 which they called the "completeness ": The quantity represents the measure of how deeply observations were carried out.

Now we will reanalyze Loh-Spillar's observational data by using $\tilde{M}_k$. Although Loh and Spillar did not give the values of C_1 explicitly in their paper, we can determine these values with their data on $x_0(z_0)$ as $C_1 = 2.94, 2.87$ and 2.10 at $z_0 = 0.25, 0.50$ and 0.75, respectively.

Next we have to determine the value of α in $\Phi(z, L)$. Following Efstathiou *et al.* (1988), we adopt their value $\alpha = -1.07$ instead of $\alpha = -1.25$ used by Loh and Spillar. The dependence of the final results on the choice of α will be discussed below.

In order to compare the flux moments in which the gravitational amplification is taken into account with those in the FRW universe, we calculate, for the same values of C_1, the ratio $\tilde{G}_0/G_0$, which is independent of ϕ^* and L^*. Fig.7.1 is for the dependence of $\tilde{G}_0/G_0$ on the value of Ω_0, and shows that the gravitational amplification effect on the number counts N of galaxies cannot be ignored. The deviation of $\tilde{G}_0/G_0$ from unity increases as redshift of the source of light becomes large, since the probability function shows the same behavior, that is, the chances that the light is gravitationally amplified increase as the distance between the source of lights and ourselves becomes large.

Let us now evaluate Ω_0 and ϕ^*, assuming that $\lambda_0 = 0$ (*i.e.*, $\Omega_0 = 2q_0$), in the cases of the FRW universe and of the clumpy universe model: this is necessary because our choice of α is different from Loh and Spillar's. We assume moreover

Table 7.1 Ω_0 and ϕ^*: the FRW universe vs. the inhomogeneous universe

	Density parameter Ω_0	$\phi^* \times 10^{-2} h^3_{[Mpc^{-3}]}$ [1)]
In the FRW universe	1.77 ± 0.89	1.59 ± 0.44
In the inhomogeneous universe	0.39 ± 0.44	1.04 ± 0.31

1) $H_0 = 100h_{[km/sMpc]}$.

that the parameters in the luminosity function are independent of redshift and galaxy-types. The results are given in Table 7.1.

It should be noticed that our value of Ω_0 in the FRW universe is larger than the corresponding value of Loh and Spillar. This shows that the value of Ω_0 depends on the choice of α

We find that the value of Ω_0 in the inhomogeneous universe is smaller than that in the FRW universe. It should be emphasized that when the gravitational lens effect is taken into account for the redshift-volume measurement the value of Ω_0 is decreased, as Hammer and Nottale (1986) showed on the Hubble diagram.

7.3 Discussion and Summary

We have discussed the influence of the gravitational amplification effect on Loh and Spillar's redshift-volume measurement and have shown that this effect decreases the value of Ω_0. This result clearly indicates that we must not ignore the gravitational lens effect when determining the cosmological parameters.

By using Loh and Spillar's unpublished data, Caditz and Petrosian (1989) estimated the first three flux moments in the FRW universe and suggested that the power-law index α in the luminosity function depends on redshift z_0. On the other hand, Bahcall and Tremaine (1988), and Yoshii and Takahara (1989) showed that the value of Ω_0 is dependent on types of galaxies considered in Φ.

In the previous sections, we have not taken into account the evolutionary effects and have restricted ourselves to discussion of the influence of the gravitational amplification effect on the redshift-volume measurement. Our result shows that in order to obtain a reliable value of Ω_0 from observation we have to take into account not only the evolutionary effects of galaxies but also the gravitational amplification effect.

As discussed by Press and Gunn (1973) and others, the approximation of point-like lenses is very good for clumps with mass $\lesssim 10^6 M_\odot$. If clumps are galaxies, our approximation, however, is not always good, and some better approximations for lenses are needed. At any rate it is important to investigate the dependence of Ω_0 on types of lens models employed, and this is one of our future problems.

8. Summary

In this thesis we have discussed various problems concerning the gravitational lens effects. In this chapter we will summarize our results of Chapter 4 – Chapter 7.

In Chapter 4 we have discussed the multiple quasar 1115+080 regarding as a multiple-image system. To specify the deflector of the system, we have adopted the dark lens model with dipole and quadrupole moments. The parameters contained in our model have been fixed by substituting observed data (*i.e.* positions of the deflector and images A_1, B and C) into the lens equation. In fixing these parameters we did not use observed flux ratios between the images. The calculated luminosity ratios need not necessarily coincide with observed data, because the intrinsic luminosity of the source may evolve with time. From these fixed parameters we can further predict the existence of a new image (the fifth image) although it may be difficult to observe the image because of its faintness.

We have evaluated the travel time differences between the images, and found that our estimation is compatible with Vanderriest *et al.*'s values (1986). From our estimation we can conclude that the intrinsic luminosity of the light source has time evolution.

Further, we have evaluated the mass of the deflector using two methods: the method proposed by Borgeest (1986) and the one proposed by ourselves. In our method, it is possible to judge whether the deflector model employed is valid or not by comparing the observed travel time differences with calculated ones, whereas this is not the case with Borgeest's method. From estimations with both methods we have found that the deflector has the mass of a typical galaxy. This fact may appear not to be consistent with Christian *et al.*'s observation. We should say, however, that richness of much faint or dark matters in the deflector is responsible for the above apparent discrepancy. Furthermore, combining our mass estimations by the two methods, we found that a constraint is imposed on the Hubble constant H_0.

In Chapter 5, we have pointed out that apparent superluminal motions are possible in a gravitationally lensed system. Our conclusion is that, if the source passes near one of the caustics on the source plane, however normally the source may move, some images appear to us to be moving away from each other with apparent superluminal velocities. We thus expect that there is a possibility of observing apparent superluminal motions in the gravitational lens system in which the bright images have small separations from each other, as in the case of images A_1 and A_2 of system 1115+080.

In Chapter 6 the rotation of the polarization plane by a weak gravitational field is discussed. First we have constructed the parallel propagator for the polarization vector in terms of a null tetrad in the post-Newtonian approximation. Next we have extended the formula given by Plebanski (1961) for a spherical deflector to the case of a spheroidal deflector. It is then found that no rotation of the polarization plane occurs in the case of any spheroidal dark lens, as Plebanski suggested for the case of a spherical deflector. It can be proved that the difference between the rotation angles of the polarization planes is absent in the general case of dark lens if the gravitational field is weak and stationary.

In Chapter 7 we have investigated the influence of the gravitational lens effect on the redshift-volume measurement of the density parameter Ω_0, and given a general formula for the kth flux moment in the clumpy universe model representing the inhomogeneous universe. In this case inhomogeneities are regarded as gravitational lens objects which amplify the flux of lights, and they are treated statistically. In so doing we have adopted the probability function given by Ehlers and Schneider (1986). It is thereby found that the gravitational amplification effect on the redshift-volume measurement is not negligible, and that the effect in fact decreases Ω_0, as Hammer and Nottale (1986) pointed out in connection with the Hubble diagram.

Finally we wish to emphasize that the gravitational lens effect does in fact provide us with a good tool for investigating dark matters, intergalactic matters,

Ly-α forests and others. At any rate, it is true indeed that no astronomical observations can be free from this effect.

ACKNOWLEDGMENTS

I would like to express my sincere gratitude to Dr. M.Omote for introducing me to the problems of the gravitational lens effect and for stimulating discussion. I also wish to thank Prof. S.Kamefuchi for careful reading of the manuscript and for useful advice. I am grateful to Prof. Y.Hara, Prof. Y.Iwasaki, Prof. A.Ukawa and other members of the institute for theoretical physics of University of Tsukuba for valuable and stimulating conversations. I am thankful, in particular, to Dr. K.Odaka and Dr. Y.Tsuboi for helpful advice and for their warm friendship.

My thanks are also due to Prof. Y.Takaku, Dr. T.Kobayashi and Mr. S.Higuchi of Fukushima Medical College for their strong support of the present research and constant encouragement.

APPENDIX A

Estimation of $|\xi_{\pm}|$

In this appendix we will estimate $|\xi_{\pm}|$ which is given by eq.(5.66) and to satisfy the equation

$$w(1+\epsilon)\xi^2 - 2\big(r_{\perp} + \frac{ie^2 \sin\gamma\cos\gamma}{1-e^2\cos^2\gamma} z_{\|}\big)\xi + w(1-\epsilon) = 0. \tag{A1}$$

Then $|\xi_+\xi_-|$ is smaller than unity because of

$$|\xi_+\xi_-| = |\frac{1-\epsilon}{1+\epsilon}|.$$

It follows from the above relation that either ξ_+ or ξ_- is in the unit circle $|\xi| = 1$. In introducing two real parameters X and Y and one complex ζ such that

$$X = r_{x_{\perp}}, \quad Y = r_{y_{\perp}} + \frac{e^2 \sin\gamma\cos\gamma}{1-e^2\cos^2\gamma} z_{\|}, \quad \zeta = X + iY, \tag{A2}$$

we can express $\xi_{\pm}$ as

$$\begin{aligned} \xi_{\pm} &= \frac{\zeta \pm \sqrt{\zeta^2 - w^2(1-\epsilon^2)}}{w(1+\epsilon)} \\ &= \frac{\zeta + A_{\pm} + iB_{\pm}}{w(1+\epsilon)}, \end{aligned} \tag{A3}$$

where

$$A_{\pm} = \pm \operatorname{sgn}(X)\sqrt{\tfrac{1}{2}\big[\sqrt{\{X^2 - Y^2 - w^2(1-\epsilon^2)\}^2 + 4X^2Y^2} + X^2 - Y^2 - w^2(1-\epsilon^2)\big]}, \tag{A4}$$

$$B_{\pm} = \pm \operatorname{sgn}(Y)\sqrt{\tfrac{1}{2}\big[\sqrt{\{X^2 - Y^2 - w^2(1-\epsilon^2)\}^2 + 4X^2Y^2} - X^2 + Y^2 + w^2(1-\epsilon^2)\big]}. \tag{A5}$$

a) In the dark lens case

In the dark lens case arbitrary w satisfies

$$w^2 \leq X^2 + \frac{Y^2}{\epsilon^2}, \tag{A6}$$

which is the condition for the dark lens. From relation (A6), we find that

$$\begin{aligned} A_{\pm}^2 &\geq \epsilon^2 X^2, \\ B_{\pm}^2 &\geq w^2 - X^2, \\ (A_+ X + B_+ Y) &\geq \epsilon w^2. \end{aligned} \tag{A7}$$

This completes the proof of $|\xi_+|^2 \geq 1$.

b) In the transparent lens case

In the transparent lens case the condition to be satisfied is: for some w,

$$w^2 \geq X^2 + \frac{Y^2}{\epsilon^2}. \tag{A8}$$

We can thus show that $|\xi_{\pm}| \leq 1$ for some w, because

$$\begin{aligned} A_{\pm}^2 &\leq \epsilon^2 X^2, \\ B_{\pm}^2 &\leq w^2 - X^2, \\ (A_+ X + B_+ Y) &\leq \epsilon w^2, \end{aligned} \tag{A9}$$

and $|\xi_+| \geq |\xi_-|$.

APPENDIX B

Evaluations of Rotation Angles for Simple Deflector models

In this appendix we give $\overline{\alpha}_0$ and P, defined in eqs.(5.56) and (5.77), respectively, for two simple examples of mass densities distribution of a deflector with spheroidal symmetry. We introduce the following parameters:

$$\xi = \frac{a_m \sin\beta}{r_\perp}, \quad \eta = \frac{A_\perp}{a_m} \quad \text{and} \quad \delta = \sqrt{1 - \frac{B_\perp^2}{a_m^2}}, \tag{B1}$$

where a_m is the major radius of the deflector beyond which the mass density vanishes, and

$$\sin\beta = e\sin\gamma, \quad A_\perp = \cot\beta\Big(r_{x_\perp} + \frac{ir_{y_\perp}}{\cos^2\beta}\Big) \text{ and } B_\perp^2 = r_{x_\perp}^2 + \frac{r_{y_\perp}^2}{\cos^2\beta}.$$

A useful relation among the above parameters is

$$\xi^{-2} + \eta^2 - \delta^2 = 1, \tag{B2}$$

(Bourassa & Kantowski 1975).

a) $\rho = Constant$

$$\rho(a) = \begin{cases} \frac{3M}{4\pi\sqrt{1-e^2}a_m^3}, & (a \le a_m), \\ 0, & (a > a_m), \end{cases} \tag{B3}$$

where M and $\sqrt{1-e^2}$ are the total mass and the axial ratio of the deflector, respectively.

The deflection angle $\overline{\alpha}_0$ obtained by ignoring the deflector rotation was given

by BK as:

$$\overline{\alpha}_0 = -\frac{3GM}{c^2 a_m \sin\beta}\Big[\frac{2}{\xi} + (1-\frac{1}{\xi^2})\ln(\frac{1+\xi}{1-\xi}) - \Big\{2\eta\delta + (1-\frac{1}{\xi^2})\ln(\frac{\eta+\delta}{\eta-\delta})\Big\}\Theta(a_m - B_\perp)\Big], \tag{B4}$$

and the rotation angle P of the polarization plane is expressed as

$$P = \frac{3GM}{c^3}\omega\cos\gamma\Big[\tfrac{4}{3}\sin\beta\delta^3 - \frac{\sin\beta}{\sqrt{1-e^2\cos^2\gamma}}Re\Big\{\Big(\frac{\delta^2-\eta^2\cot^2\beta}{\xi}\Big)\ln\Big(\frac{\eta+\delta\tan\beta}{\eta-\delta\tan\beta}\Big) + \frac{2\eta\delta\cot\beta}{\xi}\Big\} + Re\Big\{\Big(\frac{\delta^2-\eta^2}{\xi}\Big)\ln\Big(\frac{\eta+\delta}{\eta-\delta}\Big) + \frac{2\eta\delta}{\xi}\Big\}\Big]\Theta(a_m - B_\perp). \tag{B5}$$

b) $\rho \propto 1/a$

$$\rho(a) = \begin{cases} \frac{M}{2\pi\sqrt{1-e^2a_m^2}}\frac{1}{a}, & (a \le a_m), \\ 0, & (a > a_m), \end{cases} \tag{B6}$$

where M and $\sqrt{1-e^2}$ have the same meanings as in a).

The deflection angle $\overline{\alpha}_0$ is

$$\overline{\alpha}_0 = -\frac{4GM}{c^2 a_m \sin\beta}\Big[\ln(\frac{1+\xi}{1-\xi}) + \frac{1}{\xi}\ln(1-\xi^2) + \Big\{\ln(\frac{\eta-\delta}{\eta+\delta}) + \frac{1}{\xi}\ln(\frac{\eta\xi+\delta}{\eta\xi-\delta}) + \eta\ln(\frac{1-\delta}{1+\delta})\Big\}\Theta(a_m - B_\perp)\Big], \tag{B7}$$

(BK), and P is expressed as

$$P = \frac{4GM}{c^3}\omega\cos\gamma\Big[\sin\beta\Big\{\delta - \tfrac{1}{2}(1-\delta^2)\ln\tfrac{1+\delta}{1-\delta}\Big\} - \frac{\sin\beta}{\sqrt{1-e^2\cos^2\gamma}}Re\Big\{\frac{1}{\xi}\ln\Big(\frac{\eta+\delta\tan\beta}{\eta-\delta\tan\beta}\Big) + \frac{\eta}{\xi}\cot\beta\ln\frac{1+\delta}{1-\delta} + \frac{1}{\xi^2}\sqrt{1-(1-\cot^2\beta)\eta^2\xi^2}\ln\Big(\frac{\eta\xi\cot\beta - \delta\sqrt{1-(1-\cot^2\beta)\eta^2\xi^2}}{\eta\xi\cot\beta + \delta\sqrt{1-(1-\cot^2\beta)\eta^2\xi^2}}\Big)\Big\} + Re\Big\{\frac{1}{\xi}\ln\frac{\eta+\delta}{\eta-\delta} + \frac{\eta}{\xi}\ln\frac{1+\delta}{1-\delta} + \frac{1}{\xi^2}\ln\frac{\eta\xi-\delta}{\eta\xi+\delta}\Big\}\Big]\Theta(a_m - B_\perp). \tag{B8}$$

APPENDIX C

Angular Diameter Distance

In this appendix we review the derivation of the angular diameter distance both in the Friedmann-Robertson-Walker universe (hereafter abbreviated FRW universe) which is filled with isotropic and homogeneous perfect fluid and in the locally inhomogeneous universe.

a) *FRW universe*

The metric of the FRW universe is given by

$$ds^2 = c^2dt^2 - R^2(t)\Big[\frac{dr^2}{1-kr^2} + r^2(d\theta^2 + \sin^2\theta d\phi^2)\Big]. \tag{C1}$$

The energy-momentum tensor for this case is expressed as

$$T^{\mu}{}_{\nu} = diag(\rho c^2, 0, 0, 0). \tag{C2}$$

The fundamental equations in cosmology are derived from the Einstein field equations:

$$\begin{aligned} \Big(\frac{\dot{R}}{R}\Big)^2 &= \frac{8\pi G\rho}{3} - \frac{kc^2}{R^2} + \frac{\Lambda_0 c^2}{3}, \\ \frac{2\ddot{R}}{R} + \Big(\frac{\dot{R}}{R}\Big)^2 &+ \frac{kc^2}{R^2} - \Lambda_0 c^2 = 0, \end{aligned} \tag{C3}$$

where the dot denotes the derivative with respect to the comoving time 't'. Let us introduce four cosmological parameters; H_0, Ω_0, q_0 and λ_0:

$$\begin{aligned} &\text{the Hubble constant} && H_0 = \Big(\frac{\dot{R}}{R}\Big)_0^2, \\ &\text{the density parameter} && \Omega_0 = \frac{8\pi G\rho_0}{3{H_0}^2}, \\ &\text{the deceleration parameter} && q_0 = -\Big(\frac{R\ddot{R}}{\dot{R}^2}\Big)_0, \\ &\text{the cosmological constant} && \lambda_0 = \frac{\Lambda_0 c^2}{3{H_0}^2}, \end{aligned}$$

where '0' denotes the present value.

In terms of these cosmological parameters, the first equation in (C3) is given as,

$$\begin{aligned}\frac{\dot{R}}{R} =& \mathrm{H}_0\sqrt{(1+\mathrm{z})^3\Omega_0 + \lambda_0 - (1+\mathrm{z})^2 K} \\ \equiv& \mathrm{H}_0\chi(\mathrm{z}),\end{aligned} \tag{C4}$$

where z is the source redshift, and use has been made of the relations: $K = \Omega_0 + \lambda_0 - 1$, $\rho \propto R^{-3}$, $R \propto (1+\mathrm{z})^{-1}$ and $K = \frac{kc^2}{\mathrm{H}_0{}^2 R_0^2}$.

The angular diameter distance $D(\mathrm{z})$ in the FRW universe is defined as follows: (Weinberg 1972). Suppose that we observe the distance L between two points with redshift z expressed by a separation angle $\delta(\ll 1)$. There holds then the relation:

$$L = R(\mathrm{z})r(\mathrm{z})\delta. \tag{C5}$$

Thus the distance $D(\mathrm{z})$ between the two points and ourselves is given by $D(\mathrm{z}) = L/\delta$, *i.e.*

$$D(\mathrm{z}) = R(\mathrm{z})r(\mathrm{z}). \tag{C6}]$$

Lets us now express r as a function of the redshift z, which from (C1), is given by

$$r(\mathrm{z}) = \frac{1}{\sqrt{k}}\sin\Big[\sqrt{K}\int_0^{\mathrm{z}}\frac{d\mathrm{z}}{\chi(\mathrm{z})}\Big]. \tag{C7}$$

We have thus obtained $D(\mathrm{z})$ in units of $\left(\frac{c}{\mathrm{H}_0}\right)$ as follows:

$$D(\mathrm{z}) = \frac{1}{1+\mathrm{z}}\frac{1}{\sqrt{K}}\sin\Big[\sqrt{K}\int_0^{\mathrm{z}}\frac{d\mathrm{z}}{\chi(\mathrm{z})}\Big]. \tag{C8}$$

b) Clumpy universe

In order to describe the inhomogeneous universe we adopt the clumpy universe model proposed by Dyer and Roeder (1972). In this model, it is assumed that

all matters are concentrated into clumps such as galaxies, while the large scale structure of the Universe is given by the FRW universe. Moreover clumps are assumed to be distributed uniformly. Therefore all lights which are to be received by the observer propagate in an almost empty space.

Now we consider a light bundle far from any clump. The optical scalar equation (Sachs 1961) for this bundle is given by

$$\left(\mathcal{A}^{1/2}\right)'' + |\sigma|^2 \mathcal{A}^{1/2} + \frac{1}{2} R_{\mu\nu} k^\mu k^\nu \mathcal{A}^{1/2} = 0, \tag{C9}$$

where $\mathcal{A}$ denotes the cross sectional area of this light bundle and the shear σ is expressed as

$$|\sigma|^2 = \left| \frac{1}{2} k_{(\mu;\nu)} k^{\mu;\nu} - \frac{1}{4} \left(k^\mu{}_{;\mu}\right)^2 \right|, \tag{C10}$$

and the prime denotes the derivative with respect to an affine parameter τ along the light bundle.

Because the light propagates in the empty space and the large scale structure of the Universe is homogeneous, we can reduce (C9) to the following equation* :

$$\left(\mathcal{A}^{1/2}\right)'' = 0, \tag{C11}$$

Let us now consider, in particular, a conical bundle with the vertex at the observer and with the base at the source of lights. Then $\tilde{D}(\mathrm{z})$ is proportional to the square root of the cross sectional area $\mathcal{A}$ at the source. From (C11), it then follows that

$$\tilde{D}(\mathrm{z}) = \tau(\mathrm{z}), \tag{C12}$$

where the initial conditions for $\tilde{D}(\mathrm{z})$ are: $\tilde{D}|_{\tau=0} = 0$ and $\tilde{D}'|_{\tau=0} = 1$ in units of $\left(\frac{c}{\mathrm{H_0}}\right)$.

$\star$ We have taken into account the facts that $T^\mu{}_\nu = 0$ and that the shear averaged along the light trajectory does not contribute to this equation.

The relation between z and τ is given as

$$\frac{dz}{d\tau} = (1+z)^2\chi(z). \tag{C13}$$

Thus $\tilde{D}(z)$ in the clumpy universe is given by

$$\tilde{D}(z) = \int_0^z \frac{dz}{(1+z)^2\chi(z)}. \tag{C14}$$

APPENDIX D

Probability Function

In this appendix we review the derivation of the probability function proposed by Ehler and Schneider (1986). First we define the cross section $A_{L(S)}(\mu; z_S, z_L)$. For a deflector, $A_L(\mu)$ is an area of that region on the deflector plane through which the light ray whose the gravitational amplification factor is greater than μ passes. For instance, if the deflector is regarded as a point mass, the cross section $A_L(\mu; z_S, z_L)$ on the deflector plane at redshift z_L is given by

$$A_L(\mu; z_S, z_L) = \frac{8\pi GM}{c^2}\left(\frac{c}{H_0}\right)\frac{\tilde{D}(z_L)\tilde{D}_{LS}(z_S, z_L)}{\tilde{D}(z_S)}\left\{\frac{\mu}{\sqrt{\mu^2-1}} - 1\right\}, \tag{D1}$$

(Canizares 1981), whereas the cross section $A_S(\mu; z_S, z_L)$ on the source plane at redshift z_S is given by

$$\begin{aligned} A_S(\mu; z_S, z_L) =& A_L\left(\frac{\tilde{D}(z_S)}{\tilde{D}(z_L)}\right)^2 \\ =& \frac{8\pi GM}{c^2}\left(\frac{c}{H_0}\right)\frac{\tilde{D}(z_S)\tilde{D}_{LS}(z_S, z_L)}{\tilde{D}(z_L)}\left\{\frac{\mu}{\sqrt{\mu^2-1}} - 1\right\}. \end{aligned} \tag{D2}$$

Now let us evaluate the total cross section $A_{tot}(\mu; z_S)$ on the source plane for all lens galaxies within the source sphere at $z = z_S$. We obtain the quantity by integrating $A_S(\mu; z_S, z_L)$ over all lens galaxies:

$$\begin{aligned} A_{tot}(\mu; z_S) =& \int_0^{z_S} A_S(\mu; z_S, z_L) n(z_L) dV(z_L) \\ =& \left(\frac{c}{H_0}\right)^3 n_0 \int_0^{z_S} dz_L \frac{(1+z_L)^2 D^2(z_L)}{\chi(z_L)} A_S(\mu; z_S, z_L), \end{aligned} \tag{D3}$$

where $n(z_L)$, the number density of lens galaxies at $z = z_L$, is given by $n(z_L) = (1+z_L)^3 n_0$. Since we are considering the clumpy universe (see Appendix C), the present number density of lens galaxies is given by $n_0 = \rho_0/M$.

If these lens galaxies are regarded as point masses, the total cross section is then given by

$$A_{\rm tot}(\mu) = 12\pi\Big(\frac{c}{\rm H_0}\Big)^2\Omega_0\Big\{\frac{\mu}{\sqrt{\mu^2-1}}-1\Big\}\int_0^{\rm z_S} d{\rm z_L}\frac{(1+{\rm z_L})^2 D^2({\rm z_L})}{\chi({\rm z_L})}\frac{\tilde{D}({\rm z_S})\tilde{D}_{\rm LS}({\rm z_S},{\rm z_L})}{\tilde{D}({\rm z_L})}, \tag{D4}$$

On the other hand, the area of the source sphere at $z = z_S$ is given by

$$S = 4\pi\Big(\frac{c}{\rm H_0}\Big)^2 D^2({\rm z_S}). \tag{D5}$$

Thus the probability function $P(z_S; > \mu)$ with the amplification factor greater than μ is expressed as the ratio of the total cross section $A_{\rm tot}$ to the area of the whole sphere at z_S, *i.e.*:

$$P({\rm z_S};>\mu) = 3\Omega_0\Big\{\frac{\mu}{\sqrt{\mu^2-1}}-1\Big\}\Big(\frac{\tilde{D}({\rm z_S})}{D({\rm z_S})}\Big)^2\int_0^{\rm z_S} d{\rm z_L}\frac{(1+{\rm z_L})^2 D^2({\rm z_L})}{\chi({\rm z_L})}\frac{\tilde{D}_{\rm LS}({\rm z_S},{\rm z_L})}{\tilde{D}({\rm z_S})\tilde{D}({\rm z_L})}. \tag{D6}$$

Further the probability distribution $p(z_S; \mu)$ with amplification factor μ is defined as

$$p({\rm z_S};\mu) = -\frac{d}{d\mu}P({\rm z_S};>\mu), \tag{D7}$$

which is adopted in Chapter 7. The condition that p is meaningful as the probability is that $A_{\rm tot} \ll S$. This means that there are no significant overlaps of the cross sections on the source sphere.

REFERENCES

Alcock, C. and Anderson, N. 1985, *Ap.J.(Letters)*,**291**,L29.

Alcock, C. and Anderson, N. 1986, *Ap.J.*,**302**,43.

Bahcall, J.N., Bahcall, N.A. and Schneider, D.P. 1986, *Nature*,**323**,515.

Bahcall, J.N. and Tremaine, S. 1988, *Ap.J.(Letters)*,**326**,L1.

Blandford, R.D. and Kochanek, C.S. in *Jerusalem Winner School For Theoretical Physics*: vol.4 1988, *Dark Matter in the Universe*, ed. by Bahcall, J., Piran, T. and Weinberg, S., p.132.

Blandford, R.D. and Kovner, I. 1988, *Phys.Rev.*,**A38**,4028.

Blandford, R. and Narayan, R. 1986, *Ap.J.*,**310**,568.

Borgeest, U. 1983, *Astr.Ap.*,**128**,162.

Borgeest, U. 1986, *Ap.J.*,**309**,467.

Borgeest, U. and Refsdal, S. 1984, *Astr.Ap.*,**141**,318.

Bourassa, R.R. Kantowski, R. and Norton, T.D. 1973, *Ap.J.*,**185**,747.

Bourassa, R.R. and Kantowski, R. 1975, *Ap.J.*,**193**,13.

Braun, E. and Dekel, A. 1988, *Comments Astrophys.*,**12**,233.

Burke, W.L. 1981, *Ap.J.(Letters)*,**244**,L1.

Caditz, D. and Petrosian, V. 1989, *Ap.J.(Letters)*,**337**,L65.

Canizares, C.R. 1981, *Nature*,**291**,620.

Canizares, C.R. 1987, in *Observational Cosmology*, ed. by Hewitt, A., Burbidge, G. and Fang, L.Z.(Dordrecht: Reidel),p.729.

Chang, K. and Refsdal, S. 1979, *Nature*,**282**,561.

Christian, C.A., Crabtree, D. and Waddel, P. 1987, *Ap.J.*,**312**,45.

Cooke, J.H. and Kantowski, R. 1975, *Ap.J.(Letters)*,**195**,L11.

Djorgovski, S. and Soinrad, H. 1984, *Ap.J.(Letters)*,**282**,L1.

Dyer, C.C. and Oattes, L.M. 1988, *Ap.J.*,**326**,50.

Dyer, C.C. and Roeder, R.C. 1972, *Ap.J.(Letters)*,**174**,L115.

Dyer, C.C. and Roeder, R.C. 1973, *Ap.J.(Letters)*,**180**,L31.

Dyer, C.C. and Roeder, R.C. 1974, *Ap.J.*,**189**,167.

Dyer, C.C. and Roeder, R.C. 1980, *Ap.J.(Letters)*,**238**,L67.

Dyer, C.C. and Roeder, R.C. 1981, *Ap.J.(Letters)*,**241**,L133.

Efstathiou, G. Ellis, R.S. and Peterson, B.A. 1988, *M.N.R.A.S.*,**232**,431.

Einstein, A. 1936, *Science*,**84**,506.

Ehlers, J. and Schneider, P. 1986, *Astr.Ap.*,**168**,57.

Fayos, F. and Llosa, J. 1982, *Gen.Rel.Grav.*,**14**,865.

Felten, J.E. 1985, *Comments Astrophys.*,**11**,53.

Florentin-Nielsen, R. 1984, *Astr.Ap.*,**138**,L19.

Fort, B., Prieur, J.L., Mathezz, G., Mellier, Y. and Soucial, G. 1988, *Astr.Ap.*,**200**,L17.

Foy, R., Bonneau, D. and Blazit, A. 1985, *Astr.Ap.*,**149**,L13.

Futamase, T., and Sasaki, M. 1989, *Phys.Rev.*,**D40**,2502.

Giraud, E. 1988, *Ap.J.(Letters)*,**334**,L69.

Gorenstein, M.V., Shapiro, I.I., Rogers, A.E.E., Cohen, N.L., Corey, B.E., Pocas, R.W., Falco, E.E., Bonometti, R.J., Preston, R.A., Ruis, A. and Whitney, A.R. 1984, *Ap.J.*,**242**,538.

Gorenstein, M.V., Falco, E.E. and Shapiro, I.I. 1985, *Ap.J.(Letters)*,**289**,L1.

Gorenstein, M.V., Falco, E.E. and Shapiro, I.I. 1988a, *Ap.J.*,**327**,693.

Gorenstein, M.V., Cohen, N.L., Shapiro, I.I., Rogers, A.E.E., Bonometti, R.J., Falco, E.E., Bartel, N. and Marcaide, J.M. 1988b, *Ap.J.*,**334**,42.

Greenfield, P.E., Roberts, D.H. and Burke, B.F. 1985, *Ap.J.*,**293**,370.

Grossmann, S.A. and Narayan, R. 1988, *Ap.J.*,**324**,37.

Hammer, F., Le févre, O. and Nottel, L. 1987, in *Observational Cosmology,* ed. by Hewitt, A., Burbidge, G. and Fang, L.Z.(Dordrecht: Reidel),p.751.

Hammer, F., Le fé vre, O., Jones, J., Rigaut, F. and Soucial, G. 1989, *Astr.Ap.*,**208**,L7.

Hammer, F. and Nottale, L. 1986, *Astr.Ap.*,**167**,1.

Hege, E.K., Angel, J.R.P., Weymann, R.J. and Hubbard, E.N. 1980, *Nature*,**287**,416.

Hege, E.K., Hubbard, E.N., Strittmatter, P.A. and Worden, S.P. 1981, *Ap.J.(Letters)*,**248**,L1.

Henry, J.P. and Heasley, J.N. 1986, *Nature*,**321**,139.

Hewitt, J.N., Turner, E.L., Burke, B.F., Lawrence, C.R., Bennet, C.L., Langston, G.I. and Gunn, J.E. 1987 in *Observational Cosmology,* ed. by Hewitt, A., Burbidge, G. and Fang, L.Z.(Dordrecht: Reidel),p.747.

Hewitt, J.N., Turner, E.L., Lawrence, C.R., Schneider, D.P., Gunn, J.E., Bennet, C.L., Burke, B.F., Mahoney, J.H., Langston, G.I.,Schmidt, M., Oke, J.B. and Hossel, J.G. 1987b, *Ap.J.*,**321**,706.

Huchra, J., Gorenstein, M., Kent, S., Shapiro, I., Smith, G., Horine, E. and Perley, R. 1985, *A.J.*,**90**,691.

Ishihara, H., Takahashi, M. and Tomimatsu, A. 1988, *Phys.Rev.*,**D38**,472.

Issacson, J.A. and Canizares, C.R. 1989, *Ap.J.*,**336**,544.

Kantowski, R. 1968, *J.Math.Phys.*,**9**,336.

Kayser, R. and Refsdal, S. 1983, *Astr.Ap.*,**128**,156.

Katz, J.I. 1987, *Astr.Ap.*,**182**,L19.

Kent, S.M. and Falco, E.E. 1988, *A.J.*,**96**,1570.

Kovner, I. 1987a, *Ap.J.*,**312**,22.

Kovner, I. 1987b, *Ap.J.(Letters)*,**318**,L1.

Kovner, I. 1987c, *Nature*,**327**,193.

Kovner, I. and Paczyński, B. 1989, *Ap.J.(Letters)*,**335**,L9.

Kristian J., Sandage, A. and Westphal, J.A. 1978, *Ap.J.*,**221**,383.

Lapparent,V.D., Geller, M.J. and Huchra, J.P. 1989, *Ap.J.*,**342**,1.

Lavery, R.J. and Henry, J.P. 1988, *Ap.J.(Letters)*,**329**,L21.

Lawrence, J.K. 1980, *Ap.J.*,**239**,305.

Lawrence, C.R., Schneider, D.P., Schmidt, M., Bennett, C.L., Herwitt, J.N., Burke, B.F., Turner, E.L. and Gunn, J.E. 1984, *Science*,**223**,46.

Le févre, O., Hammer, F. and Nottel, L. 1987, *Nature*,**326**,268.

Liebes, S. 1964, *Phys.Rev.*,**133**,B833.

Loh, E.D. and Spillar, E.J. 1986, *Ap.J.(Letters)*,**307**,L1.

Lynds, R. and Petrosian, V. 1986 *Bull. AAS.*,**18**,1014.

Lynds, R. and Petrosian, V. 1989, *Ap.J.*,**336**,1.

Magain, P., Surdej, J., Swings, J. P., Borgeest, U., Kayser, R., Kühr, H., Refsdal,S. and Remy,M. 1988, *Nature*,**334**,325.

McKenzie, R.H. 1985, *J.Math.Phys.*,**26**,1592.

Meylan, G. and Djorgovski, S. 1989, *Ap.J.(Letters)*,**338**,L1.

Millier, J.S. and Goodrich, R.W. 1988, *Nature*,**331**,685.

Narasimha, D. and Chitre, S.M. 1988, *Ap.J.*,**332**,75.

Narasimha, D., Subramanian, K. and Chitre, S.M.
1982, *M.N.R.A.S.*,**200**,941.

Narasimha, D., Subramanian, K. and Chitre, S.M. 1984, *Ap.J.*,**283**,512.

Narasimha, D., Subramanian, K. and Chitre, S.M. 1986, *Nature*,**321**,45.

Narasimha, D., Subramanian, K. and Chitre, S.M. 1987, *Ap.J.*,**315**,434.

Narasimha, D., Subramanian, K. and Chitre, S.M. 1988 *preprint*

Nieto, J.N., Roqus, S., Llebaria, A., Vanderriest, C.H., Lelièvre, G.,
di Serego Alighieri, S., Macchetto, F. D. and Perryman, M. A. C.
1988, *Ap.J.*,**325**,644.

Omote. M. and Yoshida, H. 1989, *Phys.Lett.*,**A139**,454.

Omote. M. and Yoshida, H. 1990, *Ap.J.*,in press.

Paczyński, B. 1987, *Nature*,**325**,572.

Peacock, J.A. 1986, *M.N.R.A.S.*,**223**,113.

Pello-Descayre, R., Soucial, G., Sanahuja, B., Methez, G. and Ojero, E.
1988, *Astr.Ap.*,**190**,L11.

Pirani, F.A.E. 1964, Lectures at *Brandeis Summer Institute*
in Theoretical Physics.

Porcas, R.W., Booth, R.S., Browne, I.W.A., Walsh, D. and Wilkinson, P.N.
1981, *Nature*,**289**,758.

Press, W.H. and Gunn, J.E. 1973, *Ap.J.*,**185**,397.

Plebanski, J. 1961, *Phys.Rev.*,**118**,1396.

Refsdal, S 1964a, *M.N.R.A.S.*,**128**,295.

Refsdal, S 1964b, *M.N.R.A.S.*,**128**,307.

Refsdal, S 1966, *M.N.R.A.S.*,**132**,101.

Roberts, D.H., Greenfield, P.E., Hewitt, J.N., Burke, B.F., and Durpree, A.K. 1985, *Ap.J.*,**293**,356.

Sachs, R.K. 1961, *Proc.Roy.Soc.(London)*,**264**,A309.

Schechter, P. 1976, *Ap.J.*,**203**,297.

Schneider, P. 1985, *Astr.Ap.*,**143**,413.

Schneider, P. 1987, *Astr.Ap.*,**183**,189.

Schneider, D.P., Lawrence, C.R., Schmidt, M., Gunn, J.E., Turner, E.L., Burke, B.F. and Dhawan, V. 1985, *Ap.J.*,**294**,66.

Schneider, D.P., Gunn, J.E., Turner, E.L., Lawrence, C.R., Hewitt, J.N., Schmidt, M. and Burke, B.F. 1986, *A.J.*,**91**,991.

Schneider, D.P., Gunn, J.E., Turner, E.L., Lawrence, C.R., Schmidt, M. and Burke, B.F. 1987, *A.J.*,**94**,12.

Schneider, D.P., Turner, E.L., Gunn, J.E., Hewitt, J.N., Schmidt,M. and Lawrence, C.R. 1988, *A.J.*,**95**,1619.

Schramm, T. and Kayser, R. 1987, *Astr.Ap.*,**174**,361.

Shaklan, S.B. and Hege, E.K. 1986, *Ap.J.*,**303**,605.

Sol, H., Vanderriest, C.H., Lelievre,G., Pedersen,J. and Schneider,J. 1984, *Astr.Ap.*,**32**,105.

Soucial, G., Fort, B. Mellier, Y. and Picat, P. 1987a, *Astr.Ap.*,**172**,L14.

Soucial, G., Mellier, Y., Fort, B. Hammer, F. and Mathez, G. 1987b, *Astr.Ap.*,**184**,L7.

Soucial, G., Mellier, Y., Fort, Mathez, G. and Cailloux, M. 1988, *Astr.Ap.*,**191**,L19.

Spinrad, H. and Djorgovski, S. 1984, *Ap.J.(Letters)*,**280**,L9.

Sramek, R.A. and Weedman, D.W. 1978, *Ap.J.*,**221**,468.

Stockton, A. 1981, *Ap.J.*,**242**,141.

Su, F.S.O. and Mallett, R.L. 1980, *Ap.J.*,**238**,1111.

Surdej, J., Magain, P., Swings, J.P., Borgeest, U., Courvoisier, J.L., Kayser, R., Kellermann, K.I., Kŭhr, H. and Refsdal, S. 1987, *Nature*,**329**,695.

Surdej, J., Magain, P., Swings, J.P., Borgeest, U., Courvoisier, J.L., Kayser, R., Kellermann, K.I., Kŭhr, H. and Refsdal, S. 1988q, *Astr.Ap.*,**198**,49.

Synge, J.L. 1960, *Relativity: The General Theory*(Amsterdam, North-Holland).

Turner, E.L., Hillenbrnd, L.A. Schneider, D.P., Hewitt, J.N. and Burke, B.F. 1988, *A.J.*,**96**,1682.

Tyson, J.A., Seitzer, P., Weymann, R.D. and Foltz, C. 1986, *A.J.*,**91**,1274.

Tyson, J.A., Gorenstein, M. 1985, *Sky and Telescope*,**70**,319.

Vanderriest, C., Wlérich, G., Lelievre, G., Schneider, J., Sol, H., Horville, D., Renard, L and Servan, B. 1986, *Astr.Ap.*,**158**,L5.

Vanderriest, C., Schneider, J., Herpe, G., Chevreton, M., Moles, M., and Wlérich, G. 1989, *Astr.Ap.*,**215**,1.

Vietri, M. and Ostriker, J.P. 1983, *Ap.J.*,**267**,488.

Walsh, D., Carswell, R.F. and Weymann, R.J. 1979, *Nature*,**279**,381.

Wambsganss, J., Giraud, E., Schneider, P. and Weiss, A. 1989, *Ap.J.(Letters)*,**337**,L73.

Weedman, D.W., Weymann, R.J., Green, R.F. and Heckman, T,M. 1982, *Ap.J.(Letters)*,**255**,L5.

Weinberg, S. 1972, *Gravitation and Cosmology*(J. Wiley and Sons, Inc).

Weinberg, S. 1976, *Ap.J.(Letters)*,**208**,L1.

Weymann, R.J., Lathan, D., Angel, J.R.P., Green, R.F., Liebert, J.W., Turnshek, D.A. and Turnshek, D.E.
1980, *Nature*,**285**,641.

Weymann, R.J., Craswell, R.F. and Smith, M.G.
1981, *Ann.Rev.Ast.Ap.*,**19**,41.

Yee, H.K.C. 1988, *A.J.*,**95**,1331.

Yoshii, Y. and Takahara, F. 1989, *Ap.J.*,**346**,28.

Yoshida, H. and Omote, M. 1988 *Prog.Theo.Phys*,**79**,1095.

Young, P., Gunn, J.E., Kristian, J., Oke, J.B. and Westphal, J.A.
1980, *Ap.J.*,**241**,507.

Young, P., Gunn, J.E., Kristian, J., Oke, J.B. and Westphal, J.A.
1981a, *Ap.J.*,**244**,736.

Young, P., Deverill, R.S., Gunn, J.E. and Westphal, J.A.
1981b, *Ap.J.*,**244**,723.

Zwicky, F. 1937, *Phys.Rev.Lett.*,**51**,290.

FIGURE CAPTIONS

Fig.2.1 A gravitationally lensed system. A photon emitted from a source is deflected with an angle $\vec{\alpha}$, where $\vec{\alpha}$ is assumed to be sufficiently small, $|\vec{\alpha}| \ll 1$.

Fig.4.1 Positions and shapes of the images of 1115+080 from our calculation.

Fig.4.2 The dependence of the cosmological factor T on the deceleration parameter q_0 with $0.3 \leq z_d \leq 0.5$.

Fig.4.3 The dependence of the effective distance on redshift: a)$\gamma = -3$; b)$\gamma = -2$; c)$\gamma = -1$; d)$\gamma = 0$; e)$\gamma = 1$; f)$\gamma = 2$; and g)$\gamma = 3$.

Fig.4.4 The dependence of the cosmological factor T on γ with $-3 \leq \gamma \leq 3$.

Fig.7.1 The ratio $\tilde{G}_0/G_0$ as a function of Ω_0.

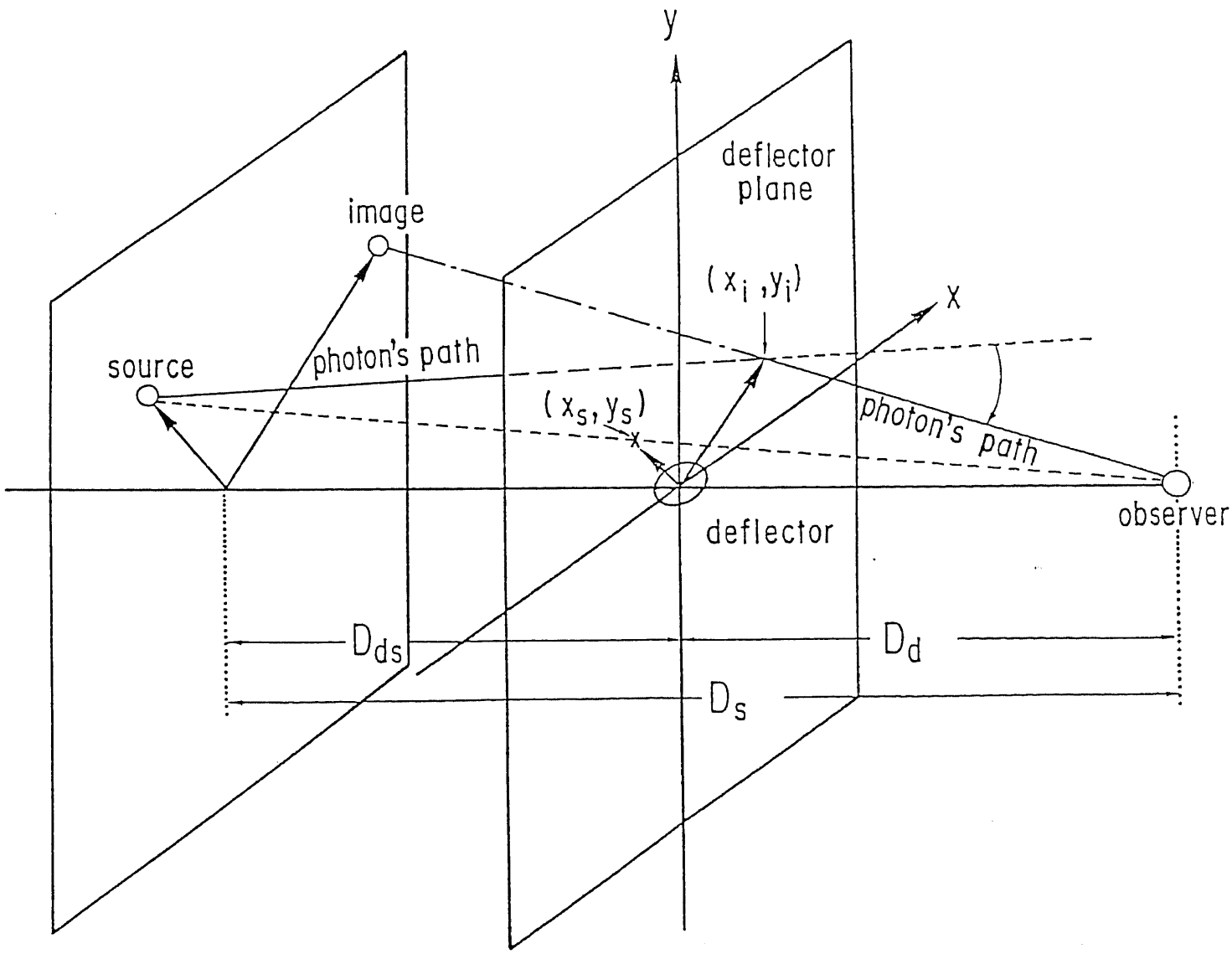
y
deflector
plane
image
(x_i, y_i)
x
source
photon's path
(x_s, y_s)
photon's path
observer
deflector
D_{ds}
D_d
D_s

Fig. 2.1

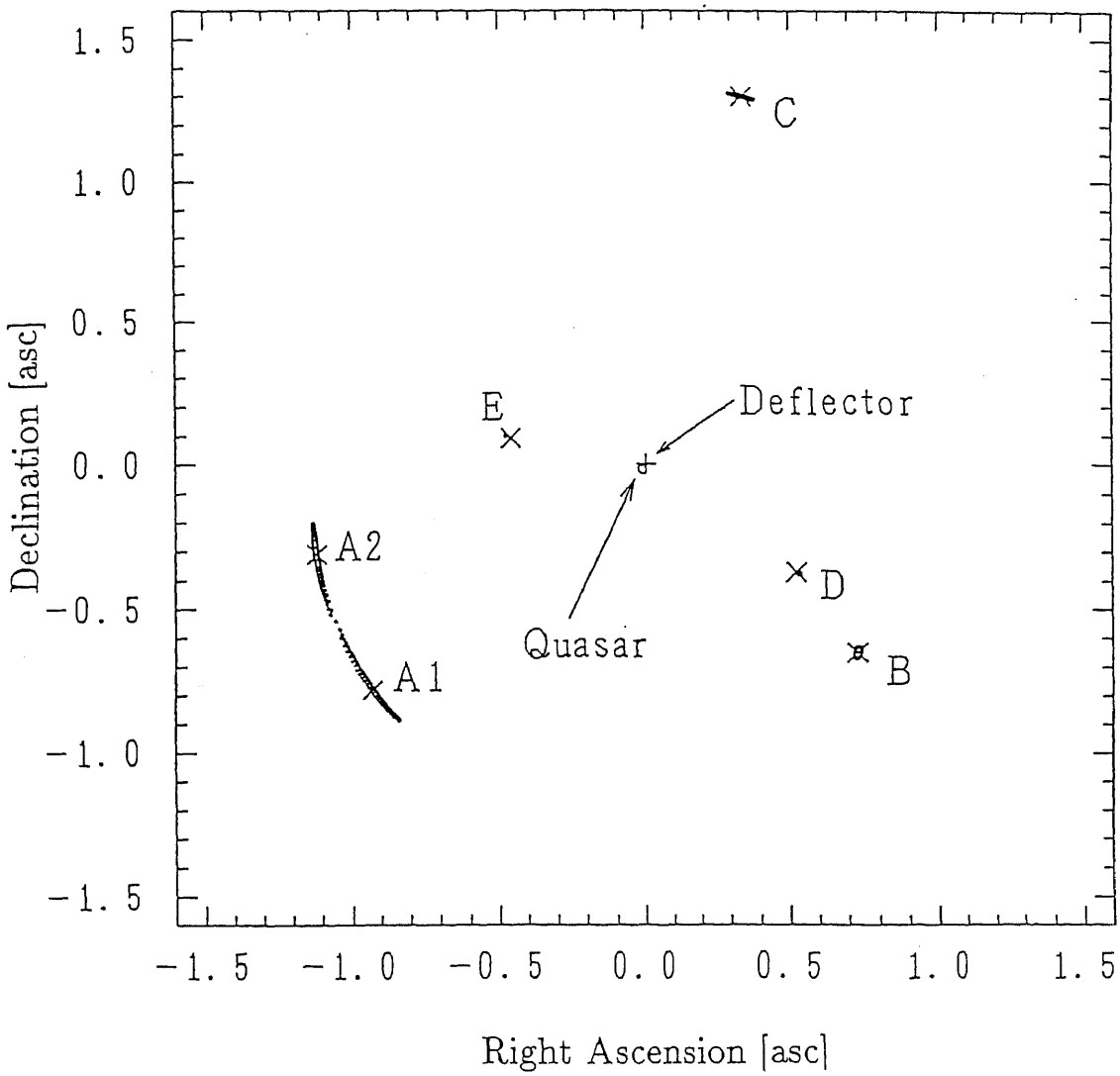
1.5
1.0
0.5
0.0
−0.5
−1.0
−1.5
Declination [asc]
−1.5
−1.0
−0.5
0.0
0.5
1.0
1.5
Right Ascension [asc]
C
E
Deflector
A2
D
Quasar
A1
B

Fig. 4.1

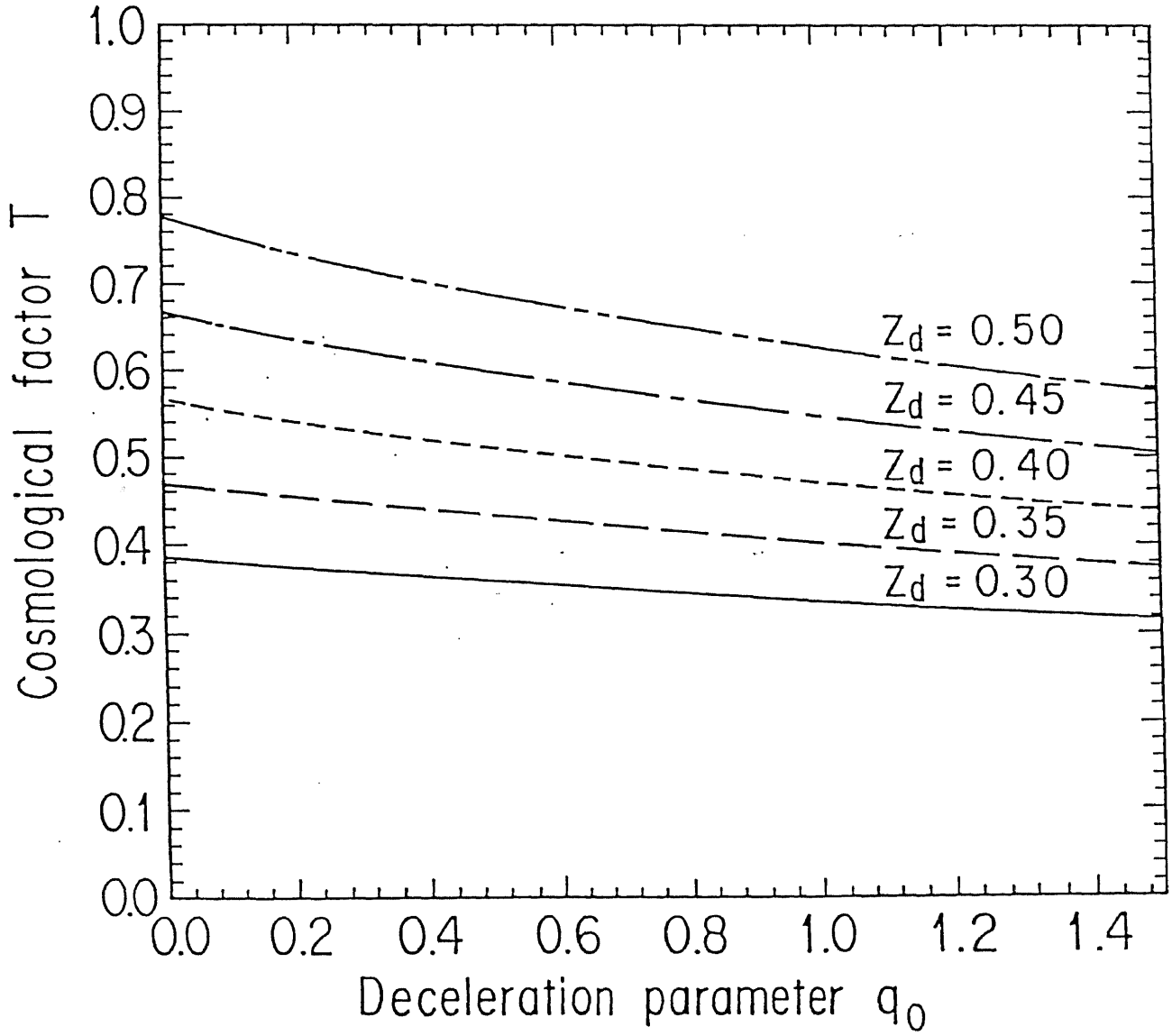
1.0
0.9
0.8
0.7
0.6
0.5
0.4
0.3
0.2
0.1
0.0
Cosmological factor T
Z_d = 0.50
Z_d = 0.45
Z_d = 0.40
Z_d = 0.35
Z_d = 0.30
0.0
0.2
0.4
0.6
0.8
1.0
1.2
1.4
Deceleration parameter q_0

Fig. 4.2

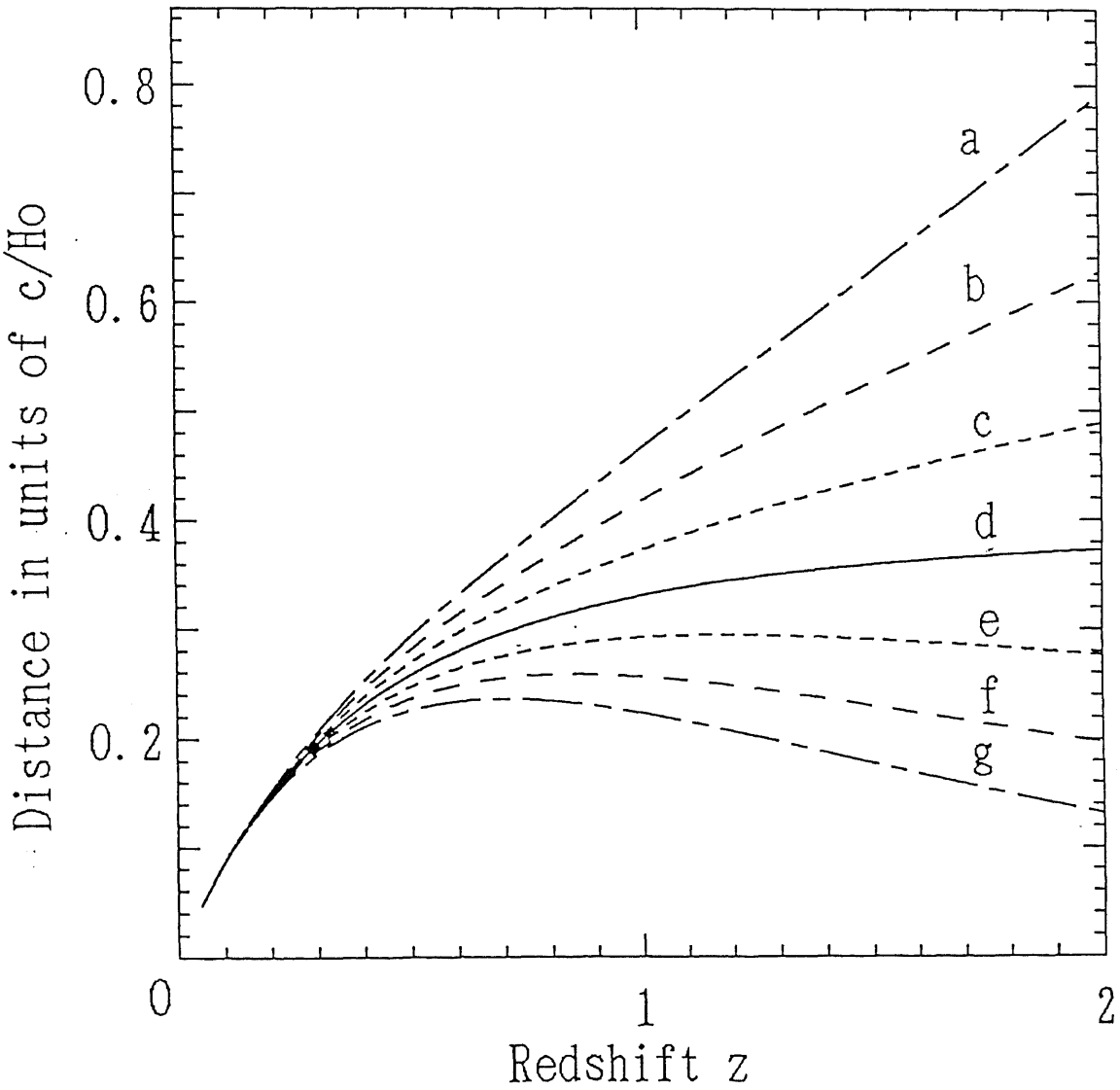

Fig. 4.3

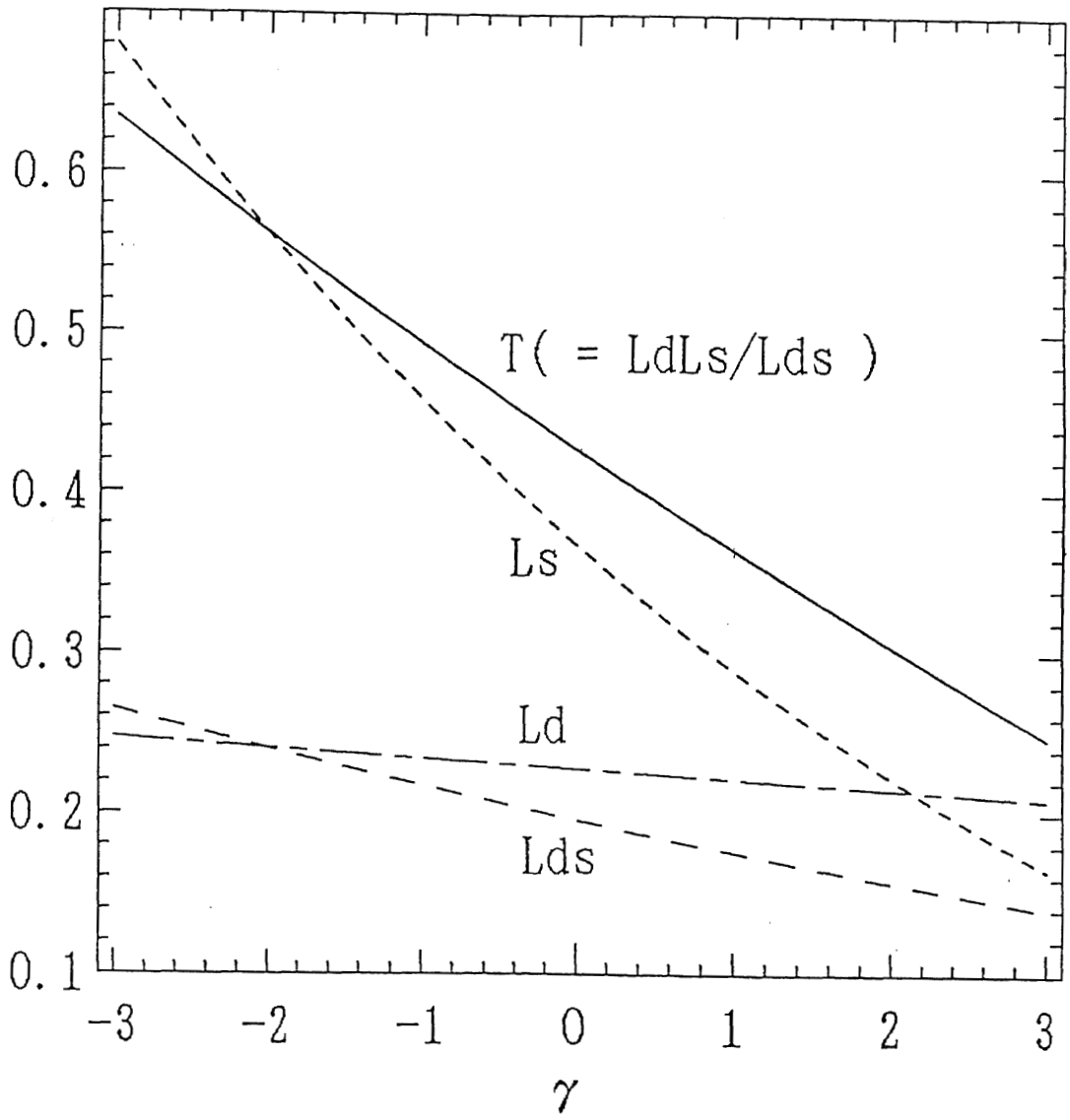

Fig. 4.4

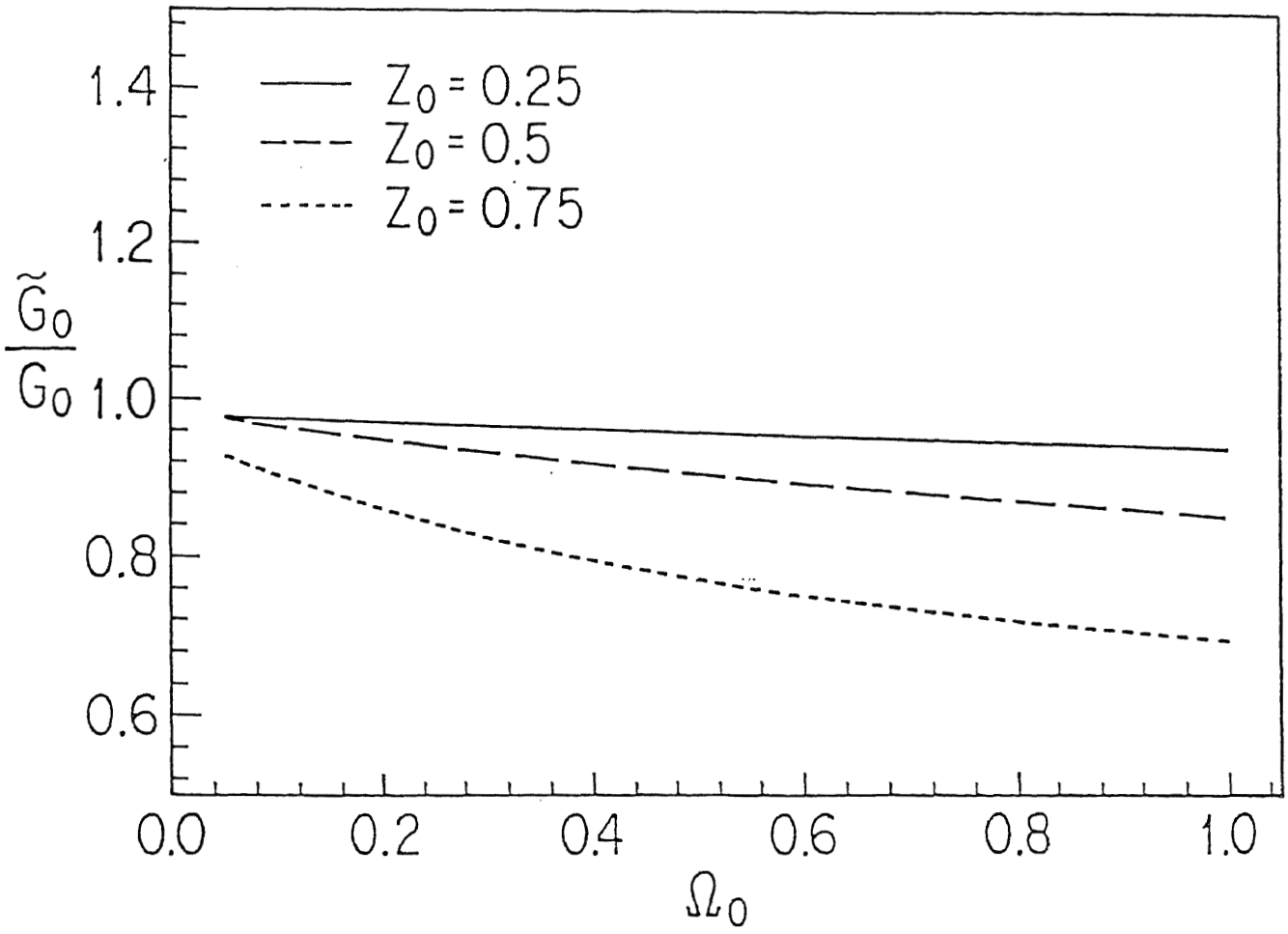
$Z_0 = 0.25$
$Z_0 = 0.5$
$Z_0 = 0.75$
$\frac{\tilde{G}_0}{G_0}$
1.4
1.2
1.0
0.8
0.6
0.0
0.2
0.4
0.6
0.8
1.0
Ω_0

Fig. 7.1